Non-supersymmetric orientifolds and chiral fermions from intersecting D6- and D8-branes

Dissertation
zur
Erlangung des Doktorgrades (Dr. rer. nat.)
der
Mathematisch-Naturwissenschaftlichen Fakultät
der
Rheinischen Friedrich-Wilhelms-Universität Bonn

vorgelegt von

Monika Gabriele Honecker

aus
Bonn

Bonn, Mai 2002

Angefertigt mit Genehmigung der Mathematisch-Naturwissenschaftlichen Fakultät
der Rheinischen Friedrich-Wilhelms-Universität Bonn

1. Referent:	Prof. Dr. Hans-Peter Nilles
2. Referent:	Prof. Dr. Rainald Flume
Tag der Promotion:	2. Juli 2002

Abstract

Brane supersymmetry breaking and chiral fermions are discussed in the context of intersecting D6- and D8-branes in compactifications of type II orientifolds. The orientifold projection contains a reflection $\mathcal{R}_i$ in i internal coordinates which leaves orientifold planes of space dimension $(9-i)$ invariant. In order to achieve partial supersymmetry breaking, a four dimensional orbifold symmetry is imposed. The reflection $\mathcal{R}_i$ is chosen such that it acts as complex conjugation on an additional two torus. Cancellation of RR charges enforces the existence of D-branes of the same dimensionality as the O-planes. The D-branes can either be chosen to lie on top of the O-planes leading to local RR charge cancellation and a $\mathcal{N}=2$ supersymmetric non-chiral spectrum or allowing for global RR charge cancellation only, the D-branes can be chosen to lie at non trivial angles on the two torus. The intersection points of two D-branes support chiral fermions in the bifundamental representation of the gauge groups which are provided by fields living on the worldvolume of the D-branes involved. These models have broken supersymmetry in the open string sector while the closed string sector, which in particular contains gravity, remains $\mathcal{N}=2$ supersymmetric.

The gauge groups and chiral spectra depend on the choice of the reflection $\mathcal{R}_i$ and the orbifold group. Several explicit examples with particle spectra close to the standard model are given.

Cancellation of gauge anomalies, the stability of the models and phenomenological implications are discussed.

Acknowledgements

Above all, I am grateful to Prof. Hans-Peter Nilles for the support of my Ph.D. and for drawing my attention to the topic of orientifold constructions.
I am very much indebted to Dr. Stefan Förste for collaborating with Dr. Ralph Schreyer and me and for patiently answering our permanent questions.
I am grateful to Dr. Ralph Schreyer for fruitful collaboration and innumerable discussions.
Furthermore, I wish to thank Dr. Ralph Blumenhagen, Dr. Athanasios Dedes, Dr. Dumitru Ghilencea, Hanno Klemm and Dr. Boris Körs for inspiring discussions.
I am grateful for the peaceful working atmosphere to my office mates Dr. Ralph Schreyer and Jasmin Pielorz as well as to the other members of the research group Florian Gmeiner, Dr. Marek Olechowski, Dr. Marco Peloso and Akın Wingerter.
Thanks a lot to Dr. Andreas Wisskirchen, Dagmar Fassbender and Patricia Zündorf for help in bureaucratic and organizational questions.
Moreover, I wish to thank Dr. Stefan Förste and Katharina Lorenz for proof-reading the manuscript.
Thanks to the Graduiertenförderung des Landes Nordrhein-Westfalen for financial support from October 1999 until July 2000.
Last but not least I am greatly indebted to my family for their love and support.

Contents

Introduction

In this thesis, orientifold models of type II superstrings are investigated where chiral fermions arise from supersymmetry breaking intersections of D-branes.

One of the major challenges of contemporary theoretical physics is the existence of two different theories which describe the known fundamental interactions at different scales but so far cannot be implemented satisfactorily into a common theory.

On the one hand, the standard model of particle physics is based on renormalizable quantum field theories. It describes earth based experiments, e.g. in particle accelerators, at an impressive accuracy.

On the other hand, the general theory of relativity is a classical theory describing gravitational interactions which become dominant at long distances. Including general relativity into quantum theories amounts to treating space and time quantum mechanically. Several different approaches have been made, which are reviewed in [102]. None of them is yet completely satisfactory, but e.g. the semi-classical approach of considering quantum field theory in curved space [17] is capable of predicting the Hawking radiation of a black hole. Additional applications of a quantized theory of gravity are expected to be relevant for astrophysics and investigations on the early universe.

Further indications to look for a theory beyond the standard model arise from the large amount of free parameters of the standard model which have to be fixed experimentally and cannot be predicted from the theory itself. In addition, astrophysical models require an extreme fine-tuning of parameters in order to contain galaxies, stars and biological life. The spectrum and gauge groups so far have no explanation from first principles, and last but not least the standard model Higgs sector prediction still needs to be confirmed.

One step beyond the standard model can be made by introducing a symmetry relating bosons and fermions, namely the supersymmetry. This theory has the technical advantage of removing quadratic divergences in the scalar masses. Furthermore, it offers the possibility of reducing the amount of free parameters of particle physics because the gauge couplings unify at the so called GUT scale and thus allow for embedding the standard model gauge groups into a single GUT group. A review article on these topics is given by [89].

Another attempt for going beyond the standard model consists in Kaluza-

Klein theories [76, 78]. This ansatz assumes that gravity propagates in more than four spacetime dimensions where the supplementary dimensions are taken to be of finite size. This ansatz, however, seems to be inconsistent if there is no underlying theory assumed. The need for string regularization schemes in Kaluza-Klein theories has recently been discussed e.g. in [52].

A very promising candidate for a theory which contains both gravity and gauge interactions is provided by string theory [58, 59, 86, 93, 94]. Interestingly, it also offers a natural explanation for the other approaches to find a theory beyond the standard model. Fermions are implemented in string theory by introducing local supersymmetry on the worldsheet. Furthermore, superstring theory is consistently defined only in ten dimensions which requires a mechanism of 'hiding dimensions' as in the Kaluza-Klein theories to make it a viable candidate for a phenomenologically appealing theory containing the known interactions. For a recent review article on strings and extra dimensions see e.g. [47].

In fact, there does not only exist one single fermionic string theory. Five different string theories are consistently defined in ten dimensions. These are the heterotic theories with gauge groups $SO(32)$ and $E_8 \times E_8$ and the type IIA, IIB and type I theory. The heterotic theories and type I superstring theory have $\mathcal{N} = 1$ supersymmetry in $D = 10$ while the type IIA and IIB theory have extended $\mathcal{N} = 2$ supersymmetry. Except for the type IIA theory, all other ten dimensional theories are chiral.

In the 1980's, the main progress in string theory focused on the formulation of the weakly coupled heterotic theories [61, 60, 62]. Compactifications on Calabi-Yau manifolds [28, 109] and orbifolds [40, 41] leading to $\mathcal{N} = 1$ supersymmetry in four dimensions were considered. The breaking of gauge groups through Wilson lines was e.g. considered in [73], and three family models with an extension of the standard model gauge group were obtained [70, 46].

Besides the heterotic theories, also the ten dimensional type I superstring is provided with a gauge group $SO(32)$. The examination of this theory also started in the 1980's [103] with the discovery of orientifold planes. The computational tools for obtaining effective lower dimensional theories from orientifold constructions were successively worked out in [99, 57, 66, 15, 16].

The picture of five distinct consistent string theories started to change dramatically with the discovery of a web of dualities which relates all theories. The two type II theories and the two heterotic theories were e.g. found to be T-dual to each other [38, 55]. Between the type I theory and the heterotic theory with gauge group $SO(32)$, S-duality has been conjectured which relates one theory at strong coupling with the other one at weak coupling [111, 98]. Furthermore, the low energy limit of the ten dimensional type IIA string theory at strong coupling is given by eleven dimensional supergravity [110, 111], and the heterotic $E_8 \times E_8$ theory at strong coupling is described by eleven dimensional supergravity on an interval with the two gauge factors confined to the ten dimensional walls [68, 67].

Implications of this on the four dimensional theories have been considered e.g. in [90, 91]. The conjectured web of dualities between the string theories and the relations to eleven dimensional supergravity led to the assumption that all known theories are special vacua of an underlying theory, called M-theory [111, 105].

In the recent years, a lot of progress has been made in the search for the standard model from type II orientifold theories. A very important ingredient is the role of the D-branes [95] which carry RR charges opposite to those of the orientifold planes. The main computational tools were worked out in [54].

The Dp-branes can either be viewed as endpoints of open strings which have Neumann boundary conditions along p spatial dimensions or as solitonic objects which couple to the closed string modes. In the latter picture, further geometric objects with couplings to closed strings are the orientifold planes. Associated to both types of couplings are physical RR charges. For a theory to be consistent, the total RR charge has to vanish. These are the 'RR tadpole cancellation conditions'. The constraints on four dimensional model building arising from the RR charge cancellations are very restrictive in the supersymmetric case.

Various approaches of obtaining phenomenologically interesting models within the supersymmetric framework include blowing-up of orbifold singularities [31, 92], locating D-branes at different points in the internal space, which is T-dual to including non-trivial Wilson lines (see e.g. [36] for a model with discrete Wilson lines and [32] for continuous ones), and considering discrete values for the NSNS antisymmetric tensor [14, 13, 113, 108, 3, 75] which reduces the rank of the gauge group and has a T-dual description in terms of deformed compactification lattices [24].

In orientifold compactifications it may make sense to go beyond the partial supersymmetry breaking by orbifold symmetries to completely broken supersymmetry. The reason is that supersymmetry may not be necessary to explain the hierarchy between the Planck and the electroweak scale. In D-brane set-ups one can sometimes keep the fundamental scale, the string scale M_s, at the weak scale and obtain the Planck scale M_P by large compact extra dimensions [6, 7].

The supersymmetry breaking in the open string sector can be realized in two different ways by D-branes while the closed string sectors are not affected. One way is the inclusion of anti-D-branes in the models which carry RR charges opposite to the D-branes. They also have the opposite GSO projection. That is the reason why tachyonic scalar excitations from strings stretching between D-branes and anti-D-branes occur for small distances of the D-branes. Many of these models are unstable and undergo phase transitions [11, 107, 84, 5, 50, 101].

The other way to break supersymmetry in the open string sector is by allowing for magnetic background fluxes on the worldvolume of the D-branes in consistency with the RR charge cancellation conditions. These magnetic fluxes also trigger the breaking of chiral and gauge symmetry. In a T-dual picture, the various fluxes of different D-branes are replaced by intersection angles of lower dimensional D-branes which wrap different cycles in the compact space. D-branes at angles in orientifold theories have first been studied for the special case where the D-branes wrap the same cycles as the orientifold planes leading to local RR charge cancellation. The six dimensional set-ups were constructed in [20] and the four dimensional models were worked out in [19, 18] for a single orbifold group generator while my collaborators and me studied products of two orbifold group generators in [49]. These models preserve $\mathcal{N} = 1$ supersymmetry in the corresponding dimension but turn out to have a non-chiral spectrum. In [21] the relation between symmetric orbifolds in orientifold theories with D-branes at angles and asymmetric orbifolds in ordinary type I theory with background fluxes was discussed for six non compact dimensions. Subsequently, in [22, 23] the chiral four dimensional spectrum for toroidal compactifications in orientifold theories with D-branes at angles was computed. All these searches for chiral fermions were derived from orientifold theories.

In [2, 1] four dimensional models were considered which descend from compactifications of type II superstring theories without any orientifold projection. The D-branes intersect on one, two or three tori while they are situated at an orbifold fixed point in the remaining compact space. Phenomenological issues, namely hierarchies of mass scales and Yukawa couplings as well as the stability of the proton were first discussed in the context of type II theories. Further attempts to derive the standard model from this class of intersecting D-branes were performed in [9].

These theories differ from the orientifold theories in three relevant features. First of all, compactifications of type II theories preserve an extended amount of supersymmetry in the closed string sector. Secondly, type II theories do not need D-branes for RR charge cancellation. If D-branes are introduced, a suitable amount of anti-D-branes is necessary for charge cancellation. Thirdly, in orientifold theories also the D-brane configurations have to be invariant under the projections. This leads to the existence of mirror images under the orientifold action which in turn restricts the total number of fermion generations to be even in ordinary compactifications on rectangular tori. This problem does not arise when considering the T-dual of a theory with a discrete NSNS background flux. The tilted tori allow for an odd number of generations, and in [24] the first example of a three generation model in four dimensions was given. In [71, 69] a three generation model which has exactly the gauge group $SU(3) \times SU(2) \times U(1)$ was found based on purely toroidal compactifications. This kind of construction contains a huge amount of free parameters, among others the numbers of identical D-branes and their wrapping numbers along all six compact directions which are only fixed by four RR tadpole conditions and the requirement of obtaining three generations. Therefore, it is relatively easy to engineer models with a standard model like chiral sector. However, the closed string sector as well as the gauge sectors of toroidal orientifolds preserve $\mathcal{N} = 4$ supersymmetry. Partial supersymmetry breaking in the closed string and gauge sectors can be achieved by orbifold compactifications. In [48] we pursued this ansatz for the special case of four dimensional orbifolds plus an additional two torus. The RR charge cancellation conditions in this class of models are far more restrictive than the toroidal ones. In [27] further non-supersymmetric chiral orientifold models with D6-branes and additional orbifold symmetries were examined. Another challenge of non-supersymmetric models, namely the issue of stability, was first addressed in [100] for the purely toroidal compactifications, and in [27, 26] it was proven that all non-supersymmetric theories with D6-branes at angles, including those where some moduli are frozen by an orbifold symmetry, suffer from a dilaton tadpole. One possible way out of this dilemma is the construction of supersymmetry preserving chiral type II orientifolds with D6-branes at angles [35, 33, 34]. For a very special choice of the orbifold symmetry, it is possible to select the non-trivial angles of D6-branes such that $\mathcal{N}=1$ supersymmetry is preserved. Further toroidal orientifold models with some locally preserved supersymmetries at D6-brane intersections [30, 29] or a Pati-Salam GUT group [79] have also been analyzed recently.

In the case of broken supersymmetry, this class of models is, however, not suitable to solve the mass hierarchy problem concerning the electroweak and the Planck scale since D6-branes at angles to not allow for large volume compactifications. Only a 'modest hierarchy problem' which relates the weak scale and the string scale in the TeV range can be explained in such models [30].

A more appropriate ansatz to handle the mass hierarchy problem is by considering orientifold models with lower dimensional intersecting D-branes with common transversal directions. I presented the first of such D4-brane models in [64] in the T-dual disguise of intersecting D8-branes with four common longitudinal compact dimensions. In [77] chiral spectra of models with intersecting D4- and D5-branes in oriented and unoriented theories were briefly discussed without, however, solving the problem of the closed string tachyonic modes arising in D5-brane models. In [65] I extended the discussion of D8-brane models to give some three generation models and discuss the stability.

The thesis is organized as follows.

Chapter 1 reviews the basic ingredients of orientifold constructions with D-branes at angles.

In chapter 2, D6-brane models on four dimensional orbifolds times an additional two torus are presented where the D6-branes intersect non-trivially on this two torus. The tadpole cancellation conditions and generic chiral spectra are computed. The generalized Green-Schwarz mechanism needed for $U(1)$ anomaly cancellation is commented on, and finally two examples are presented.

In chapter 3, models with D8-branes are considered. Tadpole and anomaly cancellation are inspected and the chiral spectrum is computed. The problem of stability of non-supersymmetric models is discussed in terms of NSNS tadpoles.

Four examples are given, and phenomenological implications are discussed.

A summary and conclusions are given in chapter 4. Technical details of the calculations are collected in the appendices A to G.

This thesis is based on

- [48]: S. Förste, G. Honecker and R. Schreyer, *Non-supersymmetric orientifolds with D-branes at angles*, JHEP **06** 2001, 004, `hep-th/0105208`,
- [65]: G. Honecker, *Intersecting brane world models from D8-branes on* $(T^2 \times T^4/\mathbb{Z}_3)/\Omega\mathcal{R}_1$ *type IIA orientifolds*, JHEP **01** 2002, 025, `hep-th/0201037`.

Chapter 1 collects basic ingredients of orientifold constructions and D-branes at angles relevant for the following chapters. Chapter 2 is based on [48] and chapter 3 on [65].

Chapter 1

Concept of D-branes at angles

1.1 Configuration in type II theories

1.1.1 Strings in constant backgrounds

Type II superstring theories are consistently defined in ten spacetime dimensions. The closed string is described by bosonic coordinates $X^\mu(\tau,\sigma)$ and their fermionic superpartners $\Psi^\mu(\tau,\sigma)$ with the spacetime index $\mu = 0\dots 9$. τ is the time-like parameter on the two dimensional worldsheet and $\sigma \in [0,2\pi)$ is the periodic space-like worldsheet parameter. Open strings can be introduced into the theory by imposing boundary conditions on $X^\mu(\tau,\sigma)$ and $\Psi^\mu(\tau,\sigma)$ at $\sigma = 0,\pi$. The bosonic part of the sigma-model action in the NS-R-formalism with trivial metric on the worldsheet which describes the ten dimensional superstring theories is then given by

$$\mathcal{S}_{bos} = \frac{1}{4\pi\alpha'}\int_M \mathrm{d}\tau\mathrm{d}\sigma \left(G_{\mu\nu}\partial_\alpha X^\mu\partial^\alpha X^\nu + \epsilon^{\alpha\beta}B_{\mu\nu}\partial_\alpha X^\mu\partial_\beta X^\nu\right) + \frac{1}{2\pi\alpha'}\int_{\partial M}\mathrm{d}\tau A_\mu\partial_\tau X^\mu, \tag{1.1}$$

where ∂M is the boundary of the worldsheet M. The fields that appear in the action (1.1) are the background metric $G_{\mu\nu}$ and the antisymmetric tensor field $B_{\mu\nu}$ which both arise from the closed string NSNS sector, as well as the gauge potential A_μ pertaining to the electro magnetic gauge field strength $F_{\mu\nu}$ localized at the boundary ∂M.

The solution to the two dimensional equation of motion in the closed string sector is given by equation (A.1) in appendix A together with the mode expansion of the left- and right-moving parts (A.2) and (A.3) which depend in a trivial background only on the light-cone coordinates $\sigma_\pm = \tau \pm \sigma$, respectively.

In the open string sector there exist two different kinds of boundary conditions consistent with the equations of motion and $(p+1)$ dimensional Lorentz-invariance $(0 \leqslant p \leqslant 9)$ if we restrict to the flat non-compact case and consider only trivial background fields, i.e. $B_{\mu\nu} = 0$, $G_{\mu\nu} = \eta_{\mu\nu}$ and $A_\mu = 0$. Neumann boundary conditions are then given by

$$\partial_\sigma X^\mu(\tau, \sigma = 0) = \partial_\sigma X^\mu(\tau, \sigma = \pi) = 0,$$

while Dirichlet conditions read

$$\partial_\tau X^\mu(\tau, \sigma = 0) = \partial_\tau X^\mu(\tau, \sigma = \pi) = 0.$$

These conditions are solved by the same ansatz as for the closed string sector (A.2), (A.3) if one takes into account that Neumann conditions preserve the momentum at the boundary, i.e. $p^\mu = \frac{1}{2}(p_L^\mu + p_R^\mu) = 0$, while Dirichlet conditions fix the coordinates of the boundary to lie on a hypersurface, i.e. $\frac{1}{2}(p_L^\mu - p_R^\mu) = 0$. In addition, left- and right moving raising- and lowering operators are identified via $\alpha_n^\mu + \tilde{\alpha}_{-n}^\mu = 0$ for Neumann and $\alpha_n^\mu - \tilde{\alpha}_{-n}^\mu = 0$ for Dirichlet boundary conditions. An open string with Neumann boundary conditions along p spatial coordinates defines a p dimensional hypersurface, the Dp-brane.

If we now consider type II superstring theories compactified on a two torus, e.g. along the $X^{4,5}$ directions with radii $R_{1,2}$, the left- and right moving momenta are quantized in units of n/R_i ($n \in \mathbb{Z}$, $i = 1, 2$). In addition, strings can wind around the compact directions, the corresponding winding modes being quantized in units of mR_i/α' ($m \in \mathbb{Z}$).

In the compact theory, Neumann- and Dirichlet boundary conditions along the direction X^i are exchanged under T-duality,

$$T : \begin{cases} X_L^i(\sigma_+) + X_R^i(\sigma_-) \to X_L^i(\sigma_+) - X_R^i(\sigma_-), \\ R_i \to R_i' = \frac{\alpha'}{R_i}, \end{cases} \tag{1.4}$$

which acts asymmetrically on the left- and right-moving sector.

For consistency of the space-time theory, the action (1.1) with generic background fields has to be invariant under gauge transformations of the potential,

$$\delta A_\mu = \partial_\mu \lambda, \tag{1.5}$$

which is trivially fulfilled since (1.5) only adds a total derivative to the integrand of the boundary term. In addition, the antisymmetric tensor variation

$$\delta B_{\mu\nu} = \partial_\mu \zeta_\nu - \partial_\nu \zeta_\mu \tag{1.6}$$

leaves the bulk action invariant, but adds a surface term which has to be canceled by a transformation of the open string gauge potential A_μ,

$$\delta A_\mu = -\zeta_\mu. \tag{1.7}$$

The combination $\mathcal{F}_{\mu\nu} = B_{\mu\nu} + F_{\mu\nu}$ is then the quantity which is invariant under (1.6) in combination with (1.7).

On the $X^{4,5}$ plane with $\mathcal{F}_{45} = -\mathcal{F}_{54} \neq 0$ and $G_{ij} = \delta_{ij}$, the boundary conditions are modified:

$$\left(\partial_\sigma X^4 + \mathcal{F}_{45}\partial_\tau X^5\right)(\sigma = 0, \pi) = 0, \tag{1.8}$$
$$\left(\partial_\sigma X^5 - \mathcal{F}_{45}\partial_\tau X^4\right)(\sigma = 0, \pi) = 0. \tag{1.9}$$

For a vanishing NSNS antisymmetric tensor background, $\mathcal{F}_{45} = F_{45}$ has to obey the Dirac quantization condition

$$\mathcal{F}_{45} = \frac{q}{p}\frac{\alpha'}{R_1 R_2}, \tag{1.10}$$

with $q, p \in \mathbb{Z}$ in order for the gauge field to be well defined on the two torus [8, 63]. This can be seen by choosing the gauge

$$\begin{aligned} A_4 &= a_4, \\ A_5 &= a_5 + F_{45}X^4, \end{aligned}$$

for a $U(1)$ bundle. Going once around the X^4 direction of the two torus, the gauge potential changes according to [88]

$$A_\mu(X^4 + R_1, X^5) = A_\mu(X^4, X^5) + \frac{\alpha'}{2\pi i}\left(g^{-1}\partial_\mu g\right)(X^4, X^5),$$

with the transition function $g = e^{2\pi i\theta(X^5)}$ and $\theta(X^5) = F_{45}R_1X^5/\alpha'$. In order for g to be single-valued on the overlap of two fundamental cells of the two torus, $\theta(X^5 = R_2) \in \mathbb{Z}$ is required which provides the quantization condition (1.10) for $p = 1$. By generalizing to the Abelian component of a $U(p)$ bundle over the same torus, (1.10) is precisely recovered. The generalization to a non-trivial NSNS antisymmetric tensor background is dealt with in section 1.2.

1.1.2 T-dual picture: D-branes at angles

Applying the T-duality transformation (1.4) along the X^5 direction exchanges $\partial_\tau X^5$ with $\partial_\sigma X^5$ at the boundaries of the string worldsheet, and the quantization condition on the background fluxes can be rephrased as $\mathcal{F}_{45} = \tan(\pi\varphi) \in R_2'/R_1 \cdot \mathbb{Q}$. The boundary conditions for D-branes with constant background flux (1.8), (1.9) can then be rewritten as

$$\partial_\sigma\left(\cos(\pi\varphi)X^4 + \sin(\pi\varphi)X^5\right)(\sigma = 0, \pi) = 0, \tag{1.12}$$
$$\partial_\tau\left(-\sin(\pi\varphi)X^4 + \cos(\pi\varphi)X^5\right)(\sigma = 0, \pi) = 0, \tag{1.13}$$

which describe a D-brane wrapping a 1-cycle in the $X^{4,5}$ plane at angle $\pi\varphi$ relative to the X^4 axis.

The correspondence between the pictures of D-branes at angles and D-branes with constant background fluxes can also be understood by comparing the corresponding fluctuation spectra of lower dimensional D-branes with those from the Born-Infeld actions of space filling D-branes with fluxes [63].

So far, we have only considered open strings with both endpoints on the same kind of D-brane. If the theory includes D-branes with different background fluxes or in the T-dual language D-branes at a relative angle $\pi\varphi$, then also strings with endpoints on two different kinds of D-branes appear. Let us for simplicity assume that one kind of D-branes wraps the 1-cycle along the X^4 direction on a two torus. A string which begins on this D-brane will have the boundary condition

$$\partial_\sigma X^4(\tau,0)=0, \qquad \partial_\tau X^5(\tau,0)=0.$$

If the string ends on a D-brane which is rotated by an angle $\pi\varphi$ relative to the first kind, it is subject to the conditions (1.12), (1.13) at $\sigma=\pi$. The solution to these conditions is given by

$$X^4(\tau,\sigma)=\sum_{m\in\mathbb{Z}+\varphi}\frac{1}{m}\alpha_m e^{-im\tau}\cos(m\sigma)+\sum_{n\in\mathbb{Z}-\varphi}\frac{1}{n}\tilde{\alpha}_n e^{-in\tau}\cos(n\sigma), \tag{1.15}$$

$$X^5(\tau,\sigma)=\sum_{m\in\mathbb{Z}+\varphi}\frac{1}{m}\alpha_m e^{-im\tau}\sin(m\sigma)-\sum_{n\in\mathbb{Z}-\varphi}\frac{1}{n}\tilde{\alpha}_n e^{-in\tau}\sin(n\sigma), \tag{1.16}$$

and neither windings nor momenta occur.

The argumentation can be extended to the fermionic sectors of the theory. The two dimensional Dirac equation for closed strings has the solution (A.4) with the mode expansions of the left- and right-moving parts given in (A.5) and (A.6). In contrast to the bosonic variables, periodicity in the variable σ and Lorentz invariance still allow for two different periodicity conditions on the worldsheet, namely

$$\begin{aligned}\text{Ramond:}\quad &\Psi^\mu(\tau,\sigma+2\pi)=\Psi^\mu(\tau,\sigma),\\ \text{Neveu-Schwarz:}\quad &\Psi^\mu(\tau,\sigma+2\pi)=-\Psi^\mu(\tau,\sigma),\end{aligned}$$

which lead to integer oscillator modings in the R and half-integer ones in the NS sector. One further subtlety in the fermionic sector is the occurrence of different spin structures $\eta=\pm1$ [106] which require in the open string sector the identifications

$$\begin{aligned}\text{Neumann:}\quad &\psi^\mu_r+i\eta\tilde{\psi}^\mu_{-r}=0,\\ \text{Dirichlet:}\quad &\psi^\mu_r-i\eta\tilde{\psi}^\mu_{-r}=0.\end{aligned}$$

The fermionic oscillator moding for open strings stretching between D-branes at angles changes completely analogous to the one for the bosonic coordinates. One important consequence of this change is the fact that the R sector of a string with pure Neumann or Dirichlet boundary conditions has zero modes ψ_0^μ whereas for a string stretching between D-branes at angles $\pi\varphi$, the zero mode on the corresponding two torus is replaced by creation- and annihilation operators $\psi^{i,\bar{i}}_{\pm\varphi}$ where $i, \bar{i}$ parameterize the two torus on which the intersection occurs. The appearance of zero modes in the spectrum signals a degeneracy of the groundstate. While the R-sector groundstate of an open string on a stack of D9-branes is eightfold degenerated, non-trivial angles on a two torus lead to a fourfold degenerated R-groundstate of strings with endpoints on different D-branes, and each further two torus with non-trivial angles reduces this degeneracy by a factor of two. This means that non-trivial angles [12] or in the T-dual picture background fields [8, 4] break chiral symmetry. For a generic choice of backgrounds or angles, supersymmetry is also broken and tachyonic modes appear in the spectrum. These effects will be worked out in detail in sections 2.2.1 and 3.1.2 for intersecting D6- and D8-branes, respectively.

1.2 Orientifold projections

The concept of T-duality between background fields and angles and the breakdown of chiral and supersymmetry is independent of the particular superstring theory under discussion. In type II theories, however, open strings and lower dimensional Dp-branes are not required for consistency. This is in contrast to type I superstring theory where a definite number of D-branes cancels the RR charges arising from orientifold planes. The amount and dimensionality of D-branes required for a consistent model depend on the particular orientifold group of the model. One further appealing feature of type I string theory is the reduced amount of supersymmetry rendering it potentially more interesting in view of deriving the standard model from string theory.

Type I superstring theory is obtained from the type IIB theory by gauging worldsheet parity Ω which acts on the closed string sector as follows [54]

$$\Omega : \begin{cases} X^\mu_L(\sigma_+) & \leftrightarrow \quad X^\mu_R(\sigma_-), \\ \Psi^\mu_L(\sigma_+) & \rightarrow \quad \Psi^\mu_R(\sigma_-), \\ \Psi^\mu_R(\sigma_-) & \rightarrow \quad -\Psi^\mu_L(\sigma_+). \end{cases} \tag{1.17}$$

The minus sign in the third line is required in order to obtain $\Omega\psi^\mu\tilde{\psi}^\mu\Omega^{-1} = \psi^\mu\tilde{\psi}^\mu$. Otherwise, the graviton would be projected out by the additional symmetry.

In total, the ten dimensional type IIB superstring theory contains as massless modes in the bosonic sector the metric $G_{\mu\nu}$, an antisymmetric tensor $B_{\mu\nu}$ and the dilaton Φ from the NSNS sector and a scalar χ, a two-form $B'_{\mu\nu}$ and a self-dual four-form $D_{\mu\nu\rho\sigma}$ from the RR sector. The NS-R and R-NS sectors provide two gravitini with spin $3/2$ and two dilatini with spin $1/2$ leading to $\mathcal{N} = 2$ supersymmetry in ten dimensions. Gauging worldsheet parity amounts to projecting out the modes with Ω eigenvalue -1. The remaining massless fields are the metric, dilaton and RR two form in the bosonic sector and one gravitino and dilatino in the fermionic sector since NS-R and R-NS states are identified under Ω. In the non-compact theory, the NSNS two-form $B_{\mu\nu}$ is gauge equivalent to $B_{\mu\nu} = 0$. It is completely projected out by Ω. Upon compactifying on a two torus, e.g. in the $X^{4,5}$ plane, however, the two-form is only defined up to lattice shifts such that effectively, a quantized non-vanishing discrete value $b = 1/2$ with $B_{45} = \epsilon_{45} b\alpha'/R_1 R_2$ remains possible [14, 13, 113, 3, 75] which cannot be gauge transformed into $B_{45} = 0$. Including a non-trivial background NSNS antisymmetric tensor of rank r on a higher dimensional torus reduces the rank of the gauge group arising from open string states by a factor of $2^{r/2}$.

The T-duality transformation (1.4) along one coordinate X^5 of the two torus mentioned in section 1.1.2 maps the non-trivial value of the NSNS tensor to a tilted shape of the compactification torus with trivial background fluxes [24]. This can be derived from expressing the metric and antisymmetric tensor background in terms of the Kähler and complex moduli and performing the T-duality transformation. The Kähler structure of the original rectangular two torus with discrete NSNS background flux $b = 0, 1/2$ and radii $R_{1,2}$ along $X^{4,5}$ is given by

$$T = T_1 + iT_2 = b + i\frac{R_1 R_2}{\alpha'},$$

and the complex structure is given by

$$U = U_1 + iU_2 = i\frac{R_2}{R_1}. \tag{1.19}$$

The T-duality transformation exchanges the role of Kähler and complex structure,

$$T' = -\frac{1}{U}, \qquad U' = -\frac{1}{T}.$$

The metric and the NSNS two form on a two torus are given in terms of the Kähler and complex structure,

$$G = \frac{T_2}{U_2}\begin{pmatrix} 1 & U_1 \\ U_1 & U_1^2 + U_2^2 \end{pmatrix} \overset{U_1=0}{=} \frac{T_2}{U_2}\begin{pmatrix} 1 & 0 \\ 0 & U_2^2 \end{pmatrix}, \qquad B = \frac{\alpha'}{R_1 R_2} T_1 \begin{pmatrix} 0 & 1 \\ -1 & 0 \end{pmatrix}.$$

Upon T-duality along X^5, these quantities transform into

$$G' = \frac{1}{\alpha'}\begin{pmatrix} R_1^2 + (bR_2')^2 & b(R_2')^2 \\ b(R_2')^2 & (R_2')^2 \end{pmatrix}, \qquad B' = 0,$$

which for $b = 1/2$ describe the tilted torus shown in figure 1.1.

The orientifold projection Ω of the original theory with background fluxes transforms under T-duality along i coordinates into $\Omega\mathcal{R}_i$ where $\mathcal{R}_i$ is the reflection along these i coordinates. In chapter 2 and 3 we will discuss the cases where

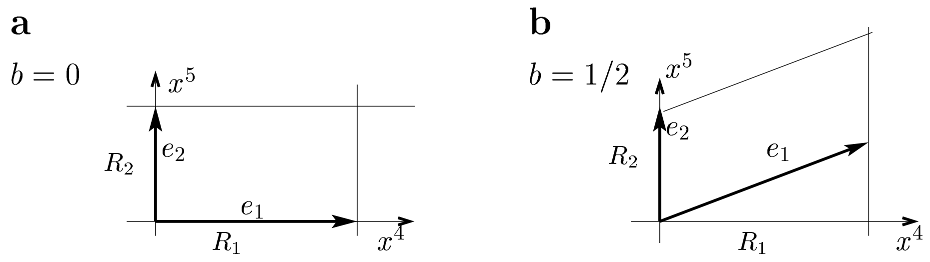

Figure 1.1: Two tori in the T-dual picture admitting D-branes at angles. The index prime on radii and basis vectors is omitted.

three and one compact coordinate, respectively, are T-dualized. In order to simplify the notation and also in view of orbifold groups discussed in section 1.3, it is convenient to introduce complex coordinates on the compact space

$$Z^1 = X^4 + iX^5, \qquad Z^2 = X^6 + iX^7, \qquad Z^3 = X^8 + iX^9. \tag{1.23}$$

In terms of these complex coordinates, the reflection $\mathcal{R}_3$ acts then as complex conjugation,

$$\mathcal{R}_3 : Z^i \to \overline{Z}^i, \qquad i = 1, 2, 3. \tag{1.24}$$

In the models discussed in chapter 3, the reflection only acts on one coordinate,

$$\mathcal{R}_1 : Z^1 \to \overline{Z}^1. \tag{1.25}$$

From the definition (1.24) it is clear that only the real axes $X^{4,6,8}$ are invariant under the orientifold projection $\Omega\mathcal{R}_3$. Similarly, according to (1.25) the real axis X^4 and the four coordinates $X^{6,7,8,9}$ are invariant under $\Omega\mathcal{R}_1$. Together with the four non compact directions, $\Omega\mathcal{R}_3$ leaves six spatial plus one time direction invariant. These are the orientifold six O6-planes. Similarly, for $\Omega\mathcal{R}_1$ one obtains O8-planes.

Consistency of the theory enforces the existence of D-branes of the same dimensionality which can be rotated by angles $\pi\varphi_j$ relative to the $\Omega\mathcal{R}_i$ invariant axes as discussed in section 1.1.2. For $\Omega\mathcal{R}_i$ to be a symmetry of the theory, also the mirror images of rotated D-branes at angles $-\pi\varphi_j$ have to exist. The details of the construction will be discussed in sections 2.1.2 and 2.1.3 in the context of D6-branes. The argumentation directly carries over to the case of intersecting D8-branes.

1.3 Orbifold groups

The ten dimensional type II superstring theories possess 32 supercharges. Torus compactifications preserve all these charges, whereas moding out the worldsheet parity Ω in combination with some target space action preserves 16 of them. Purely toroidal orientifold models thus give $\mathcal{N} = 4$ supersymmetry in four dimensions. In order to break half of the remaining supersymmetries, we incorporate an orbifold group action $\mathbb{Z}_M$ in the compactified models. The orbifold generator Θ acts as a rotation on the compact coordinates,

$$\Theta : Z^j \to e^{2\pi i v_j} Z^j. \tag{1.26}$$

A $\mathbb{Z}_M$ rotation requires $\Theta^M = \mathbb{1}$, and modular invariance of string theory requires $\sum_j v_j = 0 (\text{mod } 2)$. In the models discussed here, we restrict our attention to orbifold groups which act non-trivially only on the second and third torus. The four distinct allowed orbifolds which are listed in table 1.1 can be viewed as different singular limits of compactifying on a smooth $K3$ manifold. The

Four dimensional orbifolds	
Group	(v_2, v_3)
$\mathbb{Z}_2$	$(1/2, -1/2)$
$\mathbb{Z}_3$	$(1/3, -1/3)$
$\mathbb{Z}_4$	$(1/4, -1/4)$
$\mathbb{Z}_6$	$(1/6, -1/6)$

Table 1.1: The four orbifold limits of $K3$.

four dimensional orbifold groups listed in table 1.1 act symmetrically on left- and right-moving sectors provided that the complex conjugation does not affect these two tori. This will be the case in the models discussed in chapter 3.

If on the other hand we choose the reflection symmetry $\mathcal{R}_3$, the models are T-dual to ordinary Ω orientifolds with an asymmetric orbifold action $\hat{\Theta}$. In the complex notation (1.23), T-duality along $X^{5,7,9}$ can be rephrased as

$$T : Z_L^j + Z_R^j \to Z_L^j + \overline{Z}_R^j,$$

and the orbifold action $\hat{\Theta}$ becomes

$$\hat{\Theta} = T\Theta T^{-1} : Z_L^j + Z_R^j \to e^{2\pi i v_j} Z_L^j + e^{-2\pi i v_j} Z_R^j.$$

The T-dual picture can be used to study special classes of asymmetric orientifolds [21]. For the orbifold group $\mathbb{Z}_2$, the T-dual version acts also symmetrically, and one recovers the supersymmetric model discussed in [54]. The other six dimensional supersymmetric models of this kind have been studied in [20]. All six dimensional models are also reviewed in detail in [104].

For the heterotic theories, which are believed to be connected to open string theories by a strong/weak coupling duality, similar observations have been made in [82, 83].

Including the orbifold group $\mathbb{Z}_M$ produces additional O6-planes as can be read off from the following sequence

$$e^{-\pi i k v_j} Z^j \xrightarrow{\Theta^k} e^{\pi i k v_j} Z^j \xrightarrow{\mathcal{R}_3} e^{-\pi i k v_j} \overline{Z}^j.$$

This means that e.g. the hyperplane $(X^\mu, X^4, e^{-\pi i/3} X^6, e^{\pi i/3} X^8)$ is invariant under the combination of $\mathcal{R}_3$ with a $\mathbb{Z}_3$ rotation on the second and third torus.

1.4 RR tadpole cancellation conditions

The O-planes can be viewed as sources and drains for closed strings. The resulting tree channel interaction between two crosscaps, $\int_0^\infty \mathrm{d}l \langle C| e^{-2\pi l H} |C\rangle$, is represented by the Klein bottle amplitude diagram depicted in figure 1.2. The interaction is mediated by the bosonic closed string sectors, namely the NSNS and RR sectors. The tadpoles arising from the two different kinds of closed strings propagating in the bulk cancel each other due to supersymmetry, but in order to have a fully consistent theory, it is necessary that they also vanish separately. In the NSNS sector, this could be achieved by appropriately redefining the vacuum as suggested in [44, 45]. The procedure can, however, not be applied to the RR sector since there are conserved charges associated to the RR forms. Instead, orientifold theories contain further interactions, namely scattering of a closed string between an O-plane and a D-brane, $\int_0^\infty \mathrm{d}l \left(\langle C| e^{-2\pi l H} |B\rangle + h.c. \right)$, which has the Möbius strip as loop-channel diagram, and scattering between two D-branes, $\int_0^\infty \mathrm{d}l \langle B| e^{-2\pi l H} |B'\rangle$, represented by the cylinder at tree level. For consistency of the theory, the net RR charge of all three diagrams has to cancel. The contributions to the three diagrams can be directly calculated in the boundary state formalism [97, 50, 74], but the normalizations of boundary $|B\rangle$ and crosscap $|C\rangle$ states which determine the number of D-branes required can be more easily read off when starting from the loop channel. Furthermore, in the D8-brane models of chapter 3, the couplings of twisted closed strings to D-branes and O-planes determine the action of the orientifold and orbifold group on the Chan-Paton labels of open string states which can only be understood by starting from the loop channel. In chapter 2 we will discuss how the boundary state picture constrains the allowed compactification lattices.

The correspondence to the loop channel can be established by the two different choices of parameter ranges on the worldsheet describing the Klein bottle. The standard parameter range of a closed string is

$$0 \leqslant \sigma < 2\pi, \qquad 0 \leqslant \tau < 2\pi l. \tag{1.30}$$

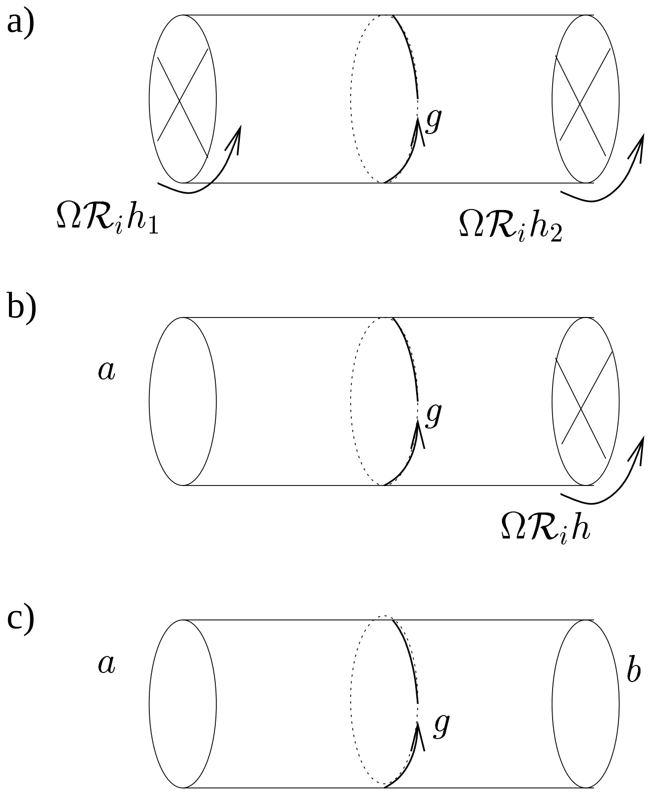

Figure 1.2: Tadpole diagrams: a) Klein bottle, b) Möbius strip, c) cylinder. $\Omega\mathcal{R}_i h_j$ denote orientifold group elements, g denotes an orbifold group element.

The Klein bottle tree channel diagram is obtained by taking a double cover, i.e. a torus with $0 \leqslant \sigma < 2\pi$, $0 \leqslant \tau < 4\pi l$, the periodic identifications $\sigma \sim \sigma + 2\pi$, $\tau \sim \tau + 4\pi l$ and a $\mathbb{Z}_2$ identification

$$(\tau, \sigma) \sim (4\pi l - \tau, \sigma + \pi).$$

The two different fundamental regions respecting these symmetries are depicted in figure 1.3. The diagram on the left hand side leads to the interpretation of a tree channel interaction, whereas the diagram on the right hand side has the interpretation of a 1-loop interaction with the closed string undergoing a twist Ω on the worldsheet. For this, the role of σ and τ have to be exchanged, and in order to obtain the standard parameter range of a closed string with $0 \leqslant \tau < 2\pi t$, a rescaling is needed which gives $t = 1/4l$. In a similar manner, by reparameterizing $t = 1/2l$, the cylinder closed string tree diagram transforms into an open string loop diagram. The Möbius strip also transforms into an open string 1-loop diagram, but this time again a double cover of the fundamental region is needed leading to the reparameterization $t = 1/8l$.

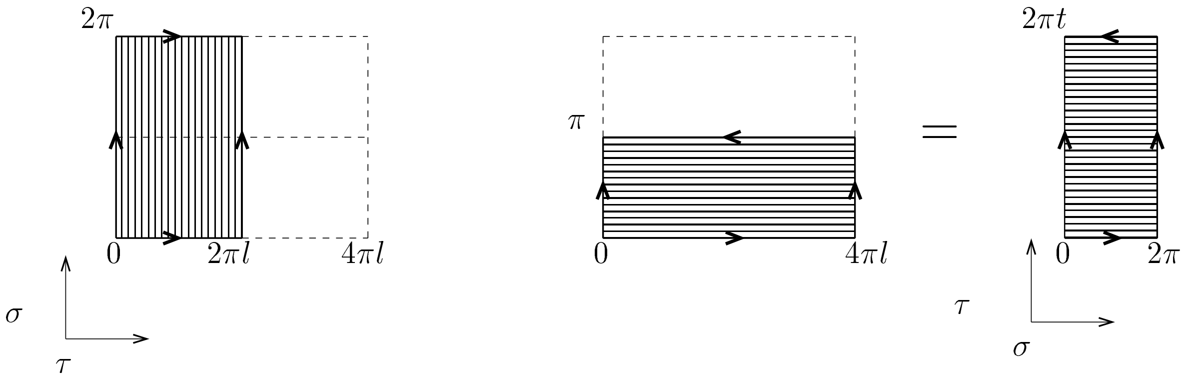

Figure 1.3: Triangulated versions of the tree channel Klein bottle diagram.

The RR charges of O-planes and D-branes can be extracted from the loop diagrams by computing the UV-limits of the following parts of the amplitudes [97]:

$$\begin{array}{rl} \text{Klein bottle:} & \text{Closed string NSNS states with } P_{orb}\Omega\mathcal{R}_i(-1)^F \text{ insertion,} \\ \text{Möbius strip:} & \text{Open string R states with } -P_{orb}\Omega\mathcal{R}_i \text{ insertion,} \\ \text{Annulus/Cylinder:} & \text{Open string NS states with } P_{orb}(-1)^F \text{ insertion,} \end{array} \tag{1.32}$$

where $P_{orb} = \left(1 + \Theta + \ldots + \Theta^{M-1}\right)/M$ projects onto states invariant under the orbifold group, F is the worldsheet fermion number and the factor $(-1)^F$ arises from the GSO projection [56] which for our models is given by (1.35) in the closed string sector, and the open string analog is obtained by restricting to e.g. the left-movers only. The minus sign in the Möbius strip takes into account the space time fermion number.

The periodicity and boundary conditions in the tree channel with the standard parameter range (1.30) on a generic bosonic worldsheet field $\phi(\tau,\sigma)$ in the g-twisted sector (see figure 1.2) are as follows [54, 37]:

$$\begin{array}{rr} \text{Klein bottle:} & \phi(0,\pi+\sigma) = \Omega\mathcal{R}_i h_1 \phi(0,\sigma), \\ & \phi(2\pi l,\pi+\sigma) = \Omega\mathcal{R}_i h_2 \phi(2\pi l,\sigma), \\ & \phi(\tau,2\pi+\sigma) = g\phi(\tau,\sigma), \\ \text{Möbius strip:} & \phi(2\pi l,\pi+\sigma) = \Omega\mathcal{R}_i h \phi(2\pi l,\sigma), \\ & \phi(\tau,2\pi+\sigma) = g\phi(\tau,\sigma). \end{array}$$

For worldsheet fermions, a phase ± 1 from the GSO projection has to be included as well [54].

For consistency of the boundary conditions, the Klein bottle has to fulfill

$$\left(\Omega\mathcal{R}_i h_1\right)^2 = \left(\Omega\mathcal{R}_i h_2\right)^2 = g^2, \tag{1.33}$$

and in the Möbius strip

$$\left(\Omega\mathcal{R}_i h\right)^2 = g^2 \tag{1.34}$$

is required. The orbifold group element g denotes the twist sector of the closed string propagating in the tree channel. Due to the choice of the orientifold group $\{\Omega\mathcal{R}_3\Theta^k\}$, only untwisted closed strings couple to the O6-planes and D6-branes in the models discussed in chapter 2, even though twisted closed string sectors exist. This is in contrast to the D8-brane models discussed in chapter 3 where all twist sectors couple to the O8-planes and D8-branes.

1.5 Low energy spectra

The physical states are given by those string excitations which are invariant under the orbifold and orientifold action and the GSO projection.

1.5.1 Closed sector

The GSO projection in the explicit examples in chapter 2 and 3 is chosen to be

$$P_{GSO} = \frac{1+(-1)^F}{2}\frac{1-(-1)^{\tilde{F}}}{2}, \tag{1.35}$$

where F and $\tilde{F}$ are left- and right-moving worldsheet fermion numbers, respectively.

The NSNS sector groundstate is odd under $(-1)^F$ and even under $(-1)^{\tilde{F}}$ and thus projected out. The reflection $\mathcal{R}_i$ does not affect the non-compact coordinates. Defining creation- and annihilation operators with complex indices as in equation (A.7), we obtain the action of the orientifold group on bosonic oscillators given in equation (A.10). The action on the fermionic sector can be easily read off from this bearing in mind the minus sign of (1.17). The orbifold group acts on the oscillators as defined in equation (1.26) with the mode expansion (A.2), (A.3) inserted. The graviton and dilaton are massless model independent states. They are represented by

$$\left(\psi^\mu_{-1/2}\tilde{\psi}^\nu_{-1/2} + \psi^\nu_{-1/2}\tilde{\psi}^\mu_{-1/2}\right)|0\rangle_{NSNS}. \tag{1.36}$$

In addition, model dependent vectors and scalars arise. The GSO projection consistent with $\Omega\mathcal{R}_3$ in the RR sector is given by ($s_i = \pm 1/2$)

$$\begin{aligned}(-1)^F|s_0,s_1,s_2,s_3\rangle &= -e^{\pi i(s_0-s_1-s_2-s_3)}|s_0,s_1,s_2,s_3\rangle, & (1.37)\\ (-1)^{\tilde{F}}|s_0,s_1,s_2,s_3\rangle &= e^{\pi i(s_0+s_1+s_2+s_3)}|s_0,s_1,s_2,s_3\rangle, & (1.38)\end{aligned}$$

while for $\Omega\mathcal{R}_1$, the GSO projection onto the left moving sector is replaced by

$$(-1)^F|s_0,s_1,s_2,s_3\rangle = -e^{\pi i(s_0-s_1+s_2+s_3)}|s_0,s_1,s_2,s_3\rangle. \tag{1.39}$$

The action of the orbifold and orientifold group on the RR sector is given by

$$\begin{aligned}
\Theta : |s_0, s_1, s_2, s_3\rangle &\rightarrow e^{2\pi i \vec{v}\cdot\vec{s}} |s_0, s_1, s_2, s_3\rangle, \\
\mathcal{R}_3 : |s_0, s_1, s_2, s_3\rangle &\rightarrow |s_0, -s_1, -s_2, -s_3\rangle, \\
\mathcal{R}_1 : |s_0, s_1, s_2, s_3\rangle &\rightarrow |s_0, -s_1, s_2, s_3\rangle,
\end{aligned}$$

with $\vec{v}$ listed in table 1.1 for the different four dimensional orbifold groups.

In the Θ^n-twisted sectors, the masses are given by

$$\frac{\alpha'}{4} m^2_{L,R} = N_{L,R} + \frac{1}{2} q^2_{L,R} + E_{vac} - \frac{1}{2}, \tag{1.40}$$

with the state represented by

$$q_{L,R} = \begin{cases} (0, 0, \pm n v_2, \pm n v_3) & \text{NS}, \\ (\frac{1}{2}, \frac{1}{2}, \frac{1}{2} \pm n v_2, \frac{1}{2} \pm n v_3) & \text{R}, \end{cases} \tag{1.41}$$

the oscillator number $N_{L,R}$ and

$$E_{vac} = \frac{1}{2} \sum_{j=2,3} |n v_j| (1 - |n v_j|), \tag{1.42}$$

where $0 \leqslant |n v_j| < 1$ is required. In the models with D6-branes, the orientifold group action $\Omega\mathcal{R}_3$ preserves the twist sector, whereas in the D8-brane models $\Omega\mathcal{R}_1$ exchanges the Θ^n and the Θ^{-n} twisted sectors.

The NS-R sectors are mapped to the R-NS sectors under the orientifold projection. Thus, the fermionic superpartners of the NSNS and RR sectors are provided by an invariant superposition of NS-R and R-NS states.

1.5.2 Open sector

The open string groundstates for strings with both ends on the same type of D-branes can be treated in the same way as one sector, e.g. the left moving one, of the closed string.

In addition, strings between D_a- and D_b-branes at angles appear. If the non-trivial angles $\pi\varphi_i$ appear only in the second and third torus with $(\pi\varphi_2, \pi\varphi_3) = \pm\pi n(v_2, v_3)$, the whole discussion of the previous section carries over. The oscillator moding is then the same as for twisted closed strings and one can therefore speak of 'twisted open string sectors'.

If on the other hand the D-branes intersect on the first torus at an angle $\pi\varphi$, equations (1.41), (1.42) have to be modified as follows,

$$q^{(\varphi)}_{L,R} = q_{L,R} + (0, \varphi, 0, 0), \tag{1.43}$$

$$E^{(\varphi)}_{vac} = E_{vac} + \frac{1}{2} |\varphi| (1 - |\varphi|). \tag{1.44}$$

The representation of open D_a-D_b string states under the gauge group is determined by regarding the orbifold and orientifold group action,

$$\begin{aligned}
\Omega\mathcal{R}_i\Theta^k : |\psi, mn\rangle\lambda^{(a,b)}_{nm} &\rightarrow |\Omega\mathcal{R}_i\Theta^k\cdot\psi, mn\rangle\left(\gamma^{(b)}_{\Omega\mathcal{R}_ik}\lambda\gamma^{(a)-1}_{\Omega\mathcal{R}_ik}\right)^T_{nm}, && (1.45)\\
\Theta^k : |\psi, mn\rangle\lambda^{(a,b)}_{nm} &\rightarrow |\Theta^k\cdot\psi, mn\rangle\left(\gamma^{(b)}_k\lambda\gamma^{(a)-1}_k\right)_{nm}, && (1.46)
\end{aligned}$$

where the γ matrices acting on the Chan-Paton labels $\lambda^{(a,b)}$ are determined by the tadpole cancellation conditions and the requirement that they form a projective representation of the orientifold group [54].

For example, applying two orientifold group elements one obtains

$$\left(\Omega\mathcal{R}_i\Theta^k\right)\left(\Omega\mathcal{R}_i\Theta^{k'}\right) : |\psi, mn\rangle\lambda^{(a,b)}_{nm} \rightarrow |\Theta^l\cdot\psi, mn\rangle\left(\gamma^{(b')-T}_{\Omega\mathcal{R}_ik}\gamma^{(b)}_{\Omega\mathcal{R}_ik'}\lambda\gamma^{(a)-1}_{\Omega\mathcal{R}_ik'}\gamma^{(a')}_{\Omega\mathcal{R}_ik}\right)_{nm}, \quad (1.47)$$

with $l = k' - k$ for $\Omega\mathcal{R}_3$ and $l = k + k'$ for $\Omega\mathcal{R}_1$. $D_{a'}$ is the $\mathcal{R}_i$ image brane of D_a. Comparing (1.47) with (1.46) leads to $\gamma^{(a)}_l \simeq \gamma^{(a')-T}_{\Omega\mathcal{R}_ik}\gamma^{(a)}_{\Omega\mathcal{R}_ik'}$ up to a phase.

If the orbifold or orientifold action is a symmetry of the D-brane configuration, i.e. it only acts as a phase on the corresponding mass eigenstates ψ, the representations of the Chan-Paton labels $\lambda^{(a,b)}$ are obtained from

$$\begin{aligned}
\lambda^{(a,b)} &= \rho_k(\psi)\left(\gamma^{(b)}_{\Omega\mathcal{R}_ik}\lambda\gamma^{(a)-1}_{\Omega\mathcal{R}_ik}\right)^T,\\
\lambda^{(a,b)} &= \tilde{\rho}_k(\psi)\gamma^{(b)}_k\lambda\gamma^{(a)-1}_k,
\end{aligned}$$

where $\rho_k(\psi), \tilde{\rho}_k(\psi) \in \mathbb{C}$ are the phases obtained from the action of the orientifold $\Omega\mathcal{R}_i\Theta^k$ and orbifold Θ^k generator on the state ψ, respectively.

For all models discussed in this thesis, $\Omega\mathcal{R}_i\Theta^k$ is a symmetry of D_a-$D_{a'}$ strings at $\mathcal{R}_i$ invariant intersections as well as D_c-D_c strings if the stack of D_c-branes is located on top of an O-plane. The gauge group supported by such D_c-branes is therefore only a subgroup of $U(N_c)$. Furthermore, in chapter 2, a $\Theta^{M/2}$ rotation for M even preserves the D6-brane configurations whereas in chapter 3, each Θ rotation leaves the D8-brane positions invariant. The corresponding low energy spectra are discussed in detail in section 2.3 for intersecting D6-branes and in section 3.1.2 for D8-branes at angles.

Chapter 2

Orientifold models with intersecting D6-branes

In this chapter, we present four dimensional orientifold compactifications of type IIA superstring theory where we combine the worldsheet parity operator Ω with a reflection $\mathcal{R}_3$ of half of the internal coordinates. In addition, we include the four dimensional orbifold groups listed in table 1.1. On the one two torus which is not affected by the orbifold projection, we allow for non-trivial angles of the D6-branes which support chiral fermions at the intersection points. The maximal rank of the gauge groups depends on the orbifold group under consideration. These models have been studied in [48].

2.1 Amplitudes and RR tadpole cancellation

Cancellation of RR tadpoles gives constraints on the allowed number of identical D6-branes and on the projection of the wrapped 1-cycles on the two torus onto the $\Omega\mathcal{R}_3$ invariant plane.

The orientifold projection $\Omega\mathcal{R}_3$ acts as defined in section 1.2 and appendix A, equation (A.10), on the oscillators. In addition, the orbifold groups of section 1.3 are moded out. At first, the Klein bottle amplitude is computed which gives an RR tadpole. In section 2.1.2 and 2.1.3, the open string loop amplitudes needed for RR charge conservation are successively computed. The strategy of determining the RR tadpoles consists of computing the loop channel expression of each amplitude, then reparameterizing the worldsheet as explained in section 1.4 and extracting the infrared divergent limit $l \to \infty$. Imposing tadpole cancellation amounts to summing over the contributions from the three contributing 1-loop amplitudes and solving a quadratic equation.

The normalizations of boundary and crosscap states are obtained by matching the direct tree channel calculation with the modular transformations of the loop channel amplitudes. Imposing worldsheet duality in this class of models results in selecting out special orbifold lattices.

2.1.1 The Klein bottle amplitude

The loop channel expression of the Klein bottle amplitude is given by

$$\mathcal{K} = 4c \int_0^\infty \frac{\mathrm{d}t}{t^3} \mathrm{Tr}_{closed}^{U+T} \left(\frac{\Omega \mathcal{R}_3}{2} P_{orb} P_{GSO} \left(-1\right)^{\mathbf{S}} e^{-2\pi t H} \right), \tag{2.1}$$

where $c = V_4 / \left(8\pi\alpha'\right)^2$ is a constant factor appearing in all three loop amplitudes, V_4 is the regularized volume of non-compact momentum space,

$$P_{orb} = \frac{1 + \Theta + \cdots + \Theta^{M-1}}{M} \tag{2.2}$$

is the orbifold projector, P_{GSO} is as defined in (1.35) with $(-1)^F$ and $(-1)^{\tilde{F}}$ given by (1.37) and (1.38), respectively, and $\mathbf{S}$ denotes the space time fermion number. The Hamiltonian H is displayed in (A.11) with mode expansion (A.12). The trace includes a sum over all lattice and oscillator contributions from untwisted and twisted sectors. The tree channel RR exchange arises from the part of the total loop channel Klein bottle amplitude (2.1) listed in (1.32).

In the following, we will discuss separately the first torus on which the orbifold group acts trivially and then the second and third torus on which the rotation acts.

In this chapter we mainly focus on the case of a trivial antisymmetric NSNS tensor background in the T-dual picture. The generalization to a non-vanishing background $b = 1/2$ on the first two torus is straightforward and will be used in chapter 3.

Lattice contributions on T^2

The torus lattice which is not subject to the orbifold projection can have the two different $\Omega\mathcal{R}_3$ invariant shapes displayed in figure 1.1 corresponding to a vanishing or non-trivial antisymmetric NSNS tensor background in the T-dual picture with D9-branes. In this chapter, we use the terminology introduced in section 1.2 of lattice orientations **a** and **b** relative to the O6-plane in the picture of D6-branes at angles if not stated otherwise.

Untwisted closed strings can have Kaluza-Klein momenta which lie in the dual lattice,

$$P = m_1 \vec{e}_1^{\,*} + m_2 \vec{e}_2^{\,*}, \tag{2.3}$$

and winding modes in the lattice,

$$\alpha' W = n_1 \vec{e}_1 + n_2 \vec{e}_2, \tag{2.4}$$

where $m_i, n_i \in \mathbb{Z}$ and the $\vec{e}_i$ ($\vec{e}_i^*$) are the basis vectors of the (dual) torus lattice. Only states invariant under the orientifold group $\Omega\mathcal{R}_3$ contribute to the Klein bottle amplitude. Kaluza-Klein momenta P are left invariant by the orientation reversal on the worldsheet, $\Omega P \Omega^{-1} = P$, while the winding directions of the string are reversed, $\Omega W \Omega^{-1} = -W$. The reflection $\mathcal{R}_3$ maps momenta and windings onto their complex conjugates on the two torus. Combining the orientation reversal on the worldsheet with the reflection, the lattice contributions to the Klein bottle amplitude in the tree channel transform as follows,

$$\begin{aligned} (\Omega\mathcal{R}_3) P^{1,\bar{1}} (\Omega\mathcal{R}_3)^{-1} &= P^{\bar{1},1}, \\ (\Omega\mathcal{R}_3) W^{1,\bar{1}} (\Omega\mathcal{R}_3)^{-1} &= -W^{\bar{1},1}. \end{aligned}$$

Only $\Omega\mathcal{R}_3$ invariant Kaluza-Klein modes contribute. Therefore, only Kaluza-Klein momenta along the direction of the O6-plane and windings perpendicular to the same contribute on the first two torus. For the **a** type lattice, the contributions to the trace are of the form

$$\frac{1}{4}\left(p_L^2 + p_R^2\right) = \frac{\alpha'}{2}(P^4)^2 + \frac{1}{2\alpha'}(W^5)^2 = \frac{\alpha'}{2}\frac{m^2}{R_1^2} + \frac{1}{2\alpha'}n^2 R_2^2,$$

where R_1, R_2 are the radii of the two torus as defined in figure 1.1.

By summing over all allowed momenta and windings $m, n \in \mathbb{Z}$, the lattice contributions can be cast into a general expression of the form

$$\mathcal{L}^{R_1,R_2}[\alpha,\beta](t) \equiv \left(\sum_{m\in\mathbb{Z}} e^{-\alpha\pi t m^2/\rho_1}\right)\left(\sum_{n\in\mathbb{Z}} e^{-\beta\pi t n^2 \rho_2}\right)$$

with $\rho_i = R_i^2/\alpha'$. The corresponding expressions for the Klein bottle amplitude for both lattice orientations **a** and **b** representing the background $b = 0, 1/2$, respectively, in the T-dual picture are listed in table B.1.

Lattice contributions on $T^4/\mathbb{Z}_M$

Lattice contributions on the orbifold only appear in the untwisted sector. The compactification lattice has to be chosen such that it remains invariant under the orbifold generator Θ. For $\mathbb{Z}_2$ and $\mathbb{Z}_4$, the $SU(2)^2$ lattice is mapped onto itself under a rotation by $e^{\pi i/2}$. The two lattice orientations **A** and **B** consistent with the reflection symmetry $\mathcal{R}_3$ are shown in figure 2.1. In fact, the $\mathbb{Z}_2$ symmetry also preserves rectangular **a** type lattices with $R_1 \neq R_2$ and the **b** type lattice with apex angle $2\alpha \neq \pi/2$ (see figure 1.1 for the definition of the lattice orientations and figure B.1 for the definition of α). The tadpole cancellation conditions are, however, independent of the variables R_1, R_2 and α. For simplicity, we utilize the quadratic lattices.

If the orbifold group is chosen to be $\mathbb{Z}_3$ or $\mathbb{Z}_6$, the $SU(3)$ lattices depicted in figure 2.2 are consistent with rotational and $\mathcal{R}_3$ symmetry. For the part of the

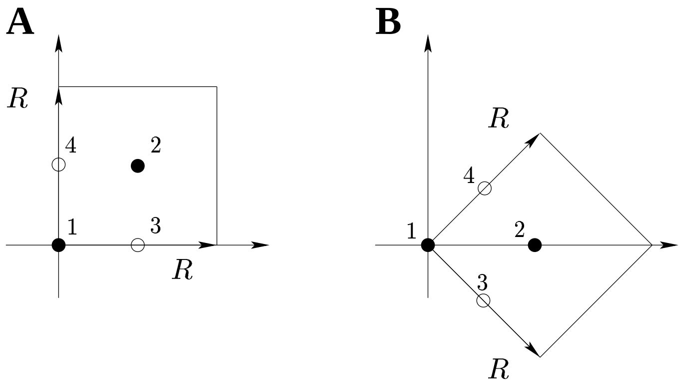

Figure 2.1: Solid circles denote $\mathbb{Z}_4$ fixed points, empty circles the additional $\mathbb{Z}_2$ fixed points which are exchanged under a $\mathbb{Z}_4$ rotation. For the **A** lattice, all fixed points are $\mathcal{R}_3$ invariant. For the **B** lattice, the $\mathbb{Z}_2$ fixed points 3 and 4 are exchanged under $\mathcal{R}_3$.

trace with trivial insertion, the lattice contributions are determined exactly in the same way as for the two torus T_1 whereas for a Θ^k insertion, the momenta and windings transform in the following way ($j = 2, 3$),

$$\begin{aligned}(\Omega\mathcal{R}_3\Theta^k)P^{j,\bar{j}}(\Omega\mathcal{R}_3\Theta^k)^{-1} &= e^{\mp 2\pi i k v_j}P^{\bar{j},j},\\ (\Omega\mathcal{R}_3\Theta^k)W^{j,\bar{j}}(\Omega\mathcal{R}_3\Theta^k)^{-1} &= -e^{\mp 2\pi i k v_j}W^{\bar{j},j}.\end{aligned}$$

This means that Kaluza-Klein momenta which are rotated by $\Theta^{-k/2}$ from the real axes and windings rotated by the same angle from the imaginary axes of the two tori $T_{2,3}$ contribute to the lattice sums. If Θ is a $\mathbb{Z}_2$ or $\mathbb{Z}_3$ rotation, $\Theta^{1/2}$ is also a symmetry of the lattice, and therefore the Kaluza-Klein and winding sums are identical to those with trivial insertion. The orbifold symmetry does not give any constraint on the choice of orientations. All possible lattice combinations **AA**, **AB** (which is equivalent to **BA**) and **BB** are allowed.

If on the other hand Θ is a $\mathbb{Z}_4$ or $\mathbb{Z}_6$ rotation, $\Theta^{1/2}$ interchanges the lattice orientations **A** and **B**. Merely the lattice **AB** gives a consistent interpretation of the Klein bottle amplitude in the tree channel. Only untwisted closed strings interact with the crosscaps, and therefore only one kind of lattice contributions on the four dimensional orbifold can appear. The **AA** and **BB** lattices lead to a linear superposition of two lattice sums which is inconsistent with worldsheet duality. This constraint is worked out in greater detail in appendix C.3.

The lattice contributions per two torus for all consistent models are listed in table B.1.

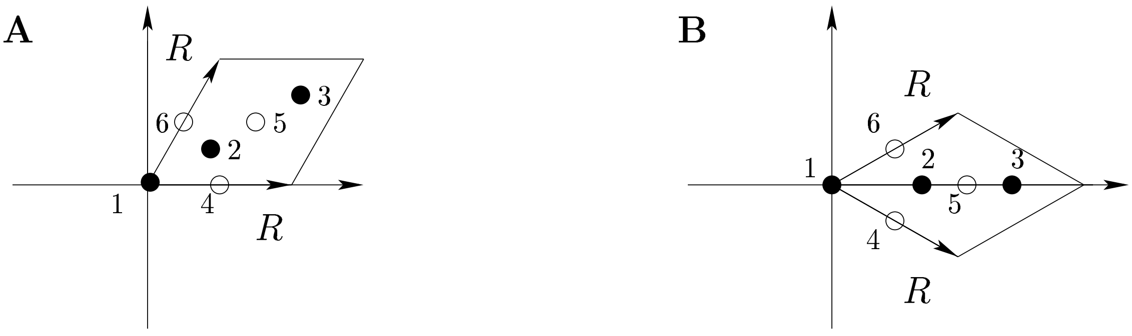

Figure 2.2: Solid circles denote $\mathbb{Z}_3$ fixed points, empty circles the $\mathbb{Z}_2$ fixed points. A $\mathbb{Z}_2$ rotation exchanges the $\mathbb{Z}_3$ fixed points 2 and 3, a $\mathbb{Z}_3$ rotation permutes the $\mathbb{Z}_2$ fixed points 4,5,6. $\mathcal{R}_3$ exchanges 5,6 in the **A** lattice and 4,6 in the **B** lattice.

The loop channel amplitude

In order to extract the RR exchange in the tree channel, only the NSNS sector with $(-1)^F$ insertion in the 1-loop channel needs to be evaluated. The non-compact directions in light-cone gauge contribute a factor $\vartheta\left[{0 \atop 1/2}\right]/\eta(2t)$ for the worldsheet fermions and $1/\eta^2(2t)$ for the worldsheet bosons. The definitions of the Dedekind eta and generalized Jacobi theta functions are given in appendix B.2. Each complex compact set of oscillators from the untwisted sector gives the same contribution. An insertion of Θ^k in the trace does not affect the oscillator part because only $\Omega\mathcal{R}_3$ invariant states $\alpha^j\tilde{\alpha}^{\bar{j}}$ and $\alpha^{\bar{j}}\tilde{\alpha}^j$ contribute and the phases cancel between left- and right-movers. Upon modular transformation, this corresponds in the tree channel to no twisted sectors coupling to the cross-caps. This result is consistent with the tree channel boundary conditions (1.33) and (1.34) which for this class of models give the twist sectors $(\Omega\mathcal{R}_3\Theta^k)^2 \equiv \mathbb{I}$.

From $(\Omega\mathcal{R}_3)\alpha_r^{j,\bar{j}}(\Omega\mathcal{R}_3)^{-1} = \tilde{\alpha}_r^{\bar{j},j}$ follows that $\Omega\mathcal{R}_3$ preserves each twist sector. Formally all twist sectors contribute to the trace, where one complex compact dimension yields the oscillator part $\vartheta\left[{nv_i \atop 1/2}\right]/\vartheta\left[{1/2+nv_i \atop 1/2}\right](2t)$ for $nv_j \neq 0$. However, the numerical result may be zero in special cases as happens for $\mathbb{Z}_2$ twist sectors.

The last ingredients needed for evaluating the trace in (2.1) are the numbers $\chi^{(n,k)}$ of Θ^n fixed points which are invariant under the insertion $\Omega\mathcal{R}_3\Theta^k$. These fixed points are displayed in figure 2.1 for $\mathbb{Z}_2$ and $\mathbb{Z}_4$ and in figure 2.2 for $\mathbb{Z}_3$ and $\mathbb{Z}_6$. Since the lattice sums and oscillator contributions are invariant under the insertions, only the total number $\chi^{(n)} = \sum_k \chi^{(n,k)}$ of Θ^n fixed points enters the computation.

In summary, the NSNS part with $(-1)^F$ insertion of the one loop Klein bottle amplitude yields

$$\mathcal{K} = c\int_0^\infty \frac{\mathrm{d}t}{t^3}\mathcal{L}_1^{\mathcal{K}}\left(\mathcal{K}^{(0)}\mathcal{L}_2^{\mathcal{K}}\mathcal{L}_3^{\mathcal{K}} + \sum_{n=1}^{M-1}\chi^{(n)}\mathcal{K}^{(n)}\right), \tag{2.7}$$

where the oscillator contributions $\mathcal{K}^{(n)}$ are given in terms of Jacobi theta functions in (B.15), $\mathcal{L}_i^{\mathcal{K}}$ denote lattice contributions arising from the i^{th} two torus listed in table B.1 and the numbers $\chi^{(n)}$ can be easily read off from figures 2.1 and 2.2.

The tree channel amplitude

The modular transformation $t = 1/4l$ leads to the RR exchange in the tree channel,

$$\tilde{\mathcal{K}} = cc_1^{\mathcal{K}}c_2^{\mathcal{K}}c_3^{\mathcal{K}}\int_0^\infty \mathrm{d}l\tilde{\mathcal{L}}_1^{\mathcal{K}}\left\{\tilde{\mathcal{L}}_2^{\mathcal{K}}\tilde{\mathcal{L}}_3^{\mathcal{K}}\tilde{\mathcal{K}}^{(0)} + 4\sum_{k=1}^{M-1}\sin^2\left(\frac{\pi k}{M}\right)\tilde{\mathcal{K}}^{(k)}\right\}, \tag{2.8}$$

where $\tilde{\mathcal{K}}^{(0)}$ and $\tilde{\mathcal{K}}^{(k)}$ are given in (B.19) and (B.20), respectively. The lattice sums $\tilde{\mathcal{L}}_i^{\mathcal{K}}$ and constants $c_i^{\mathcal{K}}$ arise from Poisson resummation of the $\mathcal{L}_i^{\mathcal{K}}$, namely $\mathcal{L}(t) = cl\tilde{\mathcal{L}}(l)$, and are listed explicitly in table B.1. The factor $4\sin^2(\pi k/M)$ reflects the fact that only $\mathbb{Z}_M$ invariant states from the closed string sector propagate in the tree channel [20]. In terms of crosscap states this can also be rephrased as the appearance of the 'complete projector' as explained in detail in appendix C.1.2, in particular formula (C.13).

The infrared limit $l \to \infty$ is obtained from the leading terms in the expansion of lattice sums and oscillator contributions. The latter can be easily read off from the product expansion of the Jacobi theta functions (B.9).

The Klein bottle amplitude can also be computed directly in the tree channel by using the boundary state approach [97, 74, 50]. The detailed calculation is given in appendices C.1 and C.3. The normalization of the crosscap state is determined via worldsheet duality to be

$$\mathcal{N}_C = \sqrt{\frac{cc_1^{\mathcal{K}}c_2^{\mathcal{K}}c_3^{\mathcal{K}}}{2M}}. \tag{2.9}$$

2.1.2 The annulus amplitude

The RR tadpole can be canceled by including open strings in the theory. One of the 1-loop amplitudes for open strings is the annulus. It is given by

$$\mathcal{A} = c\int_0^\infty \frac{\mathrm{d}t}{t^3}\mathrm{Tr}_{\mathrm{open}}\left(\frac{1}{2}P_{orb}P_{GSO}\left(-1\right)^{\mathbf{S}}e^{-2\pi tH}\right), \tag{2.10}$$

where the trace includes all possible endpoints of open strings on different D6-branes.

Lattice contributions on T^2

Let us first discuss the contributions to the one-loop amplitude from strings starting and ending on the same stack of D6-branes. Since each D6-brane wraps a 1-cycle on T_1, infinitely many parallel copies of the same stack of D6-branes have to be considered. The situation is depicted in figure 2.3. On the rectangular torus, the length L_a of the wrapped 1-cycle is determined by the wrapping numbers (n_a, m_a) along (X^4, X^5) and the corresponding radii R_1, R_2, namely $L_a = \sqrt{(n_a R_1)^2 + (m_a R_2)^2}$. The 'winding modes' are quantized in units of the distance of adjacent copies of the same D6$_a$-brane,

$$\alpha' W = \frac{s R_1 R_2}{L_a}, \tag{2.11}$$

with $s \in \mathbb{Z}$. Furthermore, strings can move along the Neumann direction of the D6$_a$-brane,

$$P = \frac{r}{L_a}, \tag{2.12}$$

with $r \in \mathbb{Z}$. The lattice contributions to the trace then appear as $\mathcal{L}^{\mathcal{A}}_{\mathbf{a}} = \sum_{r,s} e^{-2\pi t \alpha' M^2}$ with $M^2 = P^2 + (\alpha' W)^2$. The results for the **b** type lattice on T_1 can be read off from table B.1. Alternatively, the wrapping numbers along the basis vectors e_1, e_2 (see figure 1.1) on a tilted torus can be replaced with their projections onto the (X^4, X^5) directions, $(n_a, m_a + b n_a)$ with $b = 1/2$ for the tilted torus and $b = 0$ for the rectangular one.

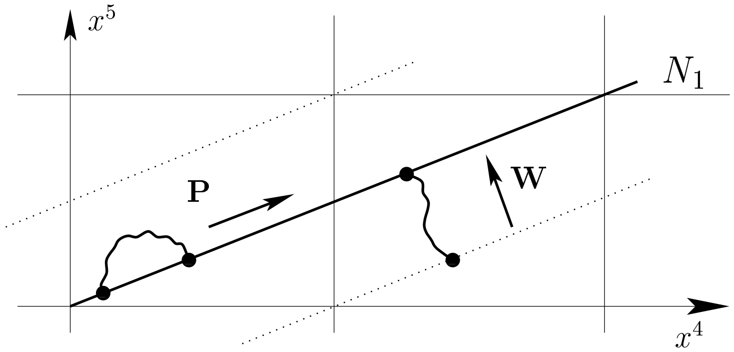

Figure 2.3: Kaluza-Klein momenta and windings from open strings with both endpoints on the same stack of D6$_1$-branes with wrapping numbers $(n_1, m_1) = (2, 1)$.

Lattice contributions on $T^4/\mathbb{Z}_M$

We restrict to the case where the D6-branes lie on top of the O6-planes along the orbifold directions. The resulting D6-brane configurations are shown in figure 2.4

for $\mathbb{Z}_2$ and $\mathbb{Z}_4$ and in figure 2.5 for $\mathbb{Z}_3$ and $\mathbb{Z}_6$ symmetries. As on T_1, momentum and winding states are quantized in units of the inverse length of the 1-cycle and the distance of parallel D6-branes on each two torus, respectively.

The loop and tree channel amplitudes

'Twisted open strings' are those strings with one endpoint located on a D6-brane which is the $\mathbb{Z}_M$ image of the other one, i.e. the position of the second D6-brane is obtained by a $\Theta^{n/2}$ rotation of the first one . The oscillators are moded in analogy with (1.15), (1.16) on $T_{2,3}$ with $\varphi = \pm n/M$. Such D6-branes can intersect multiply on the fundamental cell of the orbifold. The intersection numbers $\chi_{\mathcal{A}}^{(n)}$ can be read off from figures 2.4 and 2.5.

The 1-loop amplitude for D6$_a$-D6$_a$ strings reads

$$\mathcal{A}_{aa} = \frac{c}{4} N_a^2 \int_0^\infty \frac{\mathrm{d}t}{t^3} \mathcal{L}_1^{\mathcal{A}} \left\{ \mathcal{L}_2^{\mathcal{A}} \mathcal{L}_3^{\mathcal{A}} \mathcal{A}_{aa}^{(0,0)} + \sum_{n=1}^{M-1} \chi_{\mathcal{A}}^{(n)} \mathcal{A}_{aa}^{(n,0)} \right\}, \tag{2.13}$$

with $\mathcal{A}_{ab}^{(n,k)}$ given by (B.16) when $i\vartheta\left[{\Delta\varphi \atop 1/2}\right]/\vartheta\left[{1/2+\Delta\varphi \atop 1/2}\right](t)$ is replaced by $\vartheta\left[{0 \atop 1/2}\right]/\eta^3(t)$ for $\Delta\varphi \to 0$. The number N_a counts identical D6$_a$-branes. The square appears due to the separate counting of the endpoints $\sigma = 0, \pi$ of an open string. The lattice contributions are again collected in table B.1. In equation (2.13) we have

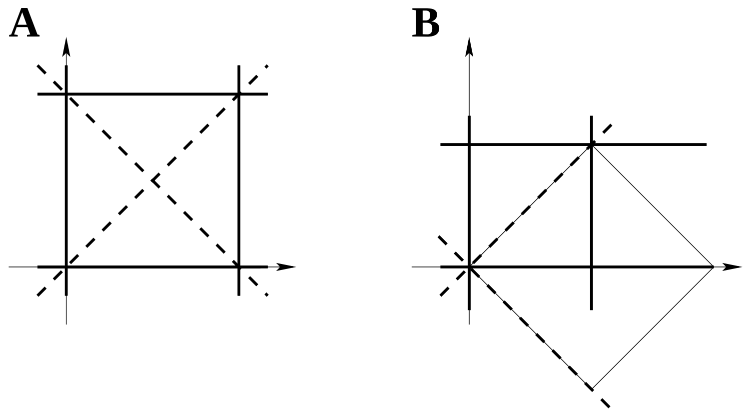

Figure 2.4: Supersymmetry preserving D6-brane configurations on T^4 for $\mathbb{Z}_2$ (solid lines) and $\mathbb{Z}_4$ (solid and dashed lines).

implicitly used the fact that the Chan-Paton representations of $\mathbb{Z}_2$ elements of the orbifold group have to be traceless as discussed below. A generic $\mathbb{Z}_M$ rotation interchanges the D6-brane positions on $T_{2,3}$. Therefore, Θ^n insertions give vanishing contributions to the annulus amplitude except for the special case of a $\mathbb{Z}_2$ rotation where D6-brane positions are mapped onto themselves. The $\mathbb{Z}_2$ rotation is accompanied by a non-trivial action on the Chan-Paton matrices

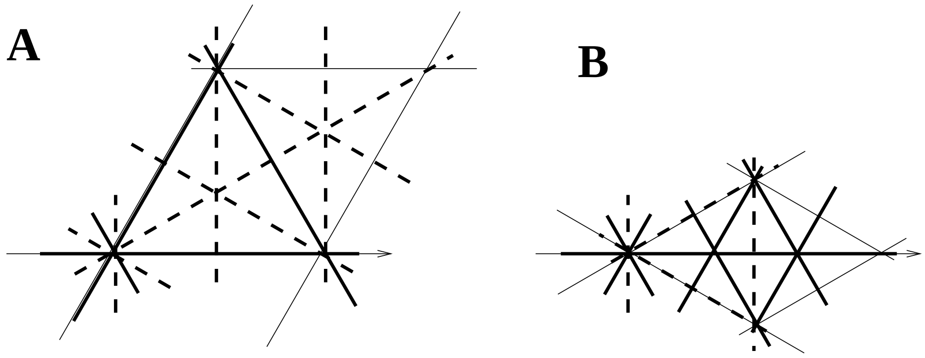

Figure 2.5: Supersymmetry preserving D6-brane configurations on T^4 for $\mathbb{Z}_3$ (solid lines) and $\mathbb{Z}_6$ (solid and dashed lines).

$\lambda^{(ab)}$ of open D6$_a$-D6$_b$ strings which provides a prefactor $\mathrm{tr}(\gamma^a_{M/2})\mathrm{tr}(\gamma^{b,-1}_{M/2})$ in the amplitude with $\Theta^{M/2}$ insertion. In order to avoid additional tadpoles from twisted closed string modes propagating in the tree channel which cannot be canceled by the Klein bottle, this prefactor has to vanish. This is exactly the condition of traceless γ matrices for $\mathbb{Z}_2$ elements, the so called 'twisted tadpole cancellation condition'.

The modular transformation $t = 1/2l$ leads to

$$\begin{aligned} \tilde{\mathcal{A}}_{aa} =& \frac{c}{2^4} N_a^2 c_1^{\mathcal{A}} c_2^{\mathcal{A}} c_3^{\mathcal{A}} \int_0^\infty \mathrm{d}l \tilde{\mathcal{L}}_1^{\mathcal{A}} \frac{\vartheta\begin{bmatrix}1/2\\0\end{bmatrix}^2}{\eta^6} \\ & \left\{ \tilde{\mathcal{L}}_2^{\mathcal{A}} \tilde{\mathcal{L}}_3^{\mathcal{A}} \frac{\vartheta\begin{bmatrix}1/2\\0\end{bmatrix}^2}{\eta^6} + 4\sum_{k=1}^{M-1} \sin^2\left(\frac{\pi k}{M}\right) \frac{\vartheta\begin{bmatrix}\frac{1}{2}\\k/M\end{bmatrix}\vartheta\begin{bmatrix}\frac{1}{2}\\-k/M\end{bmatrix}}{\vartheta\begin{bmatrix}\frac{1}{2}\\-\frac{1}{2}+k/M\end{bmatrix}\vartheta\begin{bmatrix}\frac{1}{2}\\\frac{1}{2}-k/M\end{bmatrix}} \right\}, \end{aligned} \tag{2.14}$$

where the argument of the Jacobi theta functions is $2l$. Comparing this with the result from the boundary state formalism, one obtains the normalization factor for the boundary states

$$\mathcal{N}_B = \sqrt{\frac{c c_1^{\mathcal{A}} c_2^{\mathcal{A}} c_3^{\mathcal{A}}}{2^5 M}}. \tag{2.15}$$

The details of boundary states for D6-branes are given in appendix C.2.

Having found the complete boundary and crosscap states, the calculation of the remaining amplitudes becomes a straightforward task. Open strings stretching between D6$_a$- and D6$_b$-branes at an angle $\pi\Delta\varphi$ are described by the shifted

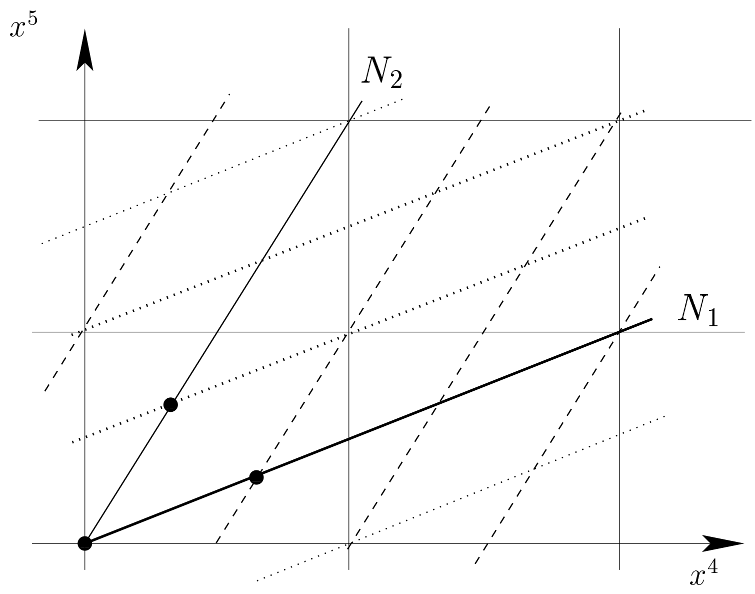

Figure 2.6: Two types of D6-branes with wrapping numbers $(n_1, m_1) = (2, 1)$ and $(n_2, m_2) = (1, 2)$ intersecting multiply on the fundamental cell of the torus.

oscillator moding $\alpha_{\mathbb{Z}+\Delta\varphi}$ according to equations (1.15), (1.16) which transforms into a phase in the tree channel. One further important ingredient is the fact that D6-branes at angles can intersect multiply on the fundamental cell of the two torus. This situation is depicted in figure 2.6. The intersection number I_{ab} is given by

$$I_{ab} = n_a m_b - m_a n_b. \tag{2.16}$$

Formally, the intersection number can take negative values. In terms of physical quantities, this means that the particles with support at the intersection locus of the D6$_a$- and D6$_b$-branes transform under the conjugate representation.

The multiplicity of intersections leads to a replication of matter which needs to be taken into account in computing the annulus amplitude in the loop channel. The tree level cylinder amplitude from strings stretched between the branes D6$_a$ and D6$_b$ intersecting at a relative angle $\pi\Delta\varphi$ reads

$$\tilde{\mathcal{A}}_{ab} = \frac{c}{2^3} N_a N_b I_{ab} c_2^{\mathcal{A}} c_3^{\mathcal{A}} \int_0^\infty \mathrm{d}l \left\{ \tilde{\mathcal{L}}_2^{\mathcal{A}} \tilde{\mathcal{L}}_3^{\mathcal{A}} \tilde{\mathcal{A}}_{ab}^{(0)} + 4 \sum_{n=1}^{M-1} \sin^2\left(\frac{\pi n}{M}\right) \tilde{\mathcal{A}}_{ab}^{(n)} \right\}, \tag{2.17}$$

with $\tilde{\mathcal{A}}_{ab}^{(0)}$ and $\tilde{\mathcal{A}}_{ab}^{(n)}$ defined in (B.21) and (B.22) respectively. The tadpole is obtained from the asymptotic behavior on the rectangular ($b = 0$) and tilted

($b = 1/2$) torus T_1,

$$\tilde{\mathcal{A}}_{ab}^{(0)} = \frac{\vartheta\begin{bmatrix}1/2\\0\end{bmatrix}^3}{\eta^9} \frac{\vartheta\begin{bmatrix}1/2\\\Delta\varphi\end{bmatrix}}{\vartheta\begin{bmatrix}1/2\\1/2+\Delta\varphi\end{bmatrix}}(2l) \stackrel{l\to\infty}{\longrightarrow} \frac{-8}{I_{ab}}\left(n_a n_b \frac{R_1}{R_2} + (m_a + bn_a)(m_b + bn_b)\frac{R_2}{R_1}\right), \tag{2.18}$$

and similarly for $\tilde{\mathcal{A}}_{ab}^{(n)}$ with the asymptotic behavior of the Jacobi theta functions belonging to the twisted oscillator contributions given by (B.10).

2.1.3 The Möbius strip amplitude

The Möbius strip amplitude in the 1-loop channel is given by the part of the total 1-loop open string amplitude with $\Omega\mathcal{R}_3$ insertion,

$$\mathcal{M} = c\int_0^\infty \frac{\mathrm{d}t}{t^3}\mathrm{Tr}_{\text{open}}\left(\frac{\Omega\mathcal{R}_3}{2}P_{orb}P_{GSO}\,(-1)^{\mathbf{S}}\,e^{-2\pi t H}\right). \tag{2.19}$$

As mentioned at the end of section 1.2, $\Omega\mathcal{R}_3$ is only a symmetry of the theory if each D6_a-brane at angle $\pi\varphi$ relative to the X^4 axis is accompanied by its mirror image under $\mathcal{R}_3$, a D$6_{a'}$-brane at angle $-\pi\varphi$. For a D6_a-brane with wrapping numbers (n_a, m_a), the mirror image D$6_{a'}$ is described by the wrapping numbers

$$(n_{a'}, m_{a'}) = (n_a, -m_a - 2bn_a), \tag{2.20}$$

where $b = 0$ and $1/2$ belong to a rectangular and tilted torus, respectively. The situation is depicted in figure 2.7 for the rectangular torus.

On $T_{2,3}$ the mirror image of a D6_a-brane rotated by $\Theta^{n/2}$ from the $\Omega\mathcal{R}_3$ invariant axis is a D$6_{a'}$-brane which is rotated by $\Theta^{-n/2}$.

The open strings which are invariant under the insertion $\Omega\mathcal{R}_3$ in the Möbius strip are those which have their endpoints on mirror D6-branes and are located at $\Omega\mathcal{R}_3$ invariant intersection points. The number of $\Omega\mathcal{R}_3$ invariant intersections on T_1 is given by

$$I_{a'a}^{\Omega\mathcal{R}_3} = 2\,(m_a + bn_a)\,. \tag{2.21}$$

The intersections on $T_{2,3}$ for $\mathbb{Z}_{2,3,4}$ are all $\Omega\mathcal{R}_3$ invariant. For $\mathbb{Z}_6$, however, one has to be more careful in counting the number of invariant intersections. For further details see figure 2.5 and the comments belonging to figure 2.2.

The contributions of the Möbius strip to the RR exchange can be calculated either from the open string R states in the 1-loop channel — with the oscillator contributions for D6-branes at non-trivial angle $\pi\varphi$ on T_1 given by (B.17) and the lattice sums for the $\Omega\mathcal{R}_3$ invariant positions listed in table B.1 — and performing a modular transformation or equivalently directly in the tree channel from

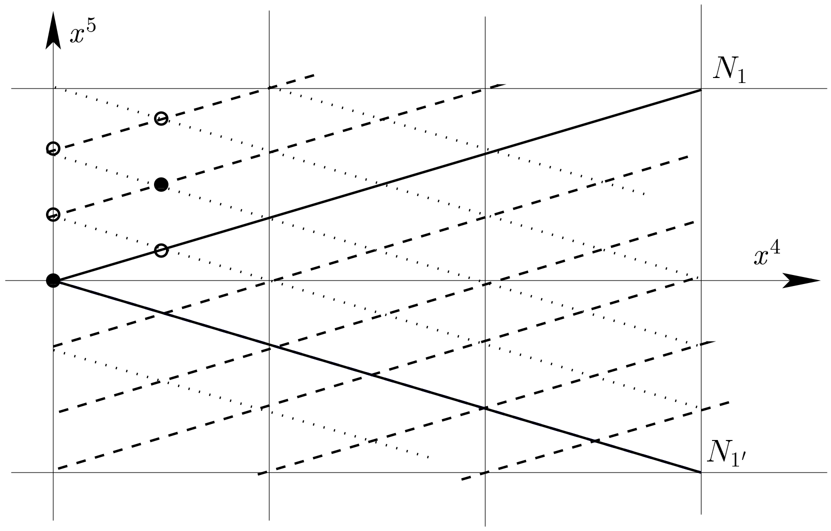

Figure 2.7: A $D6_1$-brane with $(n_1, m_1) = (3, 1)$ and its mirror image $D6_{1'}$ on a rectangular torus. Solid circles denote intersection points which are invariant under $\Omega\mathcal{R}_3$, the empty circles form pairs under $\Omega\mathcal{R}_3$.

the overlap of the corresponding boundary and crosscap states as explained in appendix C.3. For a string with both endpoints on a stack of D6-branes aligned with the X^4-axis on T_1, the RR part of the tree channel amplitude is given by

$$\tilde{\mathcal{M}}_{||} = -\frac{c}{2^4} N_a c_1^{\mathcal{M}} c_2^{\mathcal{M}} c_3^{\mathcal{M}} \int_0^\infty \mathrm{d}l \tilde{\mathcal{L}}_1^{\mathcal{M}} \frac{\vartheta\begin{bmatrix}1/2\\0\end{bmatrix}^2}{\eta^6} \times \left\{ \tilde{\mathcal{L}}_2^{\mathcal{M}} \tilde{\mathcal{L}}_3^{\mathcal{M}} \frac{\vartheta\begin{bmatrix}1/2\\0\end{bmatrix}^2}{\eta^6} + 4\sum_{n=1}^{M-1} \sin^2\left(\frac{\pi n}{M}\right) \frac{\vartheta\begin{bmatrix}1/2\\n/M\end{bmatrix}\vartheta\begin{bmatrix}1/2\\-n/M\end{bmatrix}}{\vartheta\begin{bmatrix}1/2\\-1/2+n/M\end{bmatrix}\vartheta\begin{bmatrix}1/2\\1/2-n/M\end{bmatrix}} \right\} \tag{2.22}$$

where the argument of the ϑ and η functions is $2l - \frac{i}{2}$. Similarly, we obtain the relevant contribution from a string starting on a $D6_a$-brane at angle $\pi\varphi$ with respect to the X^4-axis on T_1 and ending on its mirror image $D6_{a'}$

$$\tilde{\mathcal{M}}_a = -\frac{c}{2^2} N_a I_{a'a}^{\Omega\mathcal{R}} c_2^{\mathcal{M}} c_3^{\mathcal{M}} \int_0^\infty \mathrm{d}l \left\{ \tilde{\mathcal{L}}_2^{\mathcal{M}} \tilde{\mathcal{L}}_3^{\mathcal{M}} \tilde{\mathcal{M}}_a^{(0)} + 4\sum_{n=1}^{M-1} \sin^2\left(\frac{\pi n}{M}\right) \tilde{\mathcal{M}}_a^{(n)} \right\}, \tag{2.23}$$

where $I_{a'a}^{\Omega\mathcal{R}_3}$ is the number of $\Omega\mathcal{R}_3$-invariant intersections defined in (2.21). $\tilde{\mathcal{M}}_a^{(0)}$

and $\tilde{\mathcal{M}}_a^{(n)}$ are defined in (B.23) and (B.24), respectively.

In writing down the amplitudes, we have already used the fact that $\mathrm{tr}\left(\gamma^{a'-T}_{\Omega\mathcal{R}_3}\gamma^{a}_{\Omega\mathcal{R}_3}\right) = N_a$. This means that we can choose $\gamma^a_{\Omega\mathcal{R}_3} \equiv \mathbb{1}$ in agreement with the supersymmetric models discussed in [20, 19, 49]. Furthermore, the 'twisted tadpole cancellation condition', i.e. no tadpoles from $\mathbb{Z}_2$ insertions in the loop channel, has implicitly been used.

Finally, the tree channel 'complete projector condition' constrains the representation of the orientifold group to fulfill $\mathrm{tr}\left(\gamma^{a'-T}_{\Omega\mathcal{R}_3\frac{M}{2}}\gamma^{a}_{\Omega\mathcal{R}_3\frac{M}{2}}\right) = -N_a$ for M even.

2.1.4 Tadpole cancellation

The tadpole cancellation conditions are obtained by summing over all possible open string configurations in the annulus and Möbius strip amplitude and taking the limit $l \to \infty$. The tadpole arising from the Klein bottle amplitude is canceled provided that

$$\begin{aligned}
\mathbb{Z}_2: \quad & \sum_a N_a n_a = \begin{cases} 16 & (\mathbf{aaa}), \\ 8 & (\mathbf{aab}), \\ 4 & (\mathbf{abb}), \end{cases} \\
\mathbb{Z}_3: \quad & \sum_a N_a n_a = \ 4 \quad (\mathbf{aAA}, \mathbf{aAB}, \mathbf{aBB}), \\
\mathbb{Z}_4: \quad & \sum_a N_a n_a = \ 8 \quad (\mathbf{aAB}), \\
\mathbb{Z}_6: \quad & \sum_a N_a n_a = \ 4 \quad (\mathbf{aAB}) \ ,
\end{aligned} \tag{2.24}$$

holds. For the $\mathbf{b}$ type T_1 in the parameterization with R and α according to figure B.1, one has to replace n_a by $n_a + m_a$ so as to obtain the projection onto the $\Omega\mathcal{R}_3$ invariant axis.

If we want to include only D6-branes in the models, we are restricted to the cases $n_a > 0$ and $m_a \geq 0$. $n_a < 0$ would introduce anti-D6-branes, $m_a < 0$ labels mirror images and $n_a = 0$ corresponds to D7-branes in the T-dual type I picture. The requirement of including only D6-branes severely restricts the gauge groups. In section 2.3 we give some explicit examples.

2.2 Spectrum and anomaly cancellation

2.2.1 Spectrum

The closed string spectrum is $\mathcal{N}=2$ supersymmetric and non-chiral while the open string sector contains $\mathcal{N}=2$ supersymmetric non-chiral subsectors from strings with both endpoints on the same stack of D6-branes or $\Theta^{n/2}$ rotated ones as well as chiral non-supersymmetric subsectors from strings ending on D6-branes at angles on T_1.

Closed sector

The closed string sector consists of all states which are invariant under the orientifold projection (A.10) and the orbifold action (1.26). The untwisted sector contains the following massless states for all choices of $\mathbb{Z}_M$ ($s_i, \tilde{s}_i = \pm 1/2$):

$$
\begin{array}{lll}
\text{NSNS:} & (\psi^\mu_{-1/2}\tilde{\psi}^\nu_{-1/2} + \psi^\nu_{-1/2}\tilde{\psi}^\mu_{-1/2})|0\rangle & \text{graviton + dilaton,} \\
& (\psi^\mu_{-1/2}\tilde{\psi}^1_{-1/2} + \psi^{\overline{1}}_{-1/2}\tilde{\psi}^\mu_{-1/2})|0\rangle & \text{1 vector,} \\
& (\psi^\mu_{-1/2}\tilde{\psi}^{\overline{1}}_{-1/2} + \psi^1_{-1/2}\tilde{\psi}^\mu_{-1/2})|0\rangle & \text{1 vector,} \\
& \psi^i_{-1/2}\tilde{\psi}^{\overline{i}}_{-1/2}|0\rangle \ , \ \psi^{\overline{i}}_{-1/2}\tilde{\psi}^i_{-1/2}|0\rangle & (i=1,2,3) \text{ 6 scalars,} \\
& (\psi^1_{-1/2}\tilde{\psi}^1_{-1/2} + \psi^{\overline{1}}_{-1/2}\tilde{\psi}^{\overline{1}}_{-1/2})|0\rangle & \text{1 scalar,} \\
& (\psi^2_{-1/2}\tilde{\psi}^3_{-1/2} + \psi^{\overline{3}}_{-1/2}\tilde{\psi}^{\overline{2}}_{-1/2})|0\rangle & \text{1 scalar,} \\
& (\psi^3_{-1/2}\tilde{\psi}^2_{-1/2} + \psi^{\overline{2}}_{-1/2}\tilde{\psi}^{\overline{3}}_{-1/2})|0\rangle & \text{1 scalar,} \\
\text{RR:} & |s_0,s_1,s_2,s_3\rangle_L|\tilde{s}_0,\tilde{s}_1,\tilde{s}_2,\tilde{s}_3\rangle_R & \text{axion+ 3 scalars} \\
& \quad s_0=s_1, s_2=s_3 & + \text{ 1 vector } (H=\pm 1), \\
& \quad \tilde{s}_0=-\tilde{s}_1, \tilde{s}_2=\tilde{s}_3 & \\
& |s_0,s_1,s_2,s_3\rangle_L|\tilde{s}_0,\tilde{s}_1,\tilde{s}_2,\tilde{s}_3\rangle_R & \text{2 scalars.} \\
& \quad s_0=-s_1, s_2=-s_3 & \\
& \quad \tilde{s}_0=\tilde{s}_1, \tilde{s}_2=-\tilde{s}_3=-s_2 &
\end{array}
$$

In the RR sector, $\Omega\mathcal{R}_3$ invariant states are of the form $|s_0,s_1,s_2,s_3\rangle_L|\tilde{s}_0,\tilde{s}_1,\tilde{s}_2,\tilde{s}_3\rangle_R -$ $|\tilde{s}_0,-\tilde{s}_1,-\tilde{s}_2,-\tilde{s}_3\rangle_L|s_0,-s_1,-s_2,-s_3\rangle_R$. Only one term of the sum is listed above.

For $\mathbb{Z}_2$, additional untwisted states are invariant under the orbifold group,

$$\begin{array}{lll}
\text{NSNS:} & (\psi^2_{-1/2}\tilde{\psi}^{\overline{3}}_{-1/2} + \psi^3_{-1/2}\tilde{\psi}^{\overline{2}}_{-1/2})|0\rangle & 1 \text{ scalar,} \\
& (\psi^{\overline{2}}_{-1/2}\tilde{\psi}^{3}_{-1/2} + \psi^{\overline{3}}_{-1/2}\tilde{\psi}^{2}_{-1/2})|0\rangle & 1 \text{ scalar,} \\
& (\psi^i_{-1/2}\tilde{\psi}^{i}_{-1/2} + \psi^{\overline{i}}_{-1/2}\tilde{\psi}^{\overline{i}}_{-1/2})|0\rangle & (i=2,3)\ 2 \text{ scalars,} \\
\text{RR:} & |s_0,s_1,s_2,s_3\rangle_L|\tilde{s}_0,\tilde{s}_1,\tilde{s}_2,\tilde{s}_3\rangle_R & 2 \text{ scalars} \\
& \quad s_0=-s_1, s_2=-s_3 & +\ 1 \text{ vector } (H=\pm 1)\ . \\
& \quad \tilde{s}_0=\tilde{s}_1, \tilde{s}_2=-\tilde{s}_3=s_2 &
\end{array}$$

The strategy of computing massless states in the twisted closed sectors is explained in section 1.5.1. For example, the orbifold $\mathbb{Z}_3$ incorporates a Θ and a Θ^2 twisted sector. In the terminology of section 1.5.1, the tachyonic NSNS vacuum in the Θ twisted sector is given by

$$|0\rangle^{(\Theta)}_{NSNS} = |0,0,\tfrac{1}{3},-\tfrac{1}{3}\rangle_L|0,0,-\tfrac{1}{3},\tfrac{1}{3}\rangle_R.$$

There exist four GSO invariant massless states in the NSNS sector,

$$\psi^2_{-1/6}\tilde{\psi}^{\overline{2}}_{-1/6}|0\rangle^{(\Theta)}_{NSNS}, \qquad \psi^{\overline{3}}_{-1/6}\tilde{\psi}^{3}_{-1/6}|0\rangle^{(\Theta)}_{NSNS}, \tag{2.26}$$
$$\psi^2_{-1/6}\tilde{\psi}^{3}_{-1/6}|0\rangle^{(\Theta)}_{NSNS}, \qquad \psi^{\overline{3}}_{-1/6}\tilde{\psi}^{\overline{2}}_{-1/6}|0\rangle^{(\Theta)}_{NSNS}. \tag{2.27}$$

The $\Omega\mathcal{R}_3$ symmetry preserves the twist sector. The states in (2.26) are invariant by themselves whereas the two states in (2.27) are mapped onto each other by the orientifold symmetry. The Θ^2 twisted NSNS states are constructed correspondingly. In total, the Θ and Θ^2 twisted NSNS sectors each contribute three real scalars per $\mathbb{Z}_3$ fixed point.

In the Θ twisted RR sector, the massless GSO invariant states are fourfold degenerate due to the existence of zero modes along the non compact directions and the first two torus T_1,

$$\begin{aligned}
|0\rangle^{(\Theta,1)}_{RR} &= |\tfrac{1}{2},-\tfrac{1}{2},-\tfrac{1}{6},\tfrac{1}{6}\rangle_L|-\tfrac{1}{2},-\tfrac{1}{2},\tfrac{1}{6},-\tfrac{1}{6}\rangle_R,\\
|0\rangle^{(\Theta,2)}_{RR} &= |-\tfrac{1}{2},\tfrac{1}{2},-\tfrac{1}{6},\tfrac{1}{6}\rangle_L|\tfrac{1}{2},\tfrac{1}{2},\tfrac{1}{6},-\tfrac{1}{6}\rangle_R,\\
|0\rangle^{(\Theta,3)}_{RR} &= |\tfrac{1}{2},-\tfrac{1}{2},-\tfrac{1}{6},\tfrac{1}{6}\rangle_L|\tfrac{1}{2},\tfrac{1}{2},\tfrac{1}{6},-\tfrac{1}{6}\rangle_R,\\
|0\rangle^{(\Theta,4)}_{RR} &= |-\tfrac{1}{2},\tfrac{1}{2},-\tfrac{1}{6},\tfrac{1}{6}\rangle_L|-\tfrac{1}{2},-\tfrac{1}{2},\tfrac{1}{6},-\tfrac{1}{6}\rangle_R.
\end{aligned}$$

The states $|0\rangle^{(\Theta,1)}_{RR}$ and $|0\rangle^{(\Theta,2)}_{RR}$ provide real scalars which are identified under $\Omega\mathcal{R}_3$ while the remaining states $|0\rangle^{(\Theta,3)}_{RR}$ and $|0\rangle^{(\Theta,4)}_{RR}$ form the two helicities of a massless vector. $\Omega\mathcal{R}_3$ projects the vector out provided that the fixed point to which the state is associated transforms trivially. The Θ^2 twisted RR states are obtained along the same lines. Thus, for the **BB** type lattice, the Θ and Θ^2 twisted RR sectors each contribute one real scalar per $\mathbb{Z}_3$ fixed point. In each **A** type lattice, the two non trivial $\mathbb{Z}_3$ fixed points 2 and 3 of figure 2.2 are exchanged by the $\Omega\mathcal{R}_3$ symmetry giving rise to vectors. Again, the $\Omega\mathcal{R}_3$ invariant superposition of the NS-R and R-NS states provides the fermionic superpartners.

In $\mathbb{Z}_2$ twisted sectors, the bosonic massless GSO invariant states are given by $(s_i, \tilde{s}_i = \pm 1/2)$:

$$\begin{aligned} \text{NSNS:} \quad & |0,0,s_2,s_3\rangle_L |0,0,\tilde{s}_2,\tilde{s}_3\rangle_R, \\ & s_2 = s_3, \tilde{s}_2 = \tilde{s}_3 \\ \text{RR:} \quad & |s_0,s_1,0,0\rangle_L |\tilde{s}_0,\tilde{s}_1,0,0\rangle_R. \\ & s_0 = -s_1, \tilde{s}_0 = \tilde{s}_1 \end{aligned}$$

The exact spectrum again depends on the transformation properties of the fixed points under $\mathcal{R}_3$. The construction of the $\mathbb{Z}_4$ and $\mathbb{Z}_6$ twisted sectors goes along the same lines as the $\mathbb{Z}_3$ twisted ones.

The complete massless closed spectra for all consistent four dimensional left-right symmetric orbifolds with $\Omega\mathcal{R}_3$ projection are listed below using $\mathcal{N} = 1$ terminology. They do, however, form the $\mathcal{N} = 2$ supergravity multiplet plus $\mathcal{N} = 2$ hyper- and vectormultiplets.

Closed string spectrum for $\mathbb{Z}_2$

twist-sector	**AA**	**AB**	**BB**
untwisted	SUGRA + 11C + 4V		
Θ	32C	28C + 4V	26C + 6V

Closed spectrum of $\mathbb{Z}_3$

untwisted	SUGRA + 8C + 3V		
$\Theta + \Theta^2$	28C + 8V	30C + 6V	36C

Closed string spectrum for $\mathbb{Z}_4$

untwisted	SUGRA + 8C + 3V
$\Theta + \Theta^3$	16C
Θ^2	19C + 1V

Closed string spectrum for $\mathbb{Z}_6$

untwisted	SUGRA + 8C + 3V
$\Theta + \Theta^5$	4C
$\Theta^2 + \Theta^4$	18C + 2V
Θ^3	11C + 1V

Open sector

The open string spectrum is subdivided into two parts. Strings with both end-points on the same type of D6_a-brane provide $\mathcal{N} = 2$ non-chiral vector- and hypermultiplets and support the gauge group. Strings ending on D6_a- and D6_b-branes at angle $\pi\Delta\varphi$ on T_1 support chiral fermions and scalar pseudo-superpartners whose masses depend on the intersection angle $\pi\Delta\varphi$.

The mass formula (1.40) applied to open strings stretching between D6-branes at angle $-\frac{\pi}{2} < \pi\Delta\varphi < \frac{\pi}{2}$ on T_1 and Θ^k rotated positions on $T_{2,3}$ for the NS sector reads

$$\frac{\alpha'}{4}m^2 = N_{osc} + \frac{1}{2}(\Delta\varphi + 2\frac{k}{M} - 1), \tag{2.28}$$

with the oscillator number N^1_{osc} for a single creation operator ψ^μ given by

$$0 \leqslant N^1_{osc} \in \begin{cases} 1/2 + \mathbb{Z} & \mu = 0, \overline{0}, \\ 1/2 \mp \Delta\varphi + \mathbb{Z} & \mu = 1, \overline{1}, \\ 1/2 - k/M + \mathbb{Z} & \mu = 2, \overline{3}, \\ 1/2 + k/M + \mathbb{Z} & \mu = \overline{2}, 3. \end{cases} \tag{2.29}$$

The sector with $k = 0$ contains a tachyon $\psi^1_{\Delta\varphi-1/2}|0\rangle$ with $\frac{\alpha'}{4}m^2 = -\Delta\varphi/2$.

The lightest R sector states are massless. In table D.1, the chirality and $\mathbb{Z}_2$ eigenvalue of each groundstate are listed.

The representations under the gauge group are determined by the action of the orientifold (1.45) and orbifold group (1.46) on the Chan-Paton indices. A possible choice consistent with the tadpole cancellation conditions,

$$\begin{aligned} \mathrm{tr}\left(\gamma^{a'-T}_{\Omega\mathcal{R}_3}\gamma^a_{\Omega\mathcal{R}_3}\right) &= N_a, \\ \mathrm{tr}\gamma^a_{M/2} &= 0 \qquad \text{for } M \text{ even}, \end{aligned} \tag{2.30}$$

the property of the orbifold generator $(\Theta^{M/2})^2 = \mathbb{1}$,

$$\left(\gamma^a_{M/2}\right)^2 \simeq \mathbb{1},$$

and the constraint

$$\mathrm{tr}\left(\gamma^{a'-T}_{\Omega\mathcal{R}_3\frac{M}{2}}\gamma^a_{\Omega\mathcal{R}_3\frac{M}{2}}\right) = -N_a \tag{2.32}$$

is taken into account by

$$\gamma^a_{\Omega\mathcal{R}_3} = \mathbb{1}_{N_a}, \tag{2.33}$$

$$\gamma^a_{M/2} = \begin{pmatrix} 0 & i\mathbb{1}_{N_a/2} \\ -i\mathbb{1}_{N_a/2} & 0 \end{pmatrix}. \tag{2.34}$$

This agrees with the supersymmetric six dimensional model of [54] which is obtained from the $\mathbb{Z}_2$ model discussed here by taking the decompactification limit of the two torus T_1 in the T-dual picture with background fluxes. In the picture with D6-branes at angles this limit is given by $R_1, \frac{1}{R_2} \to \infty$.

In addition to the action on the Chan-Paton indices, the transformation properties of the mass eigenstates have to be taken into account. $\Omega\mathcal{R}_3$ maps D6$_a$-branes onto their images D6$_{a'}$. Thus, generically a D6$_a$-D6$_b$ string is mapped onto a $D6_{b'}$-$D6_{a'}$ string, and constraints on the representations arise only for $\Omega\mathcal{R}_3$ invariant configurations, namely for strings with both endpoints on $D6_a$-branes which are their own mirror image and for strings stretching between mirror branes. The largest possible gauge group obtained from a stack of N_a identical $D6_a$-branes is $U(N_a)$. If the brane position preserves some symmetry, only a subgroup appears.

A general $\mathbb{Z}_M$ rotation exchanges D6-brane positions on $T_{2,3}$. For a $\mathbb{Z}_3$ symmetry, this gives the gauge group

$$\mathbb{Z}_3: \qquad \prod_{m_a \neq 0} U(N_a) \prod_{m_a = 0} SO(N_a), \tag{2.35}$$

where $m_a = 0$ labels the position of $\Omega\mathcal{R}_3\Theta^k$ invariant D6-branes on the rectangular torus.

If the orbifold group is of even order, the $\mathbb{Z}_2$ factor preserves the positions of all D6-branes. The gauge group is reduced, $U(N_a) \xrightarrow{\mathbb{Z}_2} U(N_a/2)^2$. One further subtlety arises from the fact that in the special case of $\mathbb{Z}_3$ all D6-brane positions on $T_{2,3}$ are related by Θ^k rotations. This is not true in general. For $\mathbb{Z}_{2,4,6}$ two separate orbits occur which are displaced by a $\Theta^{1/2}$ rotation. For example in figure 2.5, when taking the orbifold symmetry $\mathbb{Z}_6$, all solid lines denote D6-branes which belong to the same orbit while all D6-branes along the dashed lines belong to the other one. The computation of RR tadpole cancellation in section 2.1.4 has been performed in terms of identical D6-branes. The gauge group before imposing symmetry constraints is therefore $U(N_a)^2$. The $\mathbb{Z}_2$ symmetry breaks the group down to $U(N_a/2)^4$, and if the stack of $D6_a$-branes with identical position on T_1 is its own mirror image under $\Omega\mathcal{R}_3$, each factor $U(N_a/2)^2$ corresponding to one orbit on $T_{2,3}$ is further reduced to $U(N_a/2)$. The resulting gauge groups are

$$\mathbb{Z}_{2,4,6}: \qquad \prod_{m_a \neq 0} U(N_a/2)^4 \prod_{m_a = 0} U(N_a/2)^2. \tag{2.36}$$

All results in this section are obtained for a rectangular torus T_1. They remain true for $D6_a$-branes on the tilted torus if one takes into account that the $\Omega\mathcal{R}_3$ invariant configuration is then given by the wrapping numbers $(n_a, m_a) = (2, -1)$ in the basis of figure 1.1. By comparison with the tadpole cancellation conditions (2.24), one can derive that the maximal rank of the gauge group is reduced by considering the tilted torus or equivalently switching on a background field b in the T-dual picture [14, 13, 113, 3, 75].

Further details of the open string spectra will be discussed in section 2.3.

2.2.2 Anomaly cancellation

The resulting spectra are free of non-Abelian gauge anomalies provided that the tadpole cancellation conditions (2.24) are fulfilled. For details see section 2.3.

The total gauge group generically contains several $U(1)$ factors arising from the decomposition $U(N) \to SU(N) \times U(1)$ and from stacks with a single D6_a-brane, i.e. $N_a = 1$. These $U(1)$ factors contribute to mixed gauge and gravitational anomalies. Only some specific linear combinations of $U(1)$ factors are anomaly free. The others should get a mass of the order of the string scale M_s by a generalized Green-Schwarz mechanism involving closed string moduli [1, 81].

In the T-dual picture of D9_a-branes with magnetic fluxes, the ten dimensional RR field C_2 and its dual C_6 have the following worldvolume couplings to the gauge fields [42, 85, 1, 71],

$$\int_{D9_a} C_6 F_a^2, \qquad \int_{D9_a} C_2 F_a^4.$$

Upon dimensional reduction, one obtains four two forms ($i \neq j \neq k \neq i$, $i, j, k = 1, 2, 3$),

$$\begin{aligned} B_2^0 &= C_2, \\ n_a^j n_a^k B_2^i &= \int_{T_j \times T_k (D9_a)} C_6, \end{aligned}$$

and their four dimensional duals

$$\begin{aligned} n_a^1 n_a^2 n_a^3 C^0 &= \int_{T_1 \times T_2 \times T_3 (D9_a)} C_6, \\ n_a^i C^i &= \int_{T_i (D9_a)} C_2, \end{aligned}$$

with $n_a^1 \equiv n_a$ depending on the specific stack of D9_a-branes and $n_a^{2,3} \equiv const.$ universal factors for the class of models under consideration where non-trivial fluxes are only implemented on T_1. The prefactors n_a^i arise from the pull-back of the RR forms on the magnetized tori T_i.

Imposing an orbifold symmetry $\mathbb{Z}_M$ on $T_{2,3}$ leaves B_2^0, B_2^1 and their four dimensional duals C^0, C^1 invariant.

The effective worldvolume couplings in the models under consideration with a rectangular T_1 are of the form

$$\begin{aligned} n_a \int_{\mathbb{R}^{1,3}} C^0 F_a^2, \qquad m_a \int_{\mathbb{R}^{1,3}} B_2^0 F_a, \\ n_a \int_{\mathbb{R}^{1,3}} C^1 F_a^2, \qquad m_a \int_{\mathbb{R}^{1,3}} B_2^1 F_a, \end{aligned} \tag{2.38}$$

where only the non-universal prefactors n_a and m_a arising from the pullback of a RR form or a gauge field on the magnetized torus, respectively, have been listed. The generalization to tilted tori is straightforward.

The anomalous $U(1)$ factors become massive due to the linear couplings to RR fields in (2.38). In [71] it was pointed out that also anomaly free $U(1)$s can have such couplings. Non-anomalous as well as anomalous $U(1)$s become massive if they couple to RR fields linearly according to (2.38). In theories with an arbitrary number of D6-branes, however, the number of massive $U(1)$ factors cannot exceed the number of RR forms involved in the Green-Schwarz mechanism.

In order to obtain phenomenologically relevant models, one has to make sure that the hypercharge does not get a mass in this way.

2.3 $\mathbb{Z}_3$ and $\mathbb{Z}_2$ models

2.3.1 The $\mathbb{Z}_3$ case

In the $\mathbb{Z}_3$ orbifold, the gauge group generated by a stack of N_a D6_a-branes with arbitrary wrapping numbers (n_a, m_a) is $U(N_a)$. For the $\Omega\mathcal{R}_3$ invariant position with $(n_a, m_a) = (1, 0)$ on the rectangular torus, the corresponding projection condition breaks the gauge group down to $SO(N_a)$.

The lattice orientations **A**, **B** can be chosen independently on $T_{2,3}$. The tadpole cancellation condition (2.24) is not affected by this choice.

Strings with endpoints on different stacks of D6_a- and D6_b-branes transform in the antifundamental of one gauge group and the fundamental of the other one, $(\overline{\mathbf{F}}_a, \mathbf{F}_b)$. The orientifold symmetry $\Omega\mathcal{R}_3$ maps a stack of D6_a-branes onto their images D$6_{a'}$ while replacing the representations by their conjugates. Therefore, a string with an endpoint on D$6_{a'}$ and the other one on D6_b transforms in the bifundamental of the gauge groups, $(\mathbf{F}_a, \mathbf{F}_b)$. The multiplicity of states is determined by the degeneracy of mass eigenstates, the intersection numbers I_{ab} on T_1 as defined in (2.16) and $I_{a'b}$ obtained from the wrapping numbers of mirror branes (2.20) and finally the intersection number χ on $T_{2,3}$ which depends on the choice of compactification lattices.

Strings with endpoints on mirror branes are subject to the $\Omega\mathcal{R}_3$ symmetry provided that the intersection point is also a $\mathcal{R}_3$ fixed point. The mass eigenstates are odd under $\Omega\mathcal{R}_3$, and inserting $\gamma^a_{\Omega\mathcal{R}_3} = \mathbb{1}_{N_a}$ in (1.45) gives states in the antisymmetric representation $(\mathbf{A}_a)$. If the intersection points are exchanged by $\Omega\mathcal{R}_3$, no projection condition emerges. $\Omega\mathcal{R}_3$ then identifies strings at different intersection points which accommodate both the antisymmetric and symmetric representation $(\mathbf{A}_a) + (\mathbf{S}_a)$.

The chiralities of fermionic states are given in table D.1. Only in the sectors with non-trivial angles on all three tori, the chiral symmetry is broken. In the case of $\mathbb{Z}_3$, two such sectors exist. This leads to an even number of copies of each representation.

The generic spectrum for the $\mathbb{Z}_3$ orbifold is listed in table 2.1. The $\Omega\mathcal{R}_3$

symmetry leads to an identification of the D6_a-D6_b and D$6_{b'}$-D$6_{a'}$ strings. The D6_b-D6_a strings provide the anti-particles for the former ones. It can be explicitly checked that the spectrum is free of non-Abelian gauge anomalies if the tadpole cancellation condition (2.24) is fulfilled. In order to do so, the following relations between the cubic Casimir operators of the fundamental, adjoint (**Adj**), symmetric and antisymmetric representation of $SU(N)$ are useful,

$$\begin{aligned} C_3(\mathbf{Adj}) &= 2NC_3(\mathbf{F}), \\ C_3(\mathbf{S}) &= (N+4)\,C_3(\mathbf{F}), \\ C_3(\mathbf{A}) &= (N-4)\,C_3(\mathbf{F}). \end{aligned} \tag{2.39}$$

Chiral fermionic spectrum for $\mathbb{Z}_3$		
	rep.	mult.
aa'	$(\mathbf{A}_a)_L$	$4m_a\chi$
aa'	$(\mathbf{A}_a)_L + (\mathbf{S}_a)_L$	$2m_a(n_a-1)\chi$
ab	$(\overline{\mathbf{F}}_a, \mathbf{F}_b)_L$	$2(n_am_b - n_bm_a)\chi$
ab'	$(\mathbf{F}_a, \mathbf{F}_b)_L$	$2(n_am_b + n_bm_a)\chi$

Table 2.1: Generic chiral spectrum for $(T^2 \times T^4/\mathbb{Z}_3)/\Omega\mathcal{R}_3$. $\chi = 1, 3, 9$ is the intersection number on $T_{2,3}$ for the lattices **AA**, **AB**, **BB**, respectively.

A $\mathbb{Z}_3$ example

As we restrict our analysis to D6_a-branes, the largest feasible gauge group which respects the tadpole condition (2.24) and yields chiral fermions is $U(3) \times U(1)$. We can split this group into $SU(3) \times U(1)^2$. Choosing the rectangular **a** torus and the wrapping numbers $(n_1, m_1) = (1, 1)$, $(n_2, m_2) = (1, 2)$, out of the two $U(1)$s the linear combination

$$Q_{nonan.} = Q_1 - \frac{3}{2}Q_2$$

is non anomalous. The D6-brane positions are depicted in figure 2.8. The remaining $U(1)$ factor should become massive by the generalized Green-Schwarz mechanism as explained in section 2.2.2. The resulting spectrum is displayed in table 2.2 for the lattice **aAA**. A different lattice on $T_{2,3}$ changes the spectrum by an overall multiplicity χ (see table 2.1).

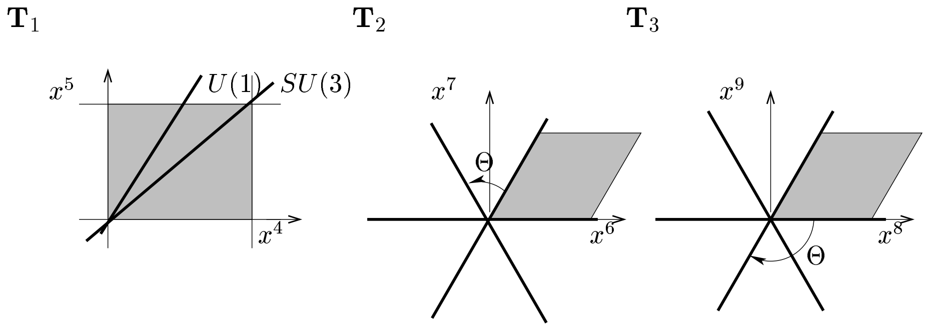

Figure 2.8: D6-brane configuration of the $(T^2 \times T^4/\mathbb{Z}_3)/\Omega\mathcal{R}_3$ example. On $T_{2,3}$ the D6-branes are evenly distributed among the three possible positions.

Chiral spectrum, Ex. 1		
	$SU(3) \times U(1)_{nonan.}$	mult.
$11'$	$(\overline{\mathbf{3}})_2$	4
12	$(\overline{\mathbf{3}})_{-5/2}$	2
$12'$	$(\mathbf{3})_{-1/2}$	6

Table 2.2: Chiral fermionic spectrum for $(T^2 \times T^4/\mathbb{Z}_3)/\Omega\mathcal{R}_3$ with $(n_1, m_1) = (1,1)$, $(n_2, m_2) = (1,2)$ and lattice **aAA**. All states are left-handed.

2.3.2 The $\mathbb{Z}_2$ case

$\mathbb{Z}_2$ models are the most simple examples for $T^4/\mathbb{Z}_M$ orbifolds where M is even. In this case, the tadpole cancellation condition depends on the choice of the orbifold lattice,

$$\sum_a \chi n_a N_a = 16, \tag{2.41}$$

where $\chi = 1, 2, 4$ is the intersection number on $T_{2,3}$ for the lattice choice **aa**, **ab**, **bb**, respectively. The breaking pattern of the gauge group is $U(N_a)^2 \xrightarrow{\mathbb{Z}_2} U(N_a/2)^2 \times U(N_a/2)^2$ $[\xrightarrow{\Omega\mathcal{R}_3} U(N_a/2)^2$ for a stack of D6-branes which are their own mirror branes] as explained in section 2.2.1 where the square arises from the existence of two orbits on $T_{2,3}$. A $\mathbb{Z}_2$ rotation maps each sector onto itself while assigning a fixed parity ± 1 to each massless state. As listed in table D.1, left-handed states are $\mathbb{Z}_2$-even and right-handed ones are $\mathbb{Z}_2$-odd in all sectors with a non-vanishing angle on T_1. Therefore, not only strings stretching between D6-branes at non-vanishing angles on all three tori contribute to the chiral spectrum but also those which merely intersect on T_1. This accounts for the fact that the intersection number χ explicitly enters the tadpole cancellation condition (2.41) in contrast to the $\mathbb{Z}_3$ models.

An alternative choice to (2.33) and (2.34) for the γ matrices consistent with the tadpole conditions (2.30) and (2.32) is given by

$$\begin{aligned}
\gamma^a_{\Omega\mathcal{R}_3} &= \begin{pmatrix} 0 & \mathbb{1}_{N_a/2} \\ \mathbb{1}_{N_a/2} & 0 \end{pmatrix}, \\
\gamma^a_{\Theta} &= \begin{pmatrix} \mathbb{1}_{N_a/2} & 0 \\ 0 & -\mathbb{1}_{N_a/2} \end{pmatrix}.
\end{aligned}$$

In this basis, the Chan-Paton labels of the gauge bosons are block-diagonal which is convenient for determining the representations of chiral fermions.

The chiral part of the open string spectrum obtained by imposing $\Omega\mathcal{R}_3$ and $\mathbb{Z}_2$ invariance is listed in table 2.3.

If the model contains an $\Omega\mathcal{R}_3$ invariant stack of D6$_c$-branes, the rank of the gauge group supported by this collection is reduced as explained above. The resulting chiral spectrum has to be modified accordingly. The relevant part is displayed in table 2.4.

The analysis of the $\mathbb{Z}_4$ and $\mathbb{Z}_6$ cases is completely analogous to the $\mathbb{Z}_2$ orbifold. There exist two independent D6-brane orbits on $T_{2,3}$ and a condition on the Chan-Paton matrices, $\mathrm{tr}\gamma_{\Theta^{M/2}} = 0$, yielding the gauge group $U(N_a/2)^4$ for given (n_a, m_a). Not only strings ending on D6-branes at non-trivial angles on all three tori provide chiral fermions, but also strings with endpoints on D6-branes of identical positions on $T_{2,3}$ contribute to the chiral spectrum since $\mathbb{Z}_2$-even and -odd states have opposite chirality. One additional subtlety enters the computation of the open spectrum in the case of $\mathbb{Z}_6$ as the intersection points of Θ and $\Theta^{3/2}$ rotated D6-branes on $T_{2,3}$ are permuted by the orbifold group. However, the tadpole conditions (2.24) already indicate that we cannot include the standard model gauge group $SU(3) \times SU(2) \times U(1)$ in $\mathbb{Z}_4$ or $\mathbb{Z}_6$ without adding anti-D6-branes. Therefore, we will not discuss these models in detail but close this chapter by giving a $\mathbb{Z}_2$ example which encloses $SU(3) \times SU(2) \times U(1)$.

Models with anti-D-branes and spatial separation of parallel D-branes corresponding to a Wilson line background in the T-dual picture will be discussed in the context of D8-brane models in chapter 3.

A $\mathbb{Z}_2$ example

If we choose not to include anti-D6-branes in our analysis, the standard model gauge group can only be enclosed for the choice $\chi = 1$ (cf. eq. (2.41)). Taking the **aaa** lattice and the minimal possible choice of three stacks of D6-branes, namely

$$\begin{aligned} N_1 &= 6, & (n_1, m_1) &= (1,1), \\ N_2 &= 4, & (n_2, m_2) &= (1,0), \\ N_3 &= 2, & (n_3, m_3) &= (4,1), \end{aligned} \tag{2.42}$$

we obtain the gauge group $SU(3)^4 \times SU(2)^2 \times U(1)^{10}$. The D6-brane positions are depicted in figure 2.9. The second stack of D6$_2$-branes is $\Omega\mathcal{R}_3$ invariant. In

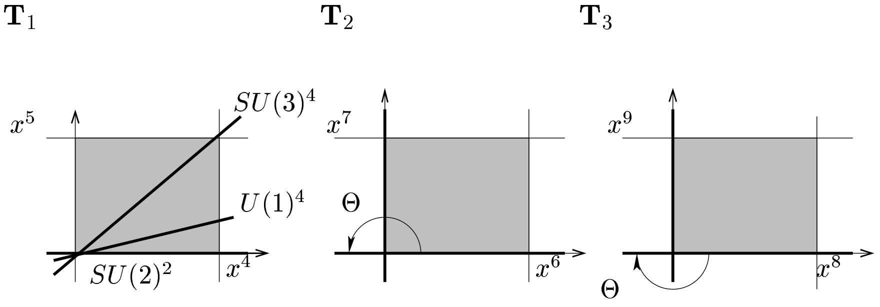

Figure 2.9: D6-brane configuration of the $\mathbb{Z}_2$ example. On $T_{2,3}$ the D6-branes with horizontal and vertical positions each accommodate the gauge group $SU(3)^2 \times SU(2) \times U(1)^5$ (before the Green-Schwarz mechanism).

this case, the tadpole condition (2.41) has to be modified,

$$\frac{N_2}{2} + \sum_{a \neq 2} n_a N_a = 16, \tag{2.43}$$

in order to avoid double counting for the strings with endpoints on the D6$_2$-branes.

This is in agreement with the fact that models containing only stacks of D6-branes with wrapping number $(n, m) = (1, 0)$ on the rectangular torus T_1 are in the decompactification limit of the T-dual two torus identical to the six dimensional supersymmetric models considered in [54] for $\mathbb{Z}_2$ and [20] for $\mathbb{Z}_3$ leading to $U(16)^2$ and $SO(8)$, respectively.

Due to the $\Omega\mathcal{R}_3$ symmetry, the sector $1'2$ provides the anti-particles for the sector 12 just as the 23 and $23'$ sectors belong together, whereas normally the sector D6$_{a'}$-D6$_{b'}$ contains the anti-particles for the sector D6$_a$-D6$_b$. Generically, since $I_{ab} + I_{a'b}$ is even, an even number of generations transforming under the same gauge factors originates from the intersections of D6$_a$ and D6$_b$-branes, half of them in the bifundamental and the other half in the antifundamental of one and the fundamental of the other gauge factor. In the model defined by (2.42), the 13 and $13'$ sectors are of this kind whereas in the sector 12, there exists a single particle in the $(\mathbf{3}_1, \mathbf{2}_2)$ of $SU(3)_1 \times SU(2)_2$. However, as the complete spectrum is symmetrically distributed among the gauge factors which are supported by a specific D6-brane configuration, the total number of $(\mathbf{3}_i, \mathbf{2}_j)$ representations of all possible $SU(3)_i \times SU(2)_j$ $(i = 1, \dots 4; j = 1, 2)$ combinations is even. The complete chiral spectrum is listed in table D.2. The model contains (at least) six non anomalous $U(1)$ factors. A possible set of linear combinations in terms of the original $U(1)$ charges Q_i $(i = 1 \dots 10)$ is given by

$$\begin{aligned}
\tilde{Q}_1 &= Q_1 + Q_2 - 3Q_7 - 3Q_8, \\
\tilde{Q}_2 &= Q_3 + Q_4 - 3Q_9 - 3Q_{10}, \\
\tilde{Q}_3 &= Q_1 - Q_2 - 3Q_5, \\
\tilde{Q}_4 &= Q_3 - Q_4 - 3Q_6, \\
\tilde{Q}_5 &= -4Q_5 + Q_7 - Q_8, \\
\tilde{Q}_6 &= -4Q_6 + Q_9 - Q_{10}.
\end{aligned} \tag{2.44}$$

The charges are also listed in table D.2. The remaining anomalous $U(1)$s are expected to become massive by the generalized Green-Schwarz mechanism.

Chiral fermionic spectrum for $\mathbb{Z}_2$		
	rep. of $U(\frac{N_a}{2})^4 \times U(\frac{N_b}{2})^4$	mult.
$aa'U$	$(\mathbf{F}_a, \mathbf{F}_a, 1, 1)_L + (1, 1, \mathbf{F}_a, \mathbf{F}_a)_L$	$4m_a n_a$
	$\underline{(\overline{\mathbf{A}}_a, 1, 1, 1)}_L$	$4m_a$
	$\underline{(\overline{\mathbf{A}}_a + \overline{\mathbf{S}}_a, 1, 1, 1)}_L$	$2m_a(n_a - 1)$
$aa'T$	$(\overline{\mathbf{F}}_a, 1, 1, \overline{\mathbf{F}}_a)_L + (1, \overline{\mathbf{F}}_a, \overline{\mathbf{F}}_a, 1)_L$	$2m_a n_a \chi$
abU	$(\mathbf{F}_a, 1, 1, 1; 1, \overline{\mathbf{F}}_b, 1, 1)_L + (1, \mathbf{F}_a, 1, 1; \overline{\mathbf{F}}_b, 1, 1, 1)_L$	$2(n_a m_b - n_b m_a)$
	$+(1, 1, \mathbf{F}_a, 1; 1, 1, 1, \overline{\mathbf{F}}_b)_L + (1, 1, 1, \mathbf{F}_a; 1, 1, \overline{\mathbf{F}}_b, 1)_L$	
	$(\overline{\mathbf{F}}_a, 1, 1, 1; \mathbf{F}_b, 1, 1, 1)_L + (1, \overline{\mathbf{F}}_a, 1, 1; 1, \mathbf{F}_b, 1, 1)_L$	$2(n_a m_b - n_b m_a)$
	$+(1, 1, \overline{\mathbf{F}}_a, 1; 1, 1, \mathbf{F}_b, 1)_L + (1, 1, 1, \overline{\mathbf{F}}_a; 1, 1, 1, \mathbf{F}_b)_L$	
$ab'U$	$(\overline{\mathbf{F}}_a, 1, 1, 1; \overline{\mathbf{F}}_b, 1, 1, 1)_L + (1, \overline{\mathbf{F}}_a, 1, 1; 1, \overline{\mathbf{F}}_b, 1, 1)_L$	$2(n_a m_b + n_b m_a)$
	$+(1, 1, \overline{\mathbf{F}}_a, 1; 1, 1, \overline{\mathbf{F}}_b, 1)_L + (1, 1, 1, \overline{\mathbf{F}}_a; 1, 1, 1, \overline{\mathbf{F}}_b)_L$	
	$(\mathbf{F}_a, 1, 1, 1; 1, \mathbf{F}_b, 1, 1)_L + (1, \mathbf{F}_a, 1, 1; \mathbf{F}_b, 1, 1, 1)_L$	$2(n_a m_b + n_b m_a)$
	$+(1, 1, \mathbf{F}_a, 1; 1, 1, 1, \mathbf{F}_b)_L + (1, 1, 1, \mathbf{F}_a; 1, 1, \mathbf{F}_b, 1)_L$	
abT	$(\mathbf{F}_a, 1, 1, 1; 1, 1, \overline{\mathbf{F}}_b, 1)_L + (1, \mathbf{F}_a, 1, 1; 1, 1, 1, \overline{\mathbf{F}}_b)_L$	$(n_a m_b - n_b m_a)\chi$
	$+(1, 1, \mathbf{F}_a, 1; \overline{\mathbf{F}}_b, 1, 1, 1,)_L + (1, 1, 1, \mathbf{F}_a; 1, \overline{\mathbf{F}}_b, 1, 1)_L$	
$ab'T$	$(\overline{\mathbf{F}}_a, 1, 1, 1; 1, 1, 1, \overline{\mathbf{F}}_b)_L + (1, \overline{\mathbf{F}}_a, 1, 1; 1, 1, \overline{\mathbf{F}}_b, 1)_L$	$(n_a m_b + n_b m_a)\chi$
	$+(1, 1, \overline{\mathbf{F}}_a, 1; 1, \overline{\mathbf{F}}_b, 1, 1,)_L + (1, 1, 1, \overline{\mathbf{F}}_a; \overline{\mathbf{F}}_b, 1, 1, 1)_L$	

Table 2.3: Generic chiral spectrum for intersecting D6-branes and $\mathbb{Z}_2$ symmetry. 'U' labels identical configurations on $T_{2,3}$, 'T' denotes D6-branes which are perpendicular on $T_{2,3}$. Permutations of entries are abbreviated by underlining.

Chiral fermionic spectrum with $\Omega\mathcal{R}_3$ invariant D6$_c$-branes		
	rep. of $U(\frac{N_c}{2})^2 \times U(\frac{N_b}{2})^4$	mult.
cbU	$(\mathbf{F}_c, 1; \overline{\mathbf{F}}_b, 1, 1, 1)_L + (1, \mathbf{F}_c; 1, 1, \overline{\mathbf{F}}_b, 1)_L$	$2m_b$
	$(\overline{\mathbf{F}}_c, 1; 1, \mathbf{F}_b, 1, 1)_L + (1, \overline{\mathbf{F}}_c; 1, 1, 1, \mathbf{F}_b)_L$	$2m_b$
	$(\overline{\mathbf{F}}_c, 1; 1, \overline{\mathbf{F}}_b, 1, 1)_L + (1, \overline{\mathbf{F}}_c; 1, 1, 1, \overline{\mathbf{F}}_b)_L$	$2m_b$
	$(\mathbf{F}_c, 1; \mathbf{F}_b, 1, 1, 1)_L + (1, \mathbf{F}_c : 1, 1, \mathbf{F}_b, 1)_L$	$2m_b$
cbT	$(\mathbf{F}_c, 1; 1, 1, \overline{\mathbf{F}}_b, 1)_L + (1, \mathbf{F}_c; \overline{\mathbf{F}}_b, 1, 1, 1,)_L$	$m_b\chi$
	$(\overline{\mathbf{F}}_c, 1; 1, 1, 1, \overline{\mathbf{F}}_b)_L + (1, \overline{\mathbf{F}}_c; 1, \overline{\mathbf{F}}_b, 1, 1,)_L$	$m_b\chi$

Table 2.4: Modification of the chiral spectrum from intersecting D6-branes for an $\Omega\mathcal{R}_3$ invariant stack of D6$_c$-branes with wrapping numbers $(n_c, m_c) = (1, 0)$ on the rectangular torus. The orbifold symmetry is $\mathbb{Z}_2$.

Chapter 3

Orientifold models with intersecting D8-branes

In this chapter, four dimensional orientifold models of type IIA theory on $T^2 \times T^4/\mathbb{Z}_3$ with D8-branes at angles [65] are presented. The orientifold projection $\Omega\mathcal{R}_1$ reflects one coordinate of the six dimensional compact space,

$$\mathcal{R}_1 : Z^1 \to \overline{Z}^1,$$

where

$$Z^1 = X^4 + iX^5$$

is the complex notation introduced in (1.23). In order to achieve partial supersymmetry breaking in the closed string sector, a $\mathbb{Z}_3$ orbifold symmetry is included

$$\Theta : \; Z^j \to e^{2\pi i v_j} Z^j,$$

with $v = (0, 1/3, -1/3)$. The sets of points which are left invariant under $\Omega\mathcal{R}_1$ constitute orientifold planes, which are extended along all non-compact directions and the four dimensional orbifold, but only along the X^4 axis on the first two torus T_1. Thus, they extend along eight spatial dimensions. In order to cancel the RR charges of these O8-planes, an appropriate configuration of D8-branes has to be added. In contrast to the D6-brane models of chapter 2, only in case of a $\mathbb{Z}_3$ symmetry the tadpole cancellation conditions are fulfilled by including merely D8-branes. For the other four dimensional orbifolds, the $\mathbb{Z}_2$ subgroup produces additional tadpoles which can only be canceled by adding D4-branes besides the D8-branes as can be seen by comparison with the supersymmetric limits of these models [53]. Since they do not admit for large volume compactifications, we restrict to the $\mathbb{Z}_3$ case.

Performing a T-duality along the X^5 direction, D8-branes at angles on T_1 correspond to D9-branes with non-trivial magnetic background flux F_{45} which is quantized in terms of the radii of the two-torus as discussed in section 1.1.2. A tilted torus T_1 in the angle picture again corresponds to a non-trivial constant background NSNS two-form flux B_{45} in the T-dual picture. As in chapter 2, due to the reflection symmetry $\mathcal{R}_1$, each $D8_a$-brane is accompanied by its mirror image $D8_{a'}$ with wrapping numbers given by (2.20), and two stacks of branes $D8_a$ and $D8_b$ generically have several intersections within the fundamental cell of the torus. The corresponding intersection numbers are as defined in (2.16).

In the class of models under consideration, the orbifold generator Θ preserves the position of each $D8_a$-brane while assigning different phases α^j (where $\alpha \equiv e^{2\pi i/3}$ and $j = 0, 1, 2$) to the mass eigenstates. Therefore, a stack of N_a $D8_a$-branes with identical positions is decomposed according to the different eigenvalues of the $\mathbb{Z}_3$ rotation, $N_a = N_a^0 + N_a^1 + N_a^2$, giving rise to the gauge group

$$U\left(N_a^0\right) \times U\left(N_a^1\right) \times U\left(N_a^2\right).$$

Particles which are supported at the intersection locus of two stacks of branes $D8_a$ and $D8_b$ with $\mathbb{Z}_3$ eigenvalue 1 transform as $(\mathbf{F}_a^i, \overline{\mathbf{F}}_b^i)$ whereas those with eigenvalue $\alpha^{\pm 1}$ transform as $(\mathbf{F}_a^i, \overline{\mathbf{F}}_b^{i\pm 1})$. This is in contrast to the D6-brane models where Θ exchanges the brane positions.

The gauge coupling constants of the $U(N_a^i)$ factors with support on a $D8_a$-brane are determined by the length L_a of the 1-cycle on T_1 which the $D8_a$-branes wrap [2]. The length of the cycle in terms of wrapping numbers and radii of the two-torus T_1 is given by the generalization of the one in section 2.1.2 to tilted tori

$$L_a = \sqrt{(n_a R_1)^2 + ((m_a + b n_a) R_2)^2}, \tag{3.5}$$

with $b = 0, 1/2$ corresponding to the rectangular and tilted torus, respectively.

The models with D8-branes do not only differ from those with D6-branes in the action of the orbifold group but also in view of solving the mass hierarchy problem. While in D6-brane models, the wrapped 3-cycles on $T_1 \times T_{2,3}$ are chosen such that there does not exist any compact direction transverse to all D6-branes, the D8-brane models admit a T-dual description in terms of D4-branes for the orbifold group $\mathbb{Z}_3$. The latter have the transverse directions along $T_{2,3}$ in common. This admits for a large orbifold volume which might serve to lower the string scale down to the TeV region and thus solve the mass hierarchy problem [7, 6].

Some phenomenological aspects of the orientifold theories with intersecting D8-branes are discussed at the end of this chapter in section 3.5.

3.1 RR tadpoles and chiral spectra

3.1.1 RR tadpole cancellation

In this section, we derive the consistency conditions of the $(T^2 \times T^4/\mathbb{Z}_3)/\Omega\mathcal{R}_1$ models which are determined by the requirement that all — untwisted and twisted — RR charges of the O8-planes are canceled by those of the D8_a-branes. The computation of untwisted tadpoles in the tree channel is similar to the one presented in chapter 2. The twisted tadpoles only occur in such classes of models where the reflection $\mathcal{R}_1$ commutes with the orbifold generator. As for the D6-brane models, the tadpole cancellation conditions can be entirely expressed in terms of the wrapping numbers n_a corresponding to the projection of the 1-cycles on T_1 onto the X^4-axis and the number of identical D8_a-branes N_a^i.

The RR tadpole cancellation conditions are again computed along the lines of section 1.4. In contrast to the models with D6-branes at angles [48] considered in chapter 2 and the supersymmetric [20, 19, 49] and non-supersymmetric orientifolds in [27], the following relation holds

$$(\Omega\mathcal{R}_1 h)^2 = h^2.$$

Therefore, twisted as well as untwisted closed strings propagate in the tree channel leading to untwisted and twisted tadpole cancellation conditions which have to be fulfilled simultaneously.

At this point, we turn to the explicit calculation of the three 1-loop-amplitudes. The direct calculation in the tree channel can be performed using the boundary state approach. For this class of models, the relevant formulas are displayed in appendix F. The normalizations of untwisted and twisted crosscap and boundary states are fixed by worldsheet duality. In this class of models, there is no further constraint on the lattices from the tree channel picture. The constraints on N_a^i arise from the action of the orbifold group on the Chan-Paton matrices of the open strings and can only be derived by starting from the 1-loop amplitudes.

Klein bottle

The closed string 1-loop contributions to the RR exchange in the tree channel are again obtained by computing the NSNS parts with $(-1)^F$ insertion where the GSO projection (1.35) in this class of models is determined by (1.38) and (1.39). The lattice contributions $\mathcal{L}_1$ on T_1 where the reflection $\mathcal{R}_1$ acts are as discussed in chapter 2 and [24, 48]. In addition, in the untwisted sector Kaluza-Klein momenta arise along all directions of the orbifold whereas windings are projected out by worldsheet parity. The explicit formulas for the lattice contributions of the orbifold to the amplitudes are listed in appendix E.1. $\Omega\mathcal{R}_1$ exchanges Θ and Θ^{-1} twisted sectors. Hence, in the 1-loop channel, only untwisted sectors contribute. The calculation of the contribution with $\mathbb{1}$ insertion goes completely along the lines discussed in chapter 2 and [24, 48] yielding

$$\mathcal{K}^U = \frac{c}{3}\int_0^\infty \frac{\mathrm{d}t}{t^3}\mathcal{L}_1^{\mathcal{K}}\mathcal{L}_2^{\mathcal{K}}\mathcal{L}_3^{\mathcal{K}}\mathcal{K}^{(0)}, \tag{3.7}$$

where c is the constant factor mentioned in section 2.1.1. $\mathcal{L}_2^{\mathcal{K}}\mathcal{L}_3^{\mathcal{K}}$ is as given in (E.4). Performing the modular transformation $t = 1/(4l)$ gives the contribution from the untwisted RR fields,

$$\tilde{\mathcal{K}}^U = \frac{c}{3}\int_0^\infty \mathrm{d}l \frac{256}{3}\frac{R_1}{R_2}\omega\tilde{\mathcal{L}}_1^{\mathcal{K}}\tilde{\mathcal{L}}_2^{\mathcal{K}}\tilde{\mathcal{L}}_3^{\mathcal{K}}\tilde{\mathcal{K}}^{(0)}, \tag{3.8}$$

where $R_{1,2}$ are the two radii of the first two-torus T_1 and ω is the dimensionless volume of the orbifold $T^4/\mathbb{Z}_3$.

In addition, $\Theta^{1,2}$ insertions create tadpoles which are independent of the internal volume of the orbifold,

$$\mathcal{K}^T = \frac{c}{3}\int_0^\infty \frac{\mathrm{d}t}{t^3}\mathcal{L}_1^{\mathcal{K}}\sum_{k=1}^{2}\mathcal{K}^{(k)}. \tag{3.9}$$

The explicit expression of $\mathcal{K}^{(k)}$ in terms of generalized Jacobi-Theta functions is given in formula (E.7). The lattice contributions $\mathcal{L}_1^{\mathcal{K}}$ are the same as in formula (3.7), whereas the Kaluza-Klein momenta on $T_{2,3}$ are not invariant under Θ. Transforming to the tree channel, the twisted Klein bottle is given by

$$\tilde{\mathcal{K}}^T = -16\frac{c}{3}\int_0^\infty \mathrm{d}l \frac{R_1}{R_2}\tilde{\mathcal{L}}_1^{\mathcal{K}}\sum_{k=1}^{2}\tilde{\mathcal{K}}^{(k)}, \tag{3.10}$$

where the contribution of the twisted oscillators $\tilde{\mathcal{K}}^{(k)}$ is listed in (E.10).

Annulus

The annulus amplitude is obtained from open strings stretching between branes $D8_a$ and $D8_b$ at angle $\pi\Delta\varphi_{ab}$ on T_1. The contributions from T_1 have been discussed in detail in chapter 2 and [24, 48]. The computation of the trace with trivial insertion is again completely analogous to the one performed there yielding the untwisted RR tadpole of the annulus in the tree channel

$$\tilde{\mathcal{A}}_{ab}^U = -N_a N_b I_{ab}\frac{c}{3}\int_0^\infty \mathrm{d}l\frac{1}{6}\omega\tilde{\mathcal{A}}^{(0)}\tilde{\mathcal{L}}_2^{\mathcal{A}}\tilde{\mathcal{L}}_3^{\mathcal{A}}. \tag{3.11}$$

N_a labels the number of $D8_a$-branes of identical position, I_{ab} is the intersection number on T_1 defined in (2.16), $\tilde{\mathcal{L}}_2^{\mathcal{A}}\tilde{\mathcal{L}}_3^{\mathcal{A}}$ is given in (E.5) and the oscillator contribution is given by (2.18). The explicit dependence of the annulus tadpole on the orbifold volume ω is due to the fact that D8$_a$-branes have Neumann directions along all four orbifold directions $X^{6\ldots9}$ leading to Kaluza-Klein momenta $P^{6\ldots9}$ in the loop channel.

In addition to the trivial insertion, each Θ^k insertion preserves the positions of D8-branes. Kaluza-Klein momenta are projected out, and the $\mathbb{Z}_3$ rotation acts non-trivially on the Chan-Paton labels of open strings with endpoints on branes D8$_a$, D8$_b$ via the matrices $\gamma^a_{\Theta^k}, \gamma^b_{\Theta^k}$ leading to

$$\mathcal{A}^T_{ab} = \frac{I_{ab}}{4}\frac{c}{3}\int_0^\infty \frac{\mathrm{d}t}{t^3}\sum_{k=1}^{2} \mathrm{tr}\gamma^a_k \mathrm{tr}\gamma_k^{-1,b}\mathcal{A}^{(k)}, \tag{3.12}$$

with $\mathcal{A}^{(k)}$ explicitly listed in (E.8). By modular transformation $t = 1/(2l)$, one arrives at the twisted RR tadpole contributions of the annulus,

$$\tilde{\mathcal{A}}^T_{ab} = -I_{ab}\frac{c}{3}\int_0^\infty \mathrm{d}l \frac{1}{2}\sum_{k=1}^{2} \mathrm{tr}\gamma^a_k \mathrm{tr}\gamma_k^{-1,b}\tilde{\mathcal{A}}^{(k)}, \tag{3.13}$$

with $\tilde{\mathcal{A}}^{(k)}$ given by (E.11). Thus, the asymptotic behavior of the annulus amplitudes is given by

$$\tilde{\mathcal{A}}^U_{ab} \stackrel{l\to\infty}{\longrightarrow} N_a N_b \frac{4}{3}\omega\frac{c}{3}\int_0^\infty \mathrm{d}l \left(n_a n_b \frac{R_1}{R_2} + (m_a + b n_a)(m_b + b n_b)\frac{R_2}{R_1}\right), \tag{3.14}$$

$$\tilde{\mathcal{A}}^T_{ab} \stackrel{l\to\infty}{\longrightarrow} -\frac{c}{3}\int_0^\infty \mathrm{d}l \sum_{k=1}^{2} \mathrm{tr}\gamma^a_k \mathrm{tr}\gamma_k^{-1,b}\left(n_a n_b \frac{R_1}{R_2} + (m_a + b n_a)(m_b + b n_b)\frac{R_2}{R_1}\right). \tag{3.15}$$

The amplitudes $\tilde{\mathcal{A}}_{aa}$ from D8$_a$-D8$_a$ strings develop the same asymptotics.

Möbius strip

The computation of the untwisted RR exchange in the tree channel arising from the Möbius strip amplitude is again very similar to the case discussed in chapter 2 and [24, 48]. Only strings stretching between mirror branes D8$_a$ and D8$_{a'}$ contribute. Their multiplicity is determined by the number of $\Omega\mathcal{R}_1$ invariant intersections $I^{\Omega\mathcal{R}_1}_{a'a}$ which is identical to (2.21). The Neumann directions on $T_{2,3}$ lead to lattice contributions from Kaluza-Klein momenta displayed in (E.6). Therefore, also the untwisted RR exchange from the Möbius strip is linearly proportional to the orbifold volume ω.

The computation of the twisted RR tadpoles in the Möbius strip is also completely analogous to the annulus case. The $\mathbb{Z}_3$ rotation acts non-trivially on the Chan-Paton matrix of the D8$_a$-D8$_{a'}$ strings, lattice contributions are projected out and the oscillator contributions in the tree channel are listed in (E.12). The corresponding loop channel oscillator contributions are given in (E.9). In summary, we obtain the asymptotic behavior

$$\mathcal{M}_a^U \stackrel{l\to\infty}{\longrightarrow} -\frac{c}{3}\int_0^\infty \mathrm{d}l \frac{256}{3}\frac{R_1}{R_2}\omega n_a \mathrm{tr}\left(\gamma_{\Omega\mathcal{R}_1}^{-1,a'}\gamma_{\Omega\mathcal{R}_1}^{T,a}\right), \tag{3.16}$$

$$\mathcal{M}_a^T \stackrel{l\to\infty}{\longrightarrow} \frac{c}{3}\int_0^\infty \mathrm{d}l 16 n_a \frac{R_1}{R_2}\sum_{k=1}^{2}\mathrm{tr}\left(\gamma_{\Omega\mathcal{R}_1 k}^{-1,a'}\gamma_{\Omega\mathcal{R}_1 k}^{T,a}\right). \tag{3.17}$$

The traces in (3.17) can be transformed due to the requirement that the γ matrices form a projective representation of the orientifold group as explained in section 1.5.2, i.e.

$$\gamma_{k+l}^a = c_{k+l}^{-1}\gamma_{\Omega\mathcal{R}_1 l}^{-T,a'}\gamma_{\Omega\mathcal{R}_1 k}^a$$

with some phases c_{k+l}.

RR tadpole cancellation

The RR tadpole cancellation conditions can be extracted from the asymptotic behavior of the Klein bottle (3.8) and (3.10), the annulus (3.14) and (3.15) and the Möbius strip (3.16) and (3.17) after summing over all possible open string configurations.

The untwisted tadpole cancellation conditions are

$$\begin{aligned}\left[\sum_a n_a N_a - 16\right]^2 &= 0, &(3.19)\\ \mathrm{tr}\left(\gamma_{\Omega\mathcal{R}_1}^{-1,a'}\gamma_{\Omega\mathcal{R}_1}^{T,a}\right) &= N_a. &(3.20)\end{aligned}$$

The twisted tadpole cancellation conditions split into the projection onto the X^4 axis proportional to R_1/R_2 and onto the X^5 direction proportional to R_2/R_1,

$$\frac{R_2}{R_1}: \sum_{k=1}^{2} \left| \sum_a (m_a + b n_a)\left(\mathrm{tr}\gamma_k^a - \mathrm{tr}\gamma_k^{a'}\right)\right|^2 = 0, \tag{3.21}$$

$$\begin{aligned}\frac{R_1}{R_2}: \sum_{k=1}^{2} \Bigg(& 8^2 + \left|\sum_a n_a\left(\mathrm{tr}\gamma_k^a + \mathrm{tr}\gamma_k^{a'}\right)\right|^2 \\ & - 2\cdot 8\cdot \sum_a n_a\left(c_{2k}\mathrm{tr}\gamma_{2k}^a + \tilde{c}_{2k}\mathrm{tr}\gamma_{2k}^{a'}\right)\Bigg) = 0.\end{aligned} \tag{3.22}$$

Condition (3.21) is trivially fulfilled if for mirror branes D8$_a$ and D8$_{a'}$ the equation $\mathrm{tr}\gamma_k^a = \mathrm{tr}\gamma_k^{a'}$ holds. Furthermore, equation (3.22) gives a total square for each twist sector k provided that $c_{2k} = \tilde{c}_{2k} = 1$ and $\mathrm{tr}\gamma_{2k} \in \mathbb{R}$. These conditions fix the form of γ_Θ^a,

$$\gamma_\Theta^a = \mathrm{diag}\left(\mathbb{I}_{N_a^0}, e_{N_a^1}^{2\pi i/3}, e_{N_a^2}^{-2\pi i/3}\right), \tag{3.23}$$

with $N_a = N_a^0 + N_a^1 + N_a^2$ and $N_a^1 = N_a^2$.

Inserting (3.23) in (3.19) and (3.22) determines the RR tadpole cancellation conditions entirely in terms of the wrapping numbers n_a corresponding to the projection of the 1-cycles onto the X^4 axis and the number of identical branes N_a^i,

$$\sum_a n_a N_a^0 = 8, \tag{3.24}$$

$$\sum_a n_a N_a^1 = 4. \tag{3.25}$$

So far, we have only considered D8$_a$-branes which are mapped to their mirror image D8$_{a'}$ under the reflection $\mathcal{R}_1$. A D8$_c$-brane which is its own mirror image contributes only half the amount to the tadpole cancellation conditions, i.e.

$$\frac{n_c N_c^0}{2} + \sum_{a \neq c} n_a N_a^0 = 8, \tag{3.26}$$

$$\frac{n_c N_c^1}{2} + \sum_{a \neq c} n_a N_a^1 = 4. \tag{3.27}$$

The wrapping numbers of the $\Omega\mathcal{R}_1$ invariant D8$_c$-brane are $(n_c, m_c) = (1, 0)$ for vanishing background antisymmetric NSNS tensor field b and $(n_c, m_c) = (2, -1)$ for $b = 1/2$ as in chapter 2. In the limit $R_1, \frac{1}{R_2} \to \infty$ where the T-dual two torus T_1 decompactifies, the supersymmetric six dimensional set-up is recovered which for vanishing antisymmetric NSNS tensor, i.e. a single stack of D8$_c$-branes with $(n_c, m_c) = (1, 0)$ and $b = 0$, is identical to the $\mathbb{Z}_3$ orientifold in [53].

3.1.2 Chiral open spectrum

The computation of the closed string spectrum is analogous to the one presented in section 2.2.1 when taking into account the altered orientifold action given by (A.10) on the oscillators. $\Omega\mathcal{R}_1$ invariant RR sector states are of the form $|s_0, s_1, s_2, s_3\rangle_L |\tilde{s}_0, \tilde{s}_1, \tilde{s}_2, \tilde{s}_3\rangle_R - |\tilde{s}_0, -\tilde{s}_1, \tilde{s}_2, \tilde{s}_3\rangle_L |s_0, -s_1, s_2, s_3\rangle_R$. The main difference in the computation of the twisted sector contributions as compared to the D6-brane models in section 2.2.1 arises from the fact that $\Omega\mathcal{R}_1$ exchanges the Θ and Θ^2 twisted sectors.

The closed string spectrum contains the $\mathcal{N} = 2$ supergravity multiplet as well as eleven hypermultiplets and ten tensor multiplets. The complete closed string sector is $\mathcal{N} = 2$ supersymmetric and non-chiral.

In order to determine the open string spectrum, we fix the Chan-Paton matrices

$$\gamma^a_{\Omega\mathcal{R}_1} = \gamma^{a'}_{\Omega\mathcal{R}_1} = \begin{pmatrix} \mathbb{1}_{N_a^0} & 0 & 0 \\ 0 & 0 & \mathbb{1}_{N_a^1} \\ 0 & \mathbb{1}_{N_a^1} & 0 \end{pmatrix},$$
$$\gamma^a_\Theta = \gamma^{a'}_\Theta = \mathrm{diag}\left(\mathbb{1}_{N_a^0}, e^{2\pi i/3}_{N_a^1}, e^{-2\pi i/3}_{N_a^1}\right)$$

in analogy to the supersymmetric case discussed in [53]. Open strings stretching between D8$_a$-branes of identical position then support the gauge groups

$$U(N_a^0) \times \left(U(N_a^1)\right)^2.$$

In the case of an $\Omega\mathcal{R}_1$ invariant stack of D8$_c$-branes, the gauge group is reduced to

$$SO(N_c^0) \times U(N_c^1).$$

The D8$_a$-D8$_a$ and D8$_c$-D8$_c$ sectors of open strings are again $\mathcal{N} = 2$ supersymmetric and non-chiral.

Finally, the sectors of strings stretching between D8$_a$ and D8$_b$-branes at angles $\pi\Delta\varphi_{ab}$ are non-supersymmetric and chiral. This part of the spectrum generically contains tachyons since the mass formula (1.40) applied to open strings for this class of models gives the following masses of states in the NS sector,

$$\frac{\alpha'}{4} m^2_{ab} = N_{osc} + \frac{\Delta\varphi_{ab}}{2} - \frac{1}{2},$$

where N_{osc} can be read off from (2.29) by setting $k/M \equiv 0$. Thus, the state $\psi^1_{\Delta\varphi-1/2}|0\rangle_{NSNS}$ is tachyonic. A complete list of lightest NS states is given in table G.1. In contrast to the models with D6-branes discussed in chapter 2, mass eigenstates in the models with D8-branes have to be classified according to their $\mathbb{Z}_3$ eigenvalues. Tachyonic states only occur in the sectors with eigenvalue 1. In principle, this introduces the possibility of choosing the brane set-up, i.e. the numbers N_a^i, such that no chiral sector with trivial eigenvalue occurs. However, the tadpole cancellation conditions (3.26), (3.27) constrain the models severely. Furthermore, in contrast to the type IIB models examined in [1, 2, 9] the orientifold projection $\Omega\mathcal{R}_1$ enforces the existence of mirror branes. D8$_a$-D8$_{a'}$ strings automatically include a sector containing tachyons which can be only projected out completely by the $\Omega\mathcal{R}_1$ symmetry in case of a single $U(1)_a$ gauge factor and the wrapping number $n_a = 1$.

The R sector of D8-branes at angles provides chiral fermions. The groundstate is fourfold degenerated as displayed in the table D.1. The degeneracy is lifted by the $\mathbb{Z}_3$ symmetry. In summary, the chiral spectrum is listed in table 3.1. For an $\Omega\mathcal{R}_1$ invariant D8$_c$-brane, the spectrum is slightly changed as displayed in table 3.2. As for D6-brane models, the sector D8$_{a'}$-D8$_{b'}$ generically provides the anti-particles of the D8$_a$-D8$_b$ sector, and the sector D8$_a$-D8$_{b'}$ is paired with D8$_{a'}$-D8$_b$. For $c = c'$, only the sectors D8$_c$-D8$_b$ and D8$_c$-D8$_{b'}$ are present and form a pair. RR tadpole cancellation ensures that the chiral spectrum is free of purely non-Abelian gauge anomalies as can be explicitly checked using (2.39). Mixed $U(1)$ anomalies will have to be cured by a generalized Green-Schwarz mechanism involving twisted RR fields from the closed string sector [43, 1, 81].

The chiral D8$_a$-D8$_{a'}$, D8$_a$-D8$_b$ and D8$_a$-D8$_{b'}$ sectors with $\mathbb{Z}_3$ eigenvalue 1 are accompanied by a tachyonic scalar pseudo-superpartner. As already mentioned in the previous paragraph, the D8$_a$-D8$_{a'}$ sector is only absent provided that $n_a = 1$ and $N_a^0 = 1, N_a^1 = N_a^2 = 0$, i.e. the D8$_a$-brane accommodates a single $U(1)_a$ gauge factor.

Massless chiral fermionic spectrum on $T^2 \times T^4/\mathbb{Z}_3$ with D8-branes			
sector	$\mathbb{Z}_3$	multiplicity	rep.
aa'	1	$2(2m_a + (2b)n_a)$	$(\mathbf{A}_a^0, 1, 1) + (1, \mathbf{F}_a^1, \mathbf{F}_a^2)$
		$(n_a - 1)(2m_a + (2b)n_a)$	$(\mathbf{A}_a^0 + \mathbf{S}_a^0, 1, 1) + 2(1, \mathbf{F}_a^1, \mathbf{F}_a^2)$
	α	$(2m_a + (2b)n_a)$	$(\bar{\mathbf{F}}_a^0, 1, \bar{\mathbf{F}}_a^2) + (1, \overline{\mathbf{A}}_a^1, 1)$
		$\frac{n_a-1}{2}(2m_a + (2b)n_a)$	$2(\bar{\mathbf{F}}_a^0, 1, \bar{\mathbf{F}}_a^2) + (1, \overline{\mathbf{A}}_a^1 + \overline{\mathbf{S}}_a^1, 1)$
	α^2	$(2m_a + (2b)n_a)$	$(\bar{\mathbf{F}}_a^0, \bar{\mathbf{F}}_a^1, 1) + (1, 1, \overline{\mathbf{A}}_a^2)$
		$\frac{n_a-1}{2}(2m_a + (2b)n_a)$	$2(\bar{\mathbf{F}}_a^0, \bar{\mathbf{F}}_a^1, 1) + (1, 1, \overline{\mathbf{A}}_a^2 + \overline{\mathbf{S}}_a^2)$
ab	1	$2(n_a m_b - n_b m_a)$	$(\bar{\mathbf{F}}_a^0, \mathbf{F}_b^0) + (\bar{\mathbf{F}}_a^1, \mathbf{F}_b^1) + (\bar{\mathbf{F}}_a^2, \mathbf{F}_b^2)$
	α	$(n_a m_b - n_b m_a)$	$(\mathbf{F}_a^0, \bar{\mathbf{F}}_b^1) + (\mathbf{F}_a^1, \bar{\mathbf{F}}_b^2) + (\mathbf{F}_a^2, \bar{\mathbf{F}}_b^0)$
	α^2	$(n_a m_b - n_b m_a)$	$(\mathbf{F}_a^0, \bar{\mathbf{F}}_b^2) + (\mathbf{F}_a^1, \bar{\mathbf{F}}_b^0) + (\mathbf{F}_a^2, \bar{\mathbf{F}}_b^1)$
ab'	1	$2(n_a m_b + n_b m_a + (2b)n_a n_b)$	$(\mathbf{F}_a^0, \mathbf{F}_b^0) + (\mathbf{F}_a^1, \mathbf{F}_b^2) + (\mathbf{F}_a^2, \mathbf{F}_b^1)$
	α	$(n_a m_b + n_b m_a + (2b)n_a n_b)$	$(\bar{\mathbf{F}}_a^0, \bar{\mathbf{F}}_b^2) + (\bar{\mathbf{F}}_a^1, \bar{\mathbf{F}}_b^1) + (\bar{\mathbf{F}}_a^2, \bar{\mathbf{F}}_b^0)$
	α^2	$(n_a m_b + n_b m_a + (2b)n_a n_b)$	$(\bar{\mathbf{F}}_a^0, \bar{\mathbf{F}}_b^1) + (\bar{\mathbf{F}}_a^1, \bar{\mathbf{F}}_b^0) + (\bar{\mathbf{F}}_a^2, \bar{\mathbf{F}}_b^2)$

Table 3.1: Chiral spectrum from intersecting D8-branes. The sectors are classified by the $\mathbb{Z}_3$ eigenvalue of the corresponding R groundstate.

3.2 Cancellation of mixed anomalies

The generic chiral open spectrum displayed in table 3.1 and 3.2 is free of purely non-Abelian gauge anomalies, but yields mixed gravitational anomalies of the

Chiral fermions for an $\Omega\mathcal{R}_1$ invariant stack of D8_c-branes			
sector	$\mathbb{Z}_3$	multiplicity	rep.
cb	1	$2n_c(m_b+bn_b)$	$(\bar{\mathbf{F}}^0_c,\mathbf{F}^0_b)+(\bar{\mathbf{F}}^1_c,\mathbf{F}^1_b)+(\mathbf{F}^1_c,\mathbf{F}^2_b)$
	α	$n_c(m_b+bn_b)$	$(\mathbf{F}^0_c,\bar{\mathbf{F}}^1_b)+(\mathbf{F}^1_c,\bar{\mathbf{F}}^2_b)+(\bar{\mathbf{F}}^1_c,\bar{\mathbf{F}}^0_b)$
	α^2	$n_c(m_b+bn_b)$	$(\mathbf{F}^0_c,\bar{\mathbf{F}}^2_b)+(\mathbf{F}^1_c,\bar{\mathbf{F}}^0_b)+(\bar{\mathbf{F}}^1_c,\bar{\mathbf{F}}^1_b)$

Table 3.2: Modification of the chiral spectrum from intersecting D8-branes involving an $\Omega\mathcal{R}_1$ invariant stack of D8_c-branes.

form

$$U(1)_{i,a}-g_{\mu\nu}:6\,(2\delta_{i,0}-\delta_{i,1}-\delta_{i,2})\,(m_a+bn_a)\,N^i_a \tag{3.31}$$

as well as mixed gauge anomalies which for $(i,a)\neq(j,b)$ are proportional to

$$\begin{aligned} U(1)_{i,a} \quad - \quad & SU(N^j_b)^2: \\ & \Big\{ (m_a+bn_a)\,n_b\,(2\delta_{i,0}-\delta_{i,1}-\delta_{i,2})\,(2\delta_{j,0}-\delta_{j,1}-\delta_{j,2}) \\ & -3n_a\,(m_b+bn_b)\,(\delta_{i,1}-\delta_{i,2})\,(\delta_{j,1}-\delta_{j,2})\Big\} N^i_a C_2(\mathbf{F}^j_b), \end{aligned} \tag{3.32}$$

where $C_2(\mathbf{F})=\frac{N^2-1}{2N}$ is the quadratic Casimir of the fundamental representation of $SU(N)$.

Consistency of the models requires anomalous gauge fields to acquire a mass and thus decouple from the effective low energy field theory. This is realized by the Green-Schwarz mechanism which in models with $K3$ orbifold compactifications involves twisted sector fields [43]. The potential candidates are the RR scalars ${}^6C^{(0)}_k$ and two-forms ${}^6C^{(2)}_k$ in six dimensions which belong to the twisted hyper- and tensormultiplets, respectively. They arise from the Kaluza-Klein reduction of the ten-dimensional two form ${}^{10}C^{(2)}$ and self-dual four form ${}^{10}C^{(4)}$ on a vanishing supersymmetric two-cycle Σ_k on the orbifold,

$${}^6C^{(2)}_k=\int_{\Sigma_k}{}^{10}C^{(4)},\qquad {}^6C^{(0)}_k=\int_{\Sigma_k}{}^{10}C^{(2)}. \tag{3.33}$$

The scalar has a dual four form in six dimensions,

$${}^6C^{(4)}_k=\int_{\Sigma_k}{}^{10}C^{(6)}.$$

Moding out the worldsheet parity amounts to mapping different cycles Σ_k onto each other such that for the $T^4/\mathbb{Z}_3$ limit, k runs over nine distinct values.

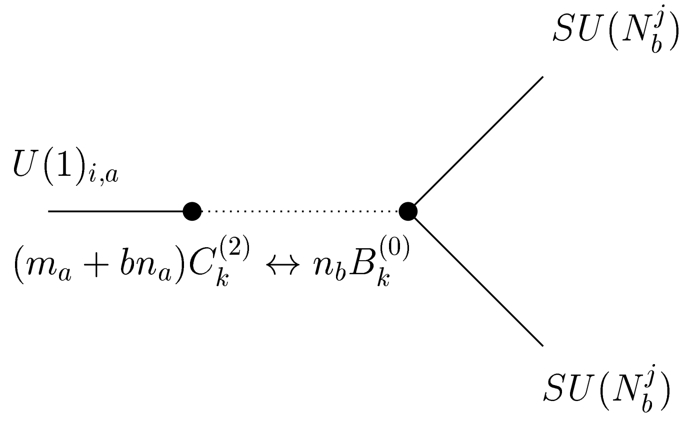

Figure 3.1: Green-Schwarz counter terms.

Reducing further down to four dimensions, the pullback of a closed RR sector k-form on a multiply wrapped brane gives a $(k-2)$-form times the wrapping number along the $\Omega\mathcal{R}_1$ invariant direction [1] of the T-dual picture,

$$n_b B_k^{(0)} = \int_{T_1(D9_b)} {}^6C_k^{(2)}, \qquad n_b B_k^{(2)} = \int_{T_1(D9_b)} {}^6C_k^{(4)},$$

while integrating out the two form $(\mathcal{F}_a)_{45} = (F_a + B)_{45} = \frac{(m_a + bn_a)\alpha'}{n_a R_1 R_2}$ on the torus yields as prefactor $m_a + bn_a$. The resulting four dimensional couplings are of the form

$$(m_a + bn_a) \int_{\mathbb{R}^{1,3}} \mathrm{tr}\left(\gamma_k^a \lambda_i^a\right) C_k^{(2)} \wedge F_{a,i}, \qquad n_b \int_{\mathbb{R}^{1,3}} \mathrm{tr}\left(\gamma_k^b \lambda_i^b \lambda_j^b\right) B_k^{(0)} F_{b,i} \wedge F_{b,j} \tag{3.36}$$
$$n_a \int_{\mathbb{R}^{1,3}} \mathrm{tr}\left(\gamma_k^a \lambda_i^a\right) B_k^{(2)} \wedge F_{a,i}, \qquad (m_b + bn_b) \int_{\mathbb{R}^{1,3}} \mathrm{tr}\left(\gamma_k^b \lambda_i^b \lambda_j^b\right) C_k^{(0)} F_{b,i} \wedge F_{b,j},$$

where λ_i^a is the Chan-Paton factor belonging to the gauge-field component $F_{a,i}$.

The expressions on the left hand side in (3.36) render the anomalous gauge fields massive. Like for the D6-brane models in section 2.2.2, also anomaly free $U(1)$ factors might acquire a mass due to the linear couplings.

Combining the two couplings (3.36) of the scalars $B_k^{(0)}$ and their dual two forms $C_k^{(2)}$, we obtain the Green-Schwarz diagram depicted in figure 3.1, similarly for the dual pairs $C_k^{(0)}$ and $B_k^{(2)}$. These diagrams have the correct form to cancel the mixed gauge anomalies (3.32). Similar diagrams exist which cancel the mixed gravitational anomalies (3.31).

3.3 NSNS tadpoles

Apart from the RR tadpoles considered in section 3.1.1, non-supersymmetric theories generically produce also NSNS tadpoles. In this section, we will follow the discussion of [27] in computing the NSNS tadpoles and deriving the effective scalar potential for the closed string moduli. The analysis will be performed at next to leading order in string perturbation theory, i.e. at open string tree level $e^{-\Phi_s}$ where Φ_s is the dilaton of type I superstring theory in ten dimensions.

The massless NSNS sector fields of our model are the four-dimensional dilaton as well as the internal metric and NSNS two form flux moduli. In our factorized ansatz on $T^2 \times T^4/\mathbb{Z}_3$, the moduli of T_1 are the two radions R_1 and R_2. The two form flux b can only take discrete values. In addition, $K3$ has 80 moduli. In the orbifold limit $T^4/\mathbb{Z}_3$, these moduli are provided by eleven hyper- and nine tensormultiplets where each of the nine orbifold fixed points contributes one hyper- and one tensormultiplet. The remaining two hypermultiplets originate from the untwisted closed string sector [53]. The twisted NSNS moduli at each fixed point group into a triplet state ρ_k^i $(i = +, -, 3,\ k = 1 \ldots 9)$ under the R-symmetry of T^4 associated to the complex structure and Kähler deformations of the manifold and a singlet state $b_k^{(0)}$ which originates from the Kaluza-Klein reduction of the ten dimensional Ω odd form $B^{(2)}$ on Σ_k. These states are listed in table 3.3.

Twisted NSNS states on $T^4/\mathbb{Z}_3$	
state	represented by
$b_k^{(0)}$	$\psi^2_{-1/6}\tilde{\psi}^{\overline{2}}_{-1/6}\|0\rangle^{(\Theta)}_{NSNS} + \psi^{\overline{2}}_{-1/6}\tilde{\psi}^2_{-1/6}\|0\rangle^{(\Theta^2)}_{NSNS}$ $+\psi^{\overline{3}}_{-1/6}\tilde{\psi}^3_{-1/6}\|0\rangle^{(\Theta)}_{NSNS} + \psi^3_{-1/6}\tilde{\psi}^{\overline{3}}_{-1/6}\|0\rangle^{(\Theta^2)}_{NSNS}$
ρ_k^3	$\psi^2_{-1/6}\tilde{\psi}^{\overline{2}}_{-1/6}\|0\rangle^{(\Theta)}_{NSNS} + \psi^{\overline{2}}_{-1/6}\tilde{\psi}^2_{-1/6}\|0\rangle^{(\Theta^2)}_{NSNS}$ $-\psi^{\overline{3}}_{-1/6}\tilde{\psi}^3_{-1/6}\|0\rangle^{(\Theta)}_{NSNS} - \psi^3_{-1/6}\tilde{\psi}^{\overline{3}}_{-1/6}\|0\rangle^{(\Theta^2)}_{NSNS}$
ρ_k^+	$\psi^2_{-1/6}\tilde{\psi}^3_{-1/6}\|0\rangle^{(\Theta)}_{NSNS} + \psi^3_{-1/6}\tilde{\psi}^2_{-1/6}\|0\rangle^{(\Theta^2)}_{NSNS}$
ρ_k^-	$\psi^{\overline{3}}_{-1/6}\tilde{\psi}^{\overline{2}}_{-1/6}\|0\rangle^{(\Theta)}_{NSNS} + \psi^{\overline{2}}_{-1/6}\tilde{\psi}^{\overline{3}}_{-1/6}\|0\rangle^{(\Theta^2)}_{NSNS}$

Table 3.3: Massless twisted NSNS states of the $(T^2 \times T^4/\mathbb{Z}_3)/\Omega\mathcal{R}_1$ orientifold. The relation of the representations to the $K3$ moduli is explained in the text.

The NSNS triplet and the RR scalar of (3.33) provide the bosonic degrees of freedom of a hypermultiplet, and the NSNS scalar together with the RR two form of (3.33) belong to a tensormultiplet at each orbifold fixed point [43] — for a lucid description see also [10].

The computation of NSNS tadpoles is completely analogous to the one of the RR tadpoles: they are extracted from the infrared divergences in the tree channel Klein bottle, annulus and Möbius strip amplitude. These three contributions lead to a sum of perfect squares which can be identified with the disc tadpoles of the various NSNS moduli of the theory. The NSNS amplitudes can be derived directly from the tree channel using the boundary states and crosscaps of appendix F. The normalizations of NSNS states are determined by the fact that for unbroken supersymmetry the NSNS tree channel amplitude of each diagram cancels the corresponding RR amplitude. The Klein bottle diagram does not feel the supersymmetry breaking. For the other two diagrams, the oscillator contributions (E.11), (E.12) involving D8-branes at generic angles can be generalized to

$$\tilde{\mathcal{A}}_{ab}^{(k)} \to (-1)^{2(\alpha+\beta)} \frac{\vartheta\begin{bmatrix}\alpha\\\beta\end{bmatrix}}{\eta^3} \frac{\vartheta\begin{bmatrix}\alpha\\\Delta\varphi+\beta\end{bmatrix}}{\vartheta\begin{bmatrix}\frac{1}{2}\\\frac{1}{2}+\Delta\varphi\end{bmatrix}} \prod_{i=2,3} \frac{\vartheta\begin{bmatrix}\alpha-kv_i\\\beta\end{bmatrix}}{\vartheta\begin{bmatrix}\frac{1}{2}-kv_i\\\frac{1}{2}\end{bmatrix}}(2l), \tag{3.37}$$

$$\tilde{\mathcal{M}}_{a}^{(k)} \to (-1)^{2(\alpha+\beta)} \frac{\vartheta\begin{bmatrix}\alpha\\\beta\end{bmatrix}}{\eta^3} \frac{\vartheta\begin{bmatrix}\alpha\\\varphi+\beta\end{bmatrix}}{\vartheta\begin{bmatrix}\frac{1}{2}\\\frac{1}{2}+\varphi\end{bmatrix}} \prod_{i=2,3} \frac{\vartheta\begin{bmatrix}\alpha+2kv_i\\\beta+kv_i\end{bmatrix}}{\vartheta\begin{bmatrix}\frac{1}{2}+2kv_i\\\frac{1}{2}+kv_i\end{bmatrix}}(2l+\frac{i}{2}). \tag{3.38}$$

These are the analogous formulas to those which are valid for D6-branes in toroidal compactifiactions derived in [22] (see also [80]). In (3.37) and (3.38) $\alpha = 0, 1/2$ corresponds to the RR and NSNS sectors, respectively, and $\beta = 0, 1/2$ arises from the overlap of states with the same or opposite spin structures, respectively. The lattice contributions remain the same as for the RR amplitudes in section 3.1.1. Each NSNS amplitude has two contributions from the different choices of the relative signs of the spin structures in the overlapping boundary states and crosscaps. The tadpoles are again read off by summing over all D8-brane configurations and taking the limit $l \to \infty$.

In the $\Omega\mathcal{R}_1$ orientifold model on $T^2 \times T^4/\mathbb{Z}_3$, three different contributions to the tadpoles arise at next to leading order. Two of them, the dilaton tadpole and the tadpole of the complex structure on T_1, originate from the untwisted part of the amplitudes. These contributions have the interpretation given in [27] which we will briefly repeat here. Additionally, a third tadpole is generated by the twisted moduli corresponding to the fixed points of $T^4/\mathbb{Z}_3$.

In detail, the dilaton tadpole of the annulus amplitude arises from a single dilaton vertex operator insertion on the disk. As observed in [95, 39, 96], this tadpole can be obtained from computing the closed string exchange between two D-branes at tree level. The coupling of the gravitational modes to a D-brane is proportional to its effective four dimensional tension which in turn is proportional to the volume of the D-brane on the compact space.

The dilaton tadpole of the orientifold theory with D8-branes is therefore obtained by evaluating all tadpole contributions and identifying the expression which is proportional to the net tension of the D8-brane configuration — or more precisely to the sum of all D8-brane tensions minus that of the O8-plane — with the dilaton exchange. The remaining untwisted tadpoles belong to the untwisted NSNS moduli of the theory, and the twisted ones arise from the twisted $K3$ moduli. The comparison with the field theory computation is presented further below in this section.

In agreement with the general expectation and the expressions in [27] valid for intersecting D6-branes, one finds for D8-branes at angles the dilaton tadpole

$$\langle \Phi_s \rangle_D = \frac{1}{\sqrt{\mathrm{Vol}(T^6)}} \left(\sum_{a=1}^{K} N_a \mathrm{Vol}(\mathrm{D8}_a) - 16 \mathrm{Vol}(\mathrm{O8}) \right), \tag{3.39}$$

with

$$\begin{aligned} \mathrm{Vol}(\mathrm{D8}_a) &= \omega L_a = \omega \sqrt{(n_a R_1)^2 + ((m_a + b n_a) R_2)^2}, \\ \mathrm{Vol}(\mathrm{O8}) &= \omega R_1, \end{aligned}$$

and the tadpole for the imaginary part of the complex structure U defined in (1.19) on T_1 is given by

$$\langle u \rangle_D = \frac{1}{\sqrt{\mathrm{Vol}(T^6)}} \left(\sum_{a=1}^{K} N_a \frac{(n_a R_1)^2 - ((m_a + b n_a) R_2)^2}{L_a} - 16 \mathrm{Vol}(\mathrm{O8}) \right). \tag{3.40}$$

In contrast to the type IIB models constructed in [1, 2], the real part of the complex structure in the T-dual picture with background fields, i.e. the antisymmetric NSNS two form, is not a modulus of the orientifold theory, and therefore we only obtain a tadpole for the imaginary part. Defining $u = \sqrt{|U_2|} = \sqrt{R_1/R_2}$, the dilaton and the complex structure tadpole can be cast into the form

$$\langle \Phi_s \rangle_D = \sqrt{\omega} \left(\sum_{a=1}^{K} N_a \mathcal{L}_a - 16 u \right), \tag{3.41}$$

$$\langle u \rangle_D = u \frac{\partial}{\partial u} \left(\sqrt{\omega} \left(\sum_{a=1}^{K} N_a \mathcal{L}_a - 16 u \right) \right), \tag{3.42}$$

with

$$\mathcal{L}_a(U) = \sqrt{(n_a u)^2 + ((m_a + U_1 n_a) \frac{1}{u})^2}.$$

The formulas (3.41) and (3.42) reflect the fact that, regarding T_1 where the reflection $\mathcal{R}_1$ acts, only the left-right symmetric states on T_1 of the closed string

Hilbert space, in this case the complex structure modulus, couple to the crosscaps and boundary states whereas the left-right antisymmetric ones, here the Kähler modulus, do not. In addition, we expect to find couplings to some moduli φ_k of $K3$.

Comparing with the boundary (F.8) and crosscap (F.7) states which in particular contain a term of the form

$$|\varphi, \Theta^2; \eta\rangle_{NSNS} \sim \exp\Big\{-i\eta \left(\psi^2_{-1/6}\tilde{\psi}^{\overline{2}}_{-1/6} + \psi^{\overline{3}}_{-1/6}\tilde{\psi}^{3}_{-1/6}\right)\Big\}|0\rangle_{NSNS},$$

one may speculate that these moduli arise from the singlet states $b_k^{(0)}$ of table 3.3. However, since neither the relative normalization of the twisted amplitudes as compared to the untwisted ones nor the explicit field theory description of the $K3$ part is known, we prefer to stick to the symbolic notation φ_k for the relevant twisted NSNS moduli.

Indeed, a third tadpole arises from the twisted sector which can be cast into the form

$$\langle\varphi_k\rangle_D = \left(\sum_a \mathrm{tr}(\gamma^a)\mathcal{L}_a - 4u\right).$$

From

$$\langle\Phi_s\rangle_D \sim \frac{\partial V}{\partial\Phi_s}, \qquad \langle u\rangle_D \sim \frac{\partial V}{\partial u}, \qquad \langle\varphi_k\rangle_D \sim \frac{\partial V}{\partial\varphi_k},$$

we can derive an ansatz for the scalar potential in the string frame of the form

$$V(\Phi_s, U, \varphi_k) = e^{-\Phi_s}\left(\sum_{a=1}^{K} N_a\mathcal{L}_a - 16u + \varphi_k\left(\sum_{a=1}^{K}\mathrm{tr}(\gamma^a)\mathcal{L}_a - 4u\right)\right). \tag{3.47}$$

This potential is computed only to non-trivial leading order in string theory even though higher powers of the complex structure modulus occur. The ansatz (3.47) for the scalar potential can be compared with the field theory expectation obtained from the Dirac-Born-Infeld action of a D9_a-brane with constant magnetic and electric background flux in the T-dual picture in the limit $\varphi_k \to 0$,

$$\mathcal{S}_{D9_a} = -T_9\int_{D9_a} \mathrm{d}^{10}x e^{-\Phi_s}\sqrt{-\det\left(G+\mathcal{F}_a\right)}, \tag{3.48}$$

with the D9-brane tension $T_9 = (2\pi)^{-9}\alpha'^{-5}$ and the constant values on T_1

$$G = \mathbb{1}_2, \qquad (\mathcal{F}_a)_{45} = (B+F_a)_{45} = \frac{(m_a + bn_a)}{n_a}\frac{\alpha'}{R_1R_2}.$$

In addition, to lowest order in the $K3$ moduli the relation

$$\det G(K3) = \mathrm{vol}(K3) = \omega$$

is valid. The dependence on the twisted sector modes φ_k in the orbifold limit $T^4/\mathbb{Z}_3$ seems to be much more complicated and will not be further pursued here.

The scalar potential (3.47) computed from string theory is unstable to lowest order. This means that the minimum of the theory is not chosen in an appropriate way and hints to an instability of the D8-brane configuration. In the T-dual theory, the tilting of D8-branes towards the X^4 axis corresponds to the dynamical decompactification to the six dimensional supersymmetric theory. A further indication of the instability arises from the fact that it seems to be impossible within the framework of intersecting D8-branes to obtain a consistent chiral theory which does not contain any tachyon at all as mentioned in section 3.1.2.

The problem of stability in the context of tachyons in a purely toroidal compactification has also been addressed in [100]. The moduli in toroidal D6-brane models with non-trivial intersection angles on all three tori can be chosen such that no tachyonic states are present. But even in this case, NSNS tadpoles signal an instability towards the decay to the supersymmetric vacuum [27].

3.4 Examples

In this section, we discuss four models in view of their phenomenological relevance. The tadpole cancellation conditions (3.26), (3.27) severely restrict the possible choices of gauge groups. For example, the GUT gauge group $SU(5)$ can only be obtained from $N_a^0 = 5$ if we restrict our attention to D8-branes (i.e. we do not want to include anti-D8-branes), and we would have to introduce at least two more stacks of D8-branes leading to exotic matter. Furthermore, the generic spectrum in table 3.1 shows that only an even number of antisymmetric representations of $SU(N_a^0 = 5)$ can be engineered. Therefore, we will not further pursue GUT models, but show two models which include the gauge group $SU(3) \times SU(2) \times U(1)_Y$ and two left-right symmetric models which contain $SU(3) \times SU(2)_L \times SU(2)_R \times U(1)_{B-L}$. In order to obtain a phenomenologically appealing spectrum, we also include parallely displaced D6-branes and anti-D6-branes. In all four models we choose the non-trivial background $b = 1/2$ as only in this case an odd number of generations is achievable.

3.4.1 Example 1a: $SU(3) \times SU(2) \times U(1)^3$ and four generations

In the first example, we choose three different stacks of D8-branes,

$$\begin{aligned} N_A^1 &= 3, \qquad && (n_A, m_A) = (2, -1), \\ N_B^0 &= 2, && (n_B, m_B) = (4, -1), \\ N_C^1 &= 1, && (n_C, m_C) = (1, 0). \end{aligned} \tag{3.51}$$

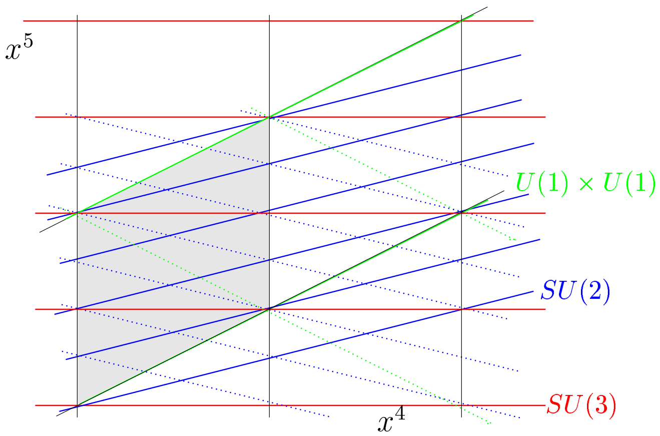

Figure 3.2: Example 1a: D8-brane configuration on T_1. The shaded area emphasizes the fundamental cell of the torus. Solid lines denote D8-branes, dotted lines denote their mirror images.

The D8-brane configuration on T_1 is depicted in figure 3.2. The stack of D8-branes of type A is $\Omega\mathcal{R}_1$ invariant. Thus, the modified tadpole cancellation conditions (3.26), (3.27) hold and the spectrum can be read off from tables 3.1 and 3.2. In this attempt, we only include D8-branes and require that quarks have no tachyonic pseudo-superpartners. In addition, we want to avoid exotic matter which would arise from additional stacks of D8-branes with non-Abelian gauge groups. This fixes the numbers N_A^1 and N_B^0 as well as the corresponding wrapping numbers n_A, n_B along the $\mathcal{R}_1$ invariant direction. It also fixes the number of quark generations to be even. The spectrum obtained from the setting (3.51) is displayed in table 3.4 where we have also listed the original (Q_a^i) and anomaly-free ($Q_Y, \tilde{Q}$) $U(1)$ charges. The factor $U(1)_{1,A}$ which arises from the $\Omega\mathcal{R}_1$ invariant stack of D8-branes is anomaly-free by itself. In addition, there are two more anomaly-free linear combinations,

$$\begin{aligned} Q_Y &= \frac{Q_A^1}{3} + Q_C^1 - Q_C^2, \\ \tilde{Q} &= \frac{Q_B^0}{4} + Q_C^1 + Q_C^2, \end{aligned} \tag{3.52}$$

where Q_Y can be interpreted as hypercharge for the left- and right-handed quarks and leptons. The remaining anomalous $U(1)$ factor acquires a mass by the generalized Green-Schwarz mechanism as described in section 3.2 and decouples from the effective theory. In the $AC\alpha^0$, $BB'\alpha^0$ and $CC'\alpha^0$ sectors, tachyonic pseudo-superpartners occur, whereas all other sectors have either massless or massive scalar partners transforming in the same representation.

Chiral fermionic spectrum for example 1a									
	mult.	rep. of $SU(3)\times SU(2)$	Q_C^1	Q_C^2	Q_B^0	Q_A^1	Q_Y	$\tilde{Q}$
$AB\alpha^1$	2	$(\overline{\mathbf{3}},\mathbf{2})$	0	0	-1	-1	$-1/3$	$-1/4$
α^2	2	$(\mathbf{3},\mathbf{2})$	0	0	-1	1	$1/3$	$-1/4$
$AC\alpha^0$	2	$(\overline{\mathbf{3}},1)$	1	0	0	-1	$2/3$	1
	2	$(\mathbf{3},1)$	0	1	0	1	$-2/3$	1
α^1	1	$(\mathbf{3},1)$	0	-1	0	1	$4/3$	-1
α^2	1	$(\overline{\mathbf{3}},1)$	-1	0	0	-1	$-4/3$	-1
$BC\alpha^1$	1	$(1,\mathbf{2})$	-1	0	1	0	-1	$-3/4$
α^2	1	$(1,\mathbf{2})$	0	-1	1	0	1	$-3/4$
$BC'\alpha^1$	3	$(1,\mathbf{2})$	-1	0	-1	0	-1	$-5/4$
α^2	3	$(1,\mathbf{2})$	0	-1	-1	0	1	$-5/4$
$BB'\alpha^0$	4	$(1,1_a)$	0	0	2	0	0	$1/2$
	6	$(1,1_a)+(1,\mathbf{3}_s)$	0	0	2	0	0	$1/2$
$CC'\alpha^0$	2	$(1,1)$	1	1	0	0	0	2

Table 3.4: Chiral fermionic spectrum from intersecting D8-branes, example 1a.

3.4.2 Example 1b: $SU(3)\times SU(2)\times U(1)^2$ and four generations

The chiral fermion content of example 1a discussed in section 3.4.1 contains a different number of particles and anti-particles , namely four candidates for quarks and six candidates for anti-quarks, and also a different amount of quarks and leptons. Bearing in mind the considerations made in engineering model 1a, we modify the third type of D8-brane C such that the amount of quarks and leptons matches. This can be achieved by

$$\begin{aligned} N_A^1 &= 3, \qquad & (n_A,m_A) &= (2,-1),\\ N_B^0 &= 2, \qquad & (n_B,m_B) &= (4,-1),\\ N_C^1 &= 1, \qquad & (n_C,m_C) &= (2,-1), \end{aligned} \tag{3.53}$$

if the stacks C and A are parallely displaced. The separation of the D8-branes serves to break $SU(4)$ down to $SU(3)\times U(1)$. In the T-dual picture, distances

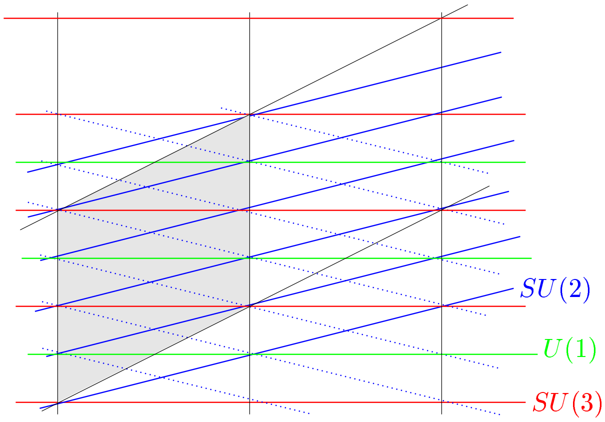

Figure 3.3: Example 1b: D8-brane configuration on T_1.

translate into Wilson lines. The D8-brane configuration is displayed in figure 3.3. As one can easily see from this figure, locating the stack C at $X^5 = R_2/4$ and taking into account lattice shifts gives again an $\Omega\mathcal{R}_1$ invariant configuration.[1] In this case, we obtain four generations of quarks and leptons as well as several exotic fermions. The complete spectrum is listed in table 3.5. In this case, Q_B^0 becomes massive while Q_A^1 and Q_C^1 are anomaly-free by themselves. The linear combination $Q_Y = \frac{Q_A^1}{3} + Q_C^1$ can be interpreted as the standard model hypercharge.

3.4.3 Example 2a: $SU(3) \times SU(2)_L \times SU(2)_R \times SO(8) \times U(1)^3$ and three generations

So far, we have only managed to engineer an even number of generations of the standard model gauge group even though we have switched on a non-trivial background field b. The following examples are chosen to be left-right symmetric and contain three generations of left-handed quarks and leptons. We again choose the $SU(3)$ factor to arise from the $\Omega\mathcal{R}_1$ invariant position and the $SU(2)_L \times SU(2)_R$ factors to be supported by D8-branes at non-trivial angles. In order to fulfill the tadpole cancellation conditions (3.26), (3.27), an additional gauge group $SO(8)$ as well as an anti-D8-brane have to be included. The D8-brane configuration of

[1] Locating a D8$_c$-brane at $X^5 = R_2/4$ is convenient, but not necessary. For $m_c + bn_c = 0$, equation (3.21) does not give any constraint on the γ matrices. The second choice consistent with the closure of the orbifold group is $\gamma^c_{\Omega\mathcal{R}_1} = \gamma^{c'}_{\Omega\mathcal{R}_1} = \mathbb{I}_{N_c}$ and $\gamma^c_\Theta = \gamma_\Theta^{-1,c'} = \mathrm{diag}\left(\mathbb{I}_{N_c^0}, e^{2\pi i/3}_{N_c^1}, e^{-2\pi i/3}_{N_c^2}\right)$ for $c \neq c'$. In this case, N_c^1 and N_c^2 can be chosen independently.

Chiral fermionic spectrum for example 1b					
	mult.	rep. of $SU(3)\times SU(2)$	Q_B^0	Q_A^1	Q_C^1
$AB\alpha^1$	2	$(\overline{\mathbf{3}},\mathbf{2})$	-1	-1	0
α^2	2	$(\mathbf{3},\mathbf{2})$	-1	1	0
$BC\alpha^1$	2	$(1,\mathbf{2})$	-1	0	-1
α^2	2	$(1,\mathbf{2})$	-1	0	1
$BB'\alpha^0$	10	$(1,1_a)$	2	0	0
	6	$(1,\mathbf{3}_s)$	2	0	0

Table 3.5: Chiral fermionic spectrum from intersecting D8-branes, example 1b.

our first choice

$$\begin{array}{rcl} \left.\begin{array}{l} N_A^0=8 \\ N_A^1=3 \end{array}\right\} & (n_A,m_A) & = & (2,-1), \\ N_B^1=2, & (n_B,m_B) & = & (1,0), \\ N_C^1=1, & (n_C,m_C) & = & (-1,0), \end{array} \tag{3.54}$$

with a parallel displacement of the D8-branes B and anti-D8-brane C is shown in figure 3.4. The complete spectrum is listed in table G.2 in the appendix. It contains three generations of quarks and leptons as well as their anti-particles. In addition, it contains exotic matter transforming in the fundamental representation of $SO(8)$, a $(\mathbf{2},\mathbf{2})$ of $SU(2)_L\times SU(2)_R$ whose tachyonic partner could be interpreted as a non-standard Higgs particle and several singlets of the non-Abelian gauge groups. The anomaly-free $U(1)$s are given by

$$\begin{aligned} Q_{B-L} &= -\frac{1}{3}Q_A^1+Q_C^1-Q_C^2, \\ Q' &= -\frac{2}{3}Q_A^1+Q_B^1-Q_B^2, \\ Q'' &= \frac{1}{4}\left(Q_B^1+Q_B^2+2Q_C^1+2Q_C^2\right), \end{aligned} \tag{3.55}$$

where Q_{B-L} can be interpreted as Baryon - Lepton number occurring in left-right symmetric models.

There are two facts which have to be taken care of when including anti-D8-branes. On the one hand, the GSO projection in the D8-brane - anti-D8-brane sector is opposite to the usual one and results in selecting the reverse

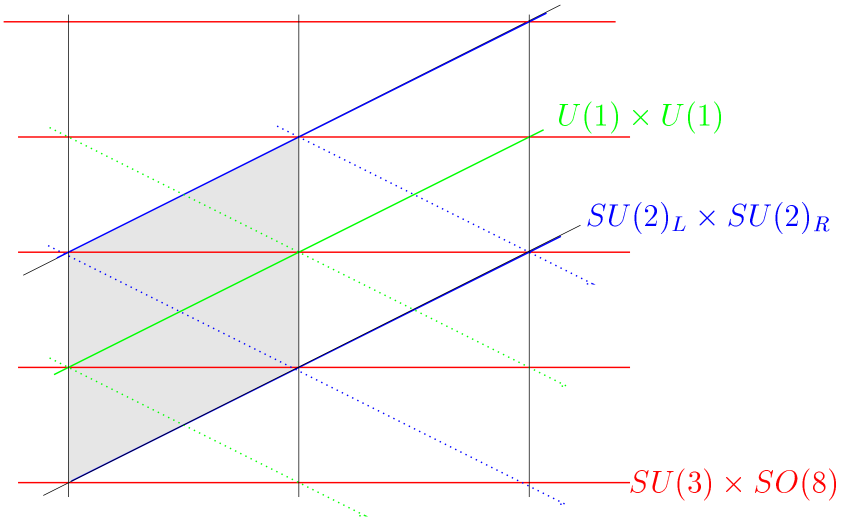

Figure 3.4: Example 2a: D8-brane configuration on T_1.

chirality. On the other hand, the $\Omega\mathcal{R}_1$ projection in the R sector of the CC' strings selects the symmetric instead of the antisymmetric representation. Due to the displacement of the stacks B and C, there will be no tachyons stretched between parallel B-branes and anti-C-branes as long as the radii R_1 and R_2 are chosen big enough.

In this example, tachyonic pseudo-superpartners $\psi^1_{\Delta\varphi-1/2}|0\rangle_{NSNS}$ occur in the $AB\alpha^0$, $BB'\alpha^0$ and $CC'\alpha^0$ sectors. In the $AC\alpha^0$ and $BC'\alpha^0$ sectors, the reversed GSO projection leaves the tachyonic groundstate $|0\rangle_{NSNS}$ invariant.

3.4.4 Example 2b: $SU(3) \times SU(2)_L \times SU(2)_R \times SO(8) \times U(1)^2$ and three generations

As a last example, we start with the same $SU(3)\times SU(2)_L\times SU(2)_R$ configuration as in example 2a, but choose the anti-D8-brane C to be $\Omega\mathcal{R}_1$ invariant and parallely displaced relative to the $SU(3)$ stack. The D8-brane positions resulting from

$$\begin{array}{rcl} \left.\begin{array}{r} N_A^0 = 8 \\ N_A^1 = 3 \end{array}\right\} & (n_A, m_A) = & (2,-1), \\ N_B^1 = 2, & (n_B, m_B) = & (1,0), \\ N_C^1 = 1, & (n_C, m_C) = & (-2,1) \end{array} \tag{3.56}$$

are displayed in figure 3.5. The complete chiral spectrum is listed in table G.3

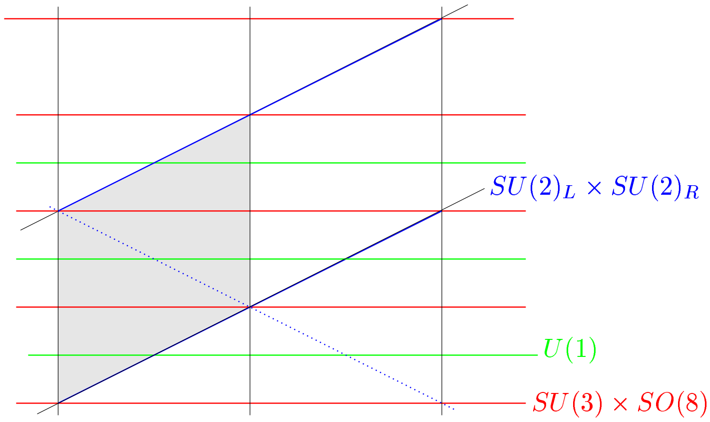

Figure 3.5: Example 2b: D8-brane configuration on T_1.

of appendix G.2, and the anomaly free $U(1)$ factors are given by

$$\begin{aligned} Q_{B-L} &= -\frac{1}{3}Q_A^1 - Q_C^1, \\ Q' &= Q_B^1 - Q_B^2 + 2Q_C^1. \end{aligned} \tag{3.57}$$

In this case, the spectrum contains three generations of left- and right-handed quarks and leptons beside some exotic matter. The GSO projection is reversed in the AC and BC sectors, and tachyons with the same representation of the gauge group as the fermions appear in the $AB\alpha^0$, $BB'\alpha^0$ and $BC\alpha^0$ sectors.

3.5 Mass and gauge hierarchies

The D8-brane models discussed in this chapter have a dual description in terms of intersecting D4-branes. Applying T-duality along all four directions $X^{6,\dots,9}$ of the orbifold, the action of the orientifold becomes $\Omega\mathcal{R}_1 I_4$ where I_4 is the reflection of all four T-dual coordinates $I_4 : X^{6,\dots,9} \to -X^{6,\dots,9}$, and the orbifold volume is transverse to all D4-branes. Within this framework, the hierarchy between the electro weak and the Planck scale can be explained by a large compact transverse volume [112, 87, 7, 6, 72].

The effective ten dimensional Lagrangian of the orientifold theory contains the relevant gravitational part [94]

$$\mathcal{S}_{10} = -\frac{1}{2\kappa^2}\int \mathrm{d}^{10}x\sqrt{-G}\frac{1}{\lambda_s^2}R_{(10)} + \dots,$$

where $\kappa^2 = \frac{1}{2}(2\pi)^7\alpha'^4$ is the ten dimensional gravitational coupling constant, $\lambda_s = e^{\Phi_s}$ contains the dilaton Φ_s of type I superstring theory and $R_{(10)}$ is the ten dimensional curvature.

The Dirac-Born-Infeld action of a Dp_a-brane is given by [94]

$$\mathcal{S}_{Dp_a} = -T_p \int_{Dp_a} \mathrm{d}^{p+1}x \frac{1}{\lambda_s} \sqrt{-\det\left(G + B + 2\pi\alpha' F_a\right)}, \tag{3.59}$$

where

$$T_p = (2\pi)^{-p} \alpha'^{-(p+1)/2}$$

is the tension of a Dp-brane and a rescaling $F_a \to 2\pi\alpha' F_a$ as compared to (3.48) has been performed in order to obtain the canonical normalization.

Upon dimensional reduction to four dimensions, the effective Lagrangian becomes

$$\mathcal{S}_4 = -\int \mathrm{d}^4x \sqrt{-G} \left(\frac{1}{2\kappa^2} \frac{V_6}{\lambda_s^2} R + \frac{V_{p-3}}{(2\pi)^{p-2} \sqrt{\alpha'}^{p-3} 4\lambda_s} F_a^2 + \dots \right),$$

where V_6 is the complete compact volume and V_{p-3} is the compact $(p-3)$ cycle wrapped by the Dp-brane. Identifying the coefficient of the curvature with $(16\pi G_N)^{-1}$ where G_N is Newton's constant and the coefficient of the field strength with $(4g_a^2)^{-1}$ where g_a is the four dimensional gauge coupling gives the following results for D4-branes [2]

$$\frac{1}{\sqrt{G_N}} = M_P = \frac{\sqrt{R_1 R_2 \omega}}{\sqrt{2}\pi^3 \lambda_s \alpha'}, \tag{3.62}$$

$$\frac{4\pi^2}{g_a^2} = \frac{M_s}{\lambda_s} L_a, \tag{3.63}$$

where $R_1 R_2$ is the volume of the two torus T_1, ω is the dimensionless volume of the four dimensional orbifold as given in appendix E.1, L_a is the length (3.5) of the 1-cycle which the D4_a-brane wraps on T_1, and $M_s = 1/\sqrt{\alpha'}$ is the string scale.

In order not to obtain too small gauge couplings, the radii R_1, R_2 may not be chosen too large according to equation (3.63). The string scale M_s can, however, be lowered down to about $1 - 10$ TeV by taking the orbifold volume $V_{orb} \equiv \omega\alpha'^2 \sim \mathcal{O}([10^9(\mathrm{TeV})^{-1}]^4)$.

One further feature of the picture with D-branes at angles is the fact that Yukawa couplings are exponentially suppressed in terms of the area A_{ijk} which is bounded by the three types of D-branes involved [2],

$$Y_{ijk} = \exp\left(-A_{ijk}\right). \tag{3.64}$$

The Higgs field H^i and the two fermions F_R^j, F_L^k involved are located at the three different vertices which the D-branes at angles generate.

As for the gauge couplings, in order to avoid too small Yukawa couplings, the areas A_{ijk} may not become too large according to formula (3.64).

Applying the relationship (3.63) to the examples discussed in section 3.4, we obtain

$$\frac{\alpha_{QCD}}{\alpha_2} = 2\sqrt{1+\frac{1}{16}\frac{1}{u^4}} \quad \text{for examples 1a and 1b,}$$
$$\frac{\alpha_{QCD}}{\alpha_2} = \frac{1}{2}\sqrt{1+\frac{1}{4}\frac{1}{u^4}} \quad \text{for examples 2a and 2b,}$$

where $u=\sqrt{R_1/R_2}$ is as defined in section 3.3. These values are only valid at tree level at the string scale M_s. In order to make contact with the observed data at the electroweak scale, the running of couplings as well as loop corrections which might be large would have to be taken into account.

The qualitative behavior of Yukawa couplings (3.64) can be nicely read off from figure 3.2 for example 1a. The sizes A_{ijk} of the smallest triangular worldsheets in units of $\frac{R_1R_2}{\alpha'}$ are $\frac{1}{48}, \frac{1}{16}, \frac{1}{12}$ and $\frac{1}{4}$. There exist, however, also trilinear couplings which arise from one single intersection point. The reason for this is that in example 1a, two quark generations $Q_L^{1,2}$ are realized as $(\overline{\mathbf{3}}, \mathbf{2})$ and the other two $Q_L^{3,4}$ as $(\mathbf{3}, \mathbf{2})$ in the AB sector. Couplings to Higgs scalars h from the BB' sector are allowed by regarding the quantum numbers. Since the position of D8-branes A is chosen to be $\Omega\mathcal{R}_1$ invariant, the intersection points of AB are also intersection points of BB'. The same argumentation applies to leptonic Yukawa couplings since the D8-brane positions of stacks B and C are chosen such that the intersection loci of BC, BC' and CC' on the $\Omega\mathcal{R}_1$ invariant axis coincide.

The AB and BB' sectors of example 1b are identical to those of example 1a. Therefore, the same Yukawa couplings for the quark sector arise. The different choice of the D8-brane C results in leptons being located at the intersections of stacks B and C which do not coincide with any intersection point of the BB' sector. As a result, all leptonic Yukawa couplings are suppressed in terms of a non-vanishing worldsheet.

Let us now briefly comment on example 2b. In this case, all left handed quarks Q_L^i $(i=1,2,3)$ are realized as $(\overline{\mathbf{3}}, \mathbf{2}_L)$ while all right handed quarks Q_R^j $(j=1,2,3)$ transform as $(\mathbf{3}, \mathbf{2}_R)$. All quarks arise from the AB sector where A is the $\Omega\mathcal{R}_1$ invariant stack of D8-branes. The BB' sector can provide Higgs scalars h in the $(\mathbf{2}_L, \mathbf{2}_R)$ with $U(1)$ charges $Q_B^1 = Q_B^2 = \pm 1$. The quantum numbers thus allow for trilinear couplings of the form $hQ_L^iQ_R^j$ for $i,j=1,2$ and $i=j=3$ since the third generation differs in the quantum numbers Q_B^1, Q_B^2 from the other two. In the same spirit, trilinear couplings $hL_L^iL_R^j$ of a Higgs particle with two leptons L_L^i, L_R^j are allowed for $i,j=1,2$ and $i=j=3$. But in contrast to the couplings involving quarks, the leptons arise from the BC sector which does not have any common intersection point with the BB' sector. Naively, one can therefore speculate that quark and lepton masses are generated from couplings to the same Higgs scalars h acquiring a vacuum expectation value, and that there will be a hierarchy of quark and lepton masses since the relevant worldsheets are of the order $A_{hQQ} = 0$ and $A_{hLL} \sim \mathcal{O}(\frac{R_1 R_2}{\alpha'})$. This naive interpretation, however, has to be handled with care since not all types of couplings to Higgses might occur, e.g. if only one type of scalar particles h with $Q_B^1 = Q_B^2 = 1$ exists and no couplings $\overline{h}QQ$ are allowed.

The same arguments hold for example 2a since the AB and BB' sectors are the same as in example 2b, and also in this case no common intersection point of BB' and BC' exists. In addition, Yukawa couplings between quarks and anti-quarks occur and are suppressed by the same mechanism as the leptonic ones.

Chapter 4

Summary and conclusions

In this thesis, supersymmetry breaking via D-branes at angles in orientifold models of type II superstring theories is investigated. Two different classes of models are discussed. In chapter 2, the orientifold projector is chosen such that D6-branes are required to cancel the RR charges of the orientifold planes, whereas in chapter 3 D8-branes are needed.

The orientifold projection contains a reflection $\mathcal{R}_i$ of i internal coordinates leading to O$(9-i)$-planes. The reflection can be rephrased as a complex conjugation of i complex coordinates. The RR charge cancellation condition enforces the existence of a suitable amount of D$(9-i)$-branes and their mirror images under the reflection. Partial supersymmetry breaking is achieved by the introduction of a four dimensional orbifold. The action of the orbifold symmetry on the Chan-Paton factors of the open string sector depends on the choice of the orientifold projection.

In chapter 2, the orientifold projection $\Omega\mathcal{R}_3$ maps the orbifold generator Θ to its inverse,

$$\Omega\mathcal{R}_3\Theta = \Theta^{-1}\Omega\mathcal{R}_3.$$

A generic $\mathbb{Z}_M$ generator rotates the positions of the D6-branes. Only a $\mathbb{Z}_2$ rotation maps D6-branes onto themselves while acting non-trivially on the Chan-Paton labels of the open string states. The D6-branes are chosen to lie on top of the O6-planes along the directions of the orbifold. Supersymmetry breaking is achieved by allowing for non-trivial intersection angles of the D6-branes on the additional two torus. The D6-branes support non-Abelian gauge groups on their worldvolume, and at the intersection point of two D6-branes chiral fermions in the bifundamental of the gauge groups are located.

We have explicitly shown the computation of the 1-loop closed and open string amplitudes, namely the Klein bottle, Möbius strip and annulus. The tree channel amplitudes have been obtained by modular transformation. In addition, we have shown the direct computation in the tree channel by means of the boundary state approach. The consistency of the two approaches, the worldsheet duality, gives additional constraints on the geometry of the compactification for the D6-brane models. Two different orientations of the tori, the **A** and **B** type lattices, are consistent with the reflection $\mathcal{R}_3$. The orbifold group acts non-trivially on the zero mode contributions to the loop amplitudes. In order to obtain the complete projector in the tree channel, only the combination **AB** for the orbifold lattice is allowed in the case of a $\mathbb{Z}_4$ and $\mathbb{Z}_6$ symmetry whereas no constraints arise for $\mathbb{Z}_2$ and $\mathbb{Z}_3$.

The tadpole cancellation conditions are given in equation (2.24). The analysis is performed for a rectangular two torus corresponding to a trivial background in the T-dual language but can easily be generalized to tilted tori or, equivalently, a non-vanishing antisymmetric NSNS tensor background in the T-dual model. The closed string spectrum is $\mathcal{N}=2$ supersymmetric in four dimensions. The open string sector contains the $\mathcal{N}=2$ supersymmetric gauge fields with gauge groups [48]

$$\begin{array}{rc} \mathbb{Z}_3: & \prod_{m_a\neq 0} U(N_a) \prod_{m_a=0} SO(N_a), \\ \mathbb{Z}_{2,4,6}: & \prod_{m_a\neq 0} U(N_a/2)^4 \prod_{m_a=0} U(N_a/2)^2. \end{array}$$

The open sector also contains strings with endpoints on two different kinds of D6-branes. These sectors provide chiral fermions in the bifundamental of the two gauge groups supported on the worldvolume of the D6-branes. Since the orbifold group $\mathbb{Z}_3$ acts trivially on the Chan-Paton labels, each chiral fermion is accompanied by a tachyon in the same representation. This situation is different for $\mathbb{Z}_{2,4,6}$. The mass eigenstates differ in their $\mathbb{Z}_2$ parity. Therefore, only chiral fermions with even parity have tachyonic pseudo superpartners. We have explicitly given examples for $\mathbb{Z}_2$ and $\mathbb{Z}_3$. Excluding anti-D-branes, for $\mathbb{Z}_3$ the maximal gauge group obtainable is $SU(3)\times U(1)$ if we require the presence of chiral fermions. The resulting spectrum is listed in table 2.2. We have also worked out an example for $\mathbb{Z}_2$ which encloses the standard model gauge group as well as several non-anomalous $U(1)$ factors and some exotic matter. We have argued that the anomalous $U(1)$s couple to untwisted closed string modes thus becoming massive by a generalized Green-Schwarz mechanism. The anomaly free $U(1)$s are displayed in equation (2.44), and the chiral spectrum is listed in table D.2. However, in this framework we can neither obtain a three generation model nor give an obvious solution to the hierarchy problem.

In chapter 3, the reflection is chosen to act only on one two torus. The orbifold group affects the other tori. Therefore the orientifold and orbifold generators commute,

$$\Omega\mathcal{R}_1\Theta = \Theta\,\Omega\mathcal{R}_1.$$

RR charge cancellation requires D8-branes which wrap a 1-cycle on the two torus and are extended along all four orbifold directions. In contrast to the models discussed in chapter 2, the orbifold group acts non-trivially on the Chan-Paton labels. While the reflection $\Omega\mathcal{R}_3$ enforces the existence of D6-branes for all kinds of four dimensional orbifolds, $\Omega\mathcal{R}_1$ generically requires both D8- and D4-branes at the same time. Only in the case of no $\mathbb{Z}_2$ subsymmetry, i.e. a $\mathbb{Z}_3$ orbifold, consistent models with only D8-branes exist. In this case, the models are T-dual to orientifolds with a different orientifold group generator $\Omega\mathcal{R}_1 I_4$ and only D4-branes where I_4 is the reflection along all transversal orbifold coordinates. This kind of model offers the possibility of solving the mass hierarchy problem by large transverse dimensions as suggested in [7, 6]. The generic RR tadpole cancellation conditions (3.26), (3.27) do not only constrain the amount of D8-branes with identical position, but determine also the action on the Chan-Paton matrices which effectively decomposes a stack of N_a $\mathrm{D8}_a$-branes into i subsystems N_a^i with $\mathbb{Z}_3$ eigenvalues α^i. The resulting gauge group is [65]

$$\mathbb{Z}_3: \qquad \prod_{m_a+bn_a\neq 0}\left[\prod_{i=0}^{2} U(N_a^i)\right]\prod_{m_a+bn_a=0} SO(N_a^0)\times U(N_a^1).$$

As for the models with D6-branes, the loop and tree channel amplitudes relevant for RR tadpole cancellation are calculated. In this class of models, worldsheet duality does not give any additional constraints on the lattices. The generic chiral spectrum is displayed in table 3.1. Only those mass eigenstates which have trivial $\mathbb{Z}_3$ eigenvalue have a tachyonic pseudo superpartner. Therefore, tachyons can be partially projected out as compared to the models discussed in chapter 2. The tadpole cancellation conditions are, however, very restrictive and therefore any model with a phenomenologically interesting gauge group and chiral spectrum will contain a tachyon. We have argued that $U(1)$ anomalies are canceled by a generalized Green-Schwarz mechanism involving closed string modes from the twisted sector. The instability of the model does not only manifest itself in the appearance of a tachyon, but also in the existence of non-vanishing NSNS tadpoles which we have computed to linear order in the moduli of the orbifold. Furthermore, we have given two explicit examples of embedding the standard model gauge group in this class of intersecting D8-brane scenarios. These examples lead to an even number of generations. A more promising ansatz consists in considering left-right symmetric models with three generations. We have also shown two examples of this type which comprise some exotic matter besides the left-right symmetric extension of the standard model. The tachyons which occur in the spectrum have the correct quantum numbers for being interpreted as non-standard Higgs particles.

In summary, in this thesis model building from type IIA orientifolds preserving $\mathcal{N}=2$ supersymmetry in the gravity and gauge sectors with chiral fermions from supersymmetry breaking intersections of D-branes have been investigated. The set-up offers a rich variety of engineering different gauge groups and obtaining replication of generations from multiple D-brane intersections. We have shown for the first time how to incorporate four dimensional chiral spectra from D-branes at angles with a reduced amount of supersymmetry in the gauge and gravity sector. Furthermore, with this requirement we have succeeded in constructing models with a reduced amount of tachyons and shown that an interpretation in terms of non-standard Higgs particles is appealing. In addition, we have for the first time performed an orientifold construction with D-branes at angles which admits for large transverse dimensions and is by this means capable of solving the hierarchy problem.

Models with intersecting D-branes clearly still deserve to be further explored. On the one hand, it will be interesting to consider the NSNS tadpoles beyond the linear order in the orbifold moduli since they might play a role in stabilizing the D8-brane models. In the T-dual models, locating D4-branes at different fixed points in the transverse space might also lead to different models, and it would be worthwhile to consider inflationary scenarios along the idea of intersecting D4-branes in purely toroidal type IIA compactifications presented in [51] for explicit orientifold models. Other possibilities of obtaining improved models consist in considering more complicated orbifold and orientifold groups. A very recent ansatz [25] uses even a different GSO projection leading to an orientifold of type 0' string theory. Also in this case, non-trivial intersection angles of D6-branes are accompanied by a non-vanishing dilaton tadpole. Therefore, another challenge within intersecting D-brane model building consists in including the Fischler Susskind mechanism [44] and exploring how it affects measurable quantities.

Appendix A

Notation and conventions

The bosonic closed string coordinates which solve the two dimensional equation of motion can be decomposed into a left- and a right-moving part depending on the light-cone coordinates of the worldsheet $\sigma_\pm = \tau \pm \sigma$,

$$X^\mu(\tau,\sigma) = X^\mu_L(\sigma_+) + X^\mu_R(\sigma_-), \tag{A.1}$$

with the mode expansions

$$X^\mu_L(\sigma_+) = \frac{x^\mu}{2} + \frac{p^\mu_L}{2}\sigma_+ + \frac{i}{\sqrt{2}}\sum_{n\neq 0}\frac{\alpha^\mu_n}{n}e^{in\sigma_+}, \tag{A.2}$$

$$X^\mu_R(\sigma_-) = \frac{x^\mu}{2} + \frac{p^\mu_R}{2}\sigma_- + \frac{i}{\sqrt{2}}\sum_{n\neq 0}\frac{\tilde{\alpha}^\mu_n}{n}e^{in\sigma_-}, \tag{A.3}$$

where x^μ and $p^\mu = \frac{1}{2}\left(p^\mu_L + p^\mu_R\right)$ are the center-of-mass position and momentum in units of α', respectively. The fermionic coordinates can be expanded in a similar manner, namely

$$\Psi^\mu(\tau,\sigma) = \Psi^\mu_L(\sigma_+) + \Psi^\mu_R(\sigma_-), \tag{A.4}$$

$$\Psi^\mu_L(\sigma_+) = \sum_r \psi^\mu_r e^{i\pi\sigma_+}, \tag{A.5}$$

$$\Psi^\mu_R(\sigma_-) = \sum_r \tilde{\psi}^\mu_r e^{i\pi\sigma_-}, \tag{A.6}$$

where the index r runs over integers in the untwisted R sector and over half-integers in the untwisted NS sector. The non-trivial commutation relations of the raising and lowering operators are given by

$$\begin{aligned}
[\alpha^\mu_n, \alpha^\nu_m] &= [\tilde{\alpha}^\mu_n, \tilde{\alpha}^\nu_m] = n\delta_{n,-m}\delta^{\mu\nu}, \\
\{\psi^\mu_r, \psi^\nu_s\} &= \left\{\tilde{\psi}^\mu_r, \tilde{\psi}^\nu_s\right\} = \delta_{r,-s}\delta^{\mu\nu}.
\end{aligned}$$

For compact coordinates on a two torus, it is useful to define complex oscillators, e.g.

$$\alpha^{1,\bar{1}} = \frac{1}{\sqrt{2}} \left(\alpha^4 \pm i\alpha^5 \right). \tag{A.7}$$

The non-trivial commutation relations then read $(i, j = 1, 2, 3)$

$$\left[\alpha_n^i, \alpha_m^{\bar{j}}\right] = \left[\tilde{\alpha}_n^i, \tilde{\alpha}_m^{\bar{j}}\right] = n\delta_{n,-m}\delta^{i\bar{j}}, \tag{A.8}$$

$$\left\{\psi_r^i, \psi_s^{\bar{j}}\right\} = \left\{\tilde{\psi}_r^i, \tilde{\psi}_s^{\bar{j}}\right\} = \delta_{r,-s}\delta^{i\bar{j}}. \tag{A.9}$$

The orientifold group action is given by (μ labels the non-compact coordinates in light cone gauge and $j = 2, 3$ the second and third torus)

$$\begin{aligned} (\Omega\mathcal{R}_i)\alpha_r^\mu(\Omega\mathcal{R}_i)^{-1} &= \tilde{\alpha}_r^\mu, \\ (\Omega\mathcal{R}_i)\alpha_r^{1,\bar{1}}(\Omega\mathcal{R}_i)^{-1} &= \tilde{\alpha}_r^{\bar{1},1}, \\ (\Omega\mathcal{R}_3)\alpha_r^{j,\bar{j}}(\Omega\mathcal{R}_3)^{-1} = \tilde{\alpha}_r^{\bar{j},j}, \qquad (\Omega\mathcal{R}_1)\alpha_r^{j,\bar{j}}(\Omega\mathcal{R}_1)^{-1} &= \tilde{\alpha}_r^{j,\bar{j}}, \end{aligned} \tag{A.10}$$

and analogously for the fermionic sectors with the minus sign included as described in section 1.2.

The Hamiltonian is given by

$$H = H_L + H_R, \tag{A.11}$$

with $(i, j = 1, 2, 3)$

$$\begin{aligned} H_L = \frac{1}{4}p_L^2 &+ \sum_{m_\mu>0} \alpha^\mu_{-m_\mu}\alpha^\mu_{m_\mu} + \sum_{r_\mu>0} r_\mu \psi^\mu_{-r_\mu}\psi^\mu_{r_\mu} \\ &+ \sum_{k_i>0} \alpha^{\bar{i}}_{-k_i}\alpha^i_{k_i} + \sum_{l_i>0} \alpha^i_{-l_i}\alpha^{\bar{i}}_{l_i} \\ &+ \sum_{s_i>0} s_i\psi^{\bar{i}}_{-s_i}\psi^i_{s_i} + \sum_{t_i>0} t_i\psi^i_{-t_i}\psi^{\bar{i}}_{t_i} + E_0 \end{aligned} \tag{A.12}$$

and similarly for H_R with energy and time measured in units of the string scale α'. In the complex notation, these definitions carry over to the twisted sectors where the oscillator indices are in $\mathbb{Z} + nv_i$ for bosons and R sector fermions and in $\mathbb{Z} + \frac{1}{2} + nv_i$ for NS sector fermions. The zero point energy for the moding $\mathbb{Z} + \nu$ of a complex boson is given by

$$E_0^{b,j} = -\frac{1}{12} + \frac{1}{2}\nu\left(1 - \nu\right) \tag{A.13}$$

and for a complex fermion by

$$E_0^{f,j} = -\frac{1}{24} + \frac{1}{2}\left(\frac{1}{2} - \nu\right)^2. \tag{A.14}$$

Appendix B

1-loop diagrams for O6-plane / D6-brane interactions

The tadpole cancellation conditions are determined by computing those diagrams in the loop channel which correspond to RR exchanges in the tree channel. As explained in section 1.4, the relevant contributions arise from the NSNS sector with $(-1)^F$ insertion for the Klein bottle, R for the Möbius strip and NS with $(-1)^F$ insertion for the annulus.

B.1 Lattice contributions

On a torus with radii $R_{1,2}$, only momenta along the $\Omega\mathcal{R}_3$ invariant direction and windings perpendicular to the former one contribute. In the loop channel, the general expression for the lattice contribution is given by

$$\mathcal{L}^{R_1,R_2}[\alpha,\beta](t) \equiv \left(\sum_{m\in\mathbb{Z}} e^{-\alpha\pi t m^2/\rho_1}\right)\left(\sum_{n\in\mathbb{Z}} e^{-\beta\pi t n^2\rho_2}\right), \tag{B.1}$$

where $\rho_i = R_i^2/\alpha'$. Using the one dimensional Poisson resummation formula

$$\sum_{n\in\mathbb{Z}} e^{-\pi/t(n+b/2\pi i)^2} = \sqrt{t}\sum_{n\in\mathbb{Z}} e^{-\pi t n^2+bn} \tag{B.2}$$

gives the general expression for the lattice contribution in the tree channel

$$\tilde{\mathcal{L}}^{R_1,R_2}[\alpha,\beta](t) \equiv \left(\sum_{m\in\mathbb{Z}} e^{-\alpha\pi t m^2\rho_1}\right)\left(\sum_{n\in\mathbb{Z}} e^{-\beta\pi t n^2/\rho_2}\right). \tag{B.3}$$

(B.1) and (B.3) are related via

$$\mathcal{L}^{R_1,R_2}[\alpha,\beta](t) = cl\tilde{\mathcal{L}}^{R_1,R_2}[\frac{\kappa}{\alpha},\frac{\kappa}{\beta}]\,(l)\,, \tag{B.4}$$

with $c = \frac{\kappa}{\sqrt{\alpha\beta}}\frac{R_1}{R_2}$, $t = 1/(\kappa l)$ and $\kappa = 4$ $(2, 8)$ for the Klein bottle (annulus, Möbius strip). The results for the different tori are summarized in table B.1.

The result for the $\mathbf{b}$ type lattice can be recast in the notation introduced in

			$\mathbb{Z}_{2,4}$		$\mathbb{Z}_{3,6}$	
	a	**b**	**A**	**B**	**A**	**B**
$\mathcal{L}^{\mathcal{K}}$	$\mathcal{L}^{R_1,R_2}[1,1]$	$\mathcal{L}^{R,R}[1/\cos^2\alpha, 4\sin^2\alpha]$	$\mathcal{L}^{R,R}[1,1]$	$\mathcal{L}^{R,R}[2,2]$	$\mathcal{L}^{R,R}[4,3]$	$\mathcal{L}^{R,R}[4/3,1]$
$\tilde{\mathcal{L}}^{\mathcal{K}}$	$\tilde{\mathcal{L}}^{R_1,R_2}[4,4]$	$\tilde{\mathcal{L}}^{R,R}[4\cos^2\alpha, 1/\sin^2\alpha]$	$\tilde{\mathcal{L}}^{R,R}[4,4]$	$\tilde{\mathcal{L}}^{R,R}[2,2]$	$\tilde{\mathcal{L}}^{R,R}[1,4/3]$	$\tilde{\mathcal{L}}^{R,R}[3,4]$
$c^{\mathcal{K}}$	$4R_1/R_2$	$2/\tan\alpha$	4	2	$2/\sqrt{3}$	$2\sqrt{3}$
$\mathcal{L}^{\mathcal{A}}$	$\mathcal{L}^{\mathcal{A}}_{\mathbf{a}}$	$\mathcal{L}^{R,R}[2/L_\alpha^2, 2\sin^2(2\alpha)/L_\alpha^2]$	$\mathcal{L}^{R,R}[2,2]$	$\mathcal{L}^{R,R}[1,1]$	$\mathcal{L}^{R,R}[2,3/2]$	$\mathcal{L}^{R,R}[2/3,1/2]$
$\tilde{\mathcal{L}}^{\mathcal{A}}$	$\tilde{\mathcal{L}}^{\mathcal{A}}_{\mathbf{a}}$	$\tilde{\mathcal{L}}^{R,R}[L_\alpha^2, L_\alpha^2/\sin^2(2\alpha)]$	$\tilde{\mathcal{L}}^{R,R}[1,1]$	$\tilde{\mathcal{L}}^{R,R}[2,2]$	$\tilde{\mathcal{L}}^{R,R}[1,4/3]$	$\tilde{\mathcal{L}}^{R,R}[3,4]$
$c^{\mathcal{A}}$	$L_a^2/(R_1R_2)$	$L_\alpha^2/\sin(2\alpha)$	1	2	$2/\sqrt{3}$	$2\sqrt{3}$
$\mathcal{L}^{\mathcal{M}}$	$\mathcal{L}^{R_1,R_2}[2,2]$	$\mathcal{L}^{R,R}[1/(2\cos^2\alpha), 8\sin^2\alpha]$	$\mathcal{L}^{R,R}[2,2]$	$\mathcal{L}^{R,R}[1,4]$	$\mathcal{L}^{R,R}[2,6]$	$\mathcal{L}^{R,R}[2/3,2]$
$\tilde{\mathcal{L}}^{\mathcal{M}}$	$\tilde{\mathcal{L}}^{R_1,R_2}[4,4]$	$\tilde{\mathcal{L}}^{R,R}[16\cos^2\alpha), 1/\sin^2\alpha]$	$\mathcal{L}^{R,R}[4,4]$	$\mathcal{L}^{R,R}[8,2]$	$\mathcal{L}^{R,R}[4,4/3]$	$\mathcal{L}^{R,R}[12,4]$
$c^{\mathcal{M}}$	$4R_1/R_2$	$4/\tan\alpha$	4	4	$4/\sqrt{3}$	$4\sqrt{3}$

Table B.1: The different lattice contributions for a two torus. $L_\alpha = \sqrt{n_a^2 + m_a^2 + 2n_a m_a \cos(2\alpha)}$ for D6-brane models on the $\mathbf{b}$ torus. The definitions of $\mathcal{L}^{\mathcal{A}}_{\mathbf{a}}$ and L_a are given in the text in section 2.1.2.
The $\mathbf{b}$ type lattice is parameterized according to the right hand side of figure B.1.

section 1.2 with non-vanishing background $b = 1/2$ field in the T-dual picture by replacing

$$\begin{aligned}
\tan\alpha &= \frac{R_2}{2R_1}, \\
R^2 &= R_1^2 + (R_2/2)^2, \\
\tilde{\mathbf{e}}_{\mathbf{1}} &= \mathbf{e}_{\mathbf{1}}, \\
\tilde{\mathbf{e}}_{\mathbf{2}} &= \mathbf{e}_{\mathbf{1}} - \mathbf{e}_{\mathbf{2}}, \\
(\tilde{n}, \tilde{m}) &= (n+m, -m),
\end{aligned} \tag{B.5}$$

where the definitions are given in figure B.1.

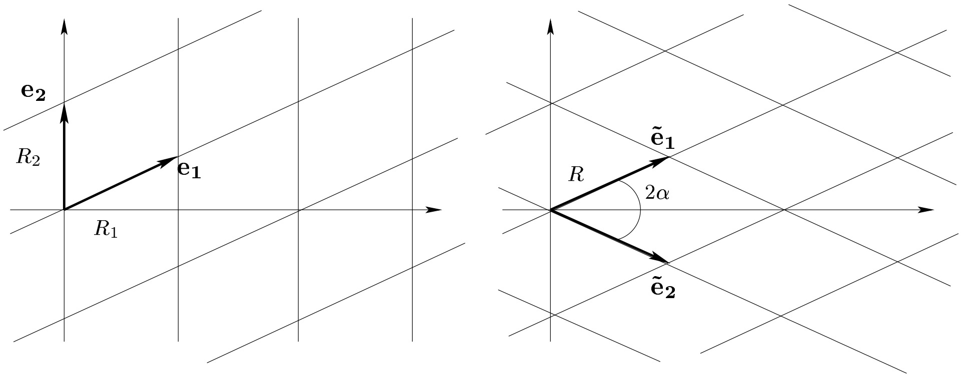

Figure B.1: Two ways to parameterize the lattice with $b = 1/2$.

B.2 Oscillator contributions

The oscillator contributions can be expressed in terms of generalized Jacobi theta functions and the Dedekind eta function ($q \equiv e^{-2\pi t}$),

$$\vartheta\left[\begin{array}{c}\alpha\\ \beta\end{array}\right](t) \equiv \sum_{n\in\mathbb{Z}} q^{(n+\alpha)^2/2} e^{2\pi i(n+\alpha)\beta}, \tag{B.6}$$

$$\eta(t) \equiv q^{1/24}\prod_{n=1}^{\infty}(1-q^n). \tag{B.7}$$

B.2.1 Theta-function-identities

The upper argument α is only defined modulo $\mathbb{Z}$, the lower argument β gives a phase when shifted by 1,

$$\vartheta\left[\begin{array}{c}\alpha\\ \beta+1\end{array}\right](t) = e^{2\pi i\alpha}\vartheta\left[\begin{array}{c}\alpha\\ \beta\end{array}\right](t), \qquad \vartheta\left[\begin{array}{c}\alpha+1\\ \beta\end{array}\right](t) = \vartheta\left[\begin{array}{c}\alpha\\ \beta\end{array}\right](t). \tag{B.8}$$

For $-1/2 < \alpha \leqslant 1/2$, the following product expansion of a Jacobi theta function holds,

$$\frac{\vartheta\left[\begin{array}{c}\alpha\\ \beta\end{array}\right]}{\eta}(t) = e^{2\pi i\alpha\beta} q^{\alpha^2/2-1/24}\prod_{n=1}^{\infty}\left[\left(1+e^{2\pi i\beta}q^{n-1/2+\alpha}\right)\left(1+e^{-2\pi i\beta}q^{n-1/2-\alpha}\right)\right], \tag{B.9}$$

from which the asymptotic behavior for $t \to \infty$ can easily be read off. For D-branes at an angle $\pi\beta \neq 0$ on a two torus, one needs in particular:

$$\frac{\vartheta\left[\begin{array}{c}\frac{1}{2}\\ \beta\end{array}\right]}{\vartheta\left[\begin{array}{c}\frac{1}{2}\\ \beta+\frac{1}{2}\end{array}\right]}(2l) \stackrel{l\to\infty}{\longrightarrow} -\frac{1}{\tan(\pi\beta)}. \tag{B.10}$$

Jacobi theta functions and the Dedekind eta function have the following modular transformation properties:

$$\begin{aligned}\vartheta\left[\begin{array}{c}\alpha\\ \beta\end{array}\right](t) &= e^{2\pi i\alpha\beta}\frac{1}{\sqrt{t}}\vartheta\left[\begin{array}{c}-\beta\\ \alpha\end{array}\right]\left(\frac{1}{t}\right),\\ \eta(t) &= \frac{1}{\sqrt{t}}\eta\left(\frac{1}{t}\right).\end{aligned}$$

For the loop – tree channel correspondence of the Möbius strip, the additional identities for $\alpha \in (-1, 0]$ are useful:

$$\frac{\vartheta\left[\begin{array}{c}\alpha+\frac{1}{2}\\ \beta\end{array}\right]}{\vartheta\left[\begin{array}{c}\alpha+\frac{1}{2}\\ \beta+\frac{1}{2}\end{array}\right]}(t-\frac{i}{2}) = e^{-\pi i\alpha}\frac{\vartheta\left[\begin{array}{c}\frac{\alpha+1}{2}\\ \frac{\alpha}{2}+\beta\end{array}\right]\vartheta\left[\begin{array}{c}\frac{\alpha}{2}\\ \frac{\alpha+1}{2}+\beta\end{array}\right]}{\vartheta\left[\begin{array}{c}\frac{\alpha+1}{2}\\ \frac{\alpha+1}{2}+\beta\end{array}\right]\vartheta\left[\begin{array}{c}\frac{\alpha}{2}\\ \frac{\alpha}{2}+\beta\end{array}\right]}(2t), \tag{B.11}$$

$$\frac{\vartheta\left[\begin{array}{c}\frac{1}{2}\\ 0\end{array}\right]}{\eta^3}(t-\frac{i}{2}) = \frac{\vartheta\left[\begin{array}{c}\frac{1}{2}\\ 0\end{array}\right]\vartheta\left[\begin{array}{c}0\\ \frac{1}{2}\end{array}\right]}{\eta^3\vartheta\left[\begin{array}{c}0\\ 0\end{array}\right]}(2t). \tag{B.12}$$

For $\frac{1}{2t} = 4l$, these lead to the modular transformations

$$\frac{\vartheta\left[\begin{array}{c}\alpha+\frac{1}{2}\\ \beta\end{array}\right]}{\vartheta\left[\begin{array}{c}\alpha+\frac{1}{2}\\ \beta+\frac{1}{2}\end{array}\right]}(t-\frac{i}{2}) = -ie^{-2\pi i(\alpha+\beta)}\frac{\vartheta\left[\begin{array}{c}-(\alpha+2\beta)+\frac{1}{2}\\ (\alpha+\beta)\end{array}\right]}{\vartheta\left[\begin{array}{c}-(\alpha+2\beta)+\frac{1}{2}\\ (\alpha+\beta)+\frac{1}{2}\end{array}\right]}(2l-\frac{i}{2}), \tag{B.13}$$

$$\frac{\vartheta\left[\begin{array}{c}\frac{1}{2}\\ 0\end{array}\right]}{\eta^3}(t-\frac{i}{2}) = \frac{1}{4l}\frac{\vartheta\left[\begin{array}{c}\frac{1}{2}\\ 0\end{array}\right]}{\eta^3}(2l-\frac{i}{2}). \tag{B.14}$$

B.2.2 Oscillator contributions to loop diagrams in D6-brane models

The oscillator contributions in the loop channel in terms of generalized Jacobi theta functions are given by

$$
\begin{aligned}
\mathcal{K}^{(n)} &= \frac{\vartheta\begin{bmatrix} 0 \\ \frac{1}{2} \end{bmatrix}}{\eta^3} \prod_{nv_i \notin \mathbb{Z}} \left(\frac{\vartheta\begin{bmatrix} nv_i \\ \frac{1}{2} \end{bmatrix}}{\vartheta\begin{bmatrix} \frac{1}{2}+nv_i \\ \frac{1}{2} \end{bmatrix}} \right) \prod_{nv_i \in \mathbb{Z}} \left(\frac{\vartheta\begin{bmatrix} 0 \\ \frac{1}{2} \end{bmatrix}}{\eta^3} \right) (2t), && \text{(B.15)} \\
\mathcal{A}_{ab}^{(n,k)} &= i\frac{\vartheta\begin{bmatrix} 0 \\ \frac{1}{2} \end{bmatrix}}{\eta^3} \frac{\vartheta\begin{bmatrix} \Delta\varphi \\ \frac{1}{2} \end{bmatrix}}{\vartheta\begin{bmatrix} \frac{1}{2}+\Delta\varphi \\ \frac{1}{2} \end{bmatrix}} \prod_{(nv_i,kv_i) \notin \mathbb{Z}^2} \left(\frac{(-2i)^{\delta}\,\vartheta\begin{bmatrix} nv_i \\ \frac{1}{2}+kv_i \end{bmatrix}}{\vartheta\begin{bmatrix} \frac{1}{2}+nv_i \\ \frac{1}{2}+kv_i \end{bmatrix}} \right) \\
&\quad \times \prod_{(nv_i,kv_i) \in \mathbb{Z}^2} \left(\frac{\vartheta\begin{bmatrix} 0 \\ \frac{1}{2} \end{bmatrix}}{\eta^3} \right) (t), && \text{(B.16)} \\
\mathcal{M}_{a}^{(n,k)} &= ie^{2\pi i\varphi}\frac{\vartheta\begin{bmatrix} \frac{1}{2} \\ 0 \end{bmatrix}}{\eta^3} \frac{\vartheta\begin{bmatrix} \frac{1}{2}+2\varphi \\ -\varphi \end{bmatrix}}{\vartheta\begin{bmatrix} \frac{1}{2}+2\varphi \\ \frac{1}{2}-\varphi \end{bmatrix}} \prod_{(nv_i,kv_i) \notin \mathbb{Z}^2} \left(\frac{(-2i)^{\delta}\,\vartheta\begin{bmatrix} \frac{1}{2}+nv_i \\ kv_i \end{bmatrix}}{\vartheta\begin{bmatrix} \frac{1}{2}+nv_i \\ \frac{1}{2}+kv_i \end{bmatrix}} \right) \\
&\quad \times \prod_{(nv_i,kv_i) \in \mathbb{Z}^2} \left(\frac{\vartheta\begin{bmatrix} \frac{1}{2} \\ 0 \end{bmatrix}}{\eta^3} \right) (t-\frac{i}{2}), && \text{(B.17)}
\end{aligned}
$$

where

$$
\delta = \begin{cases} 1 & \text{if} \quad (nv_i, kv_i) \in \mathbb{Z} \times \mathbb{Z} + \frac{1}{2}, \\ 0 & \text{else.} \end{cases} \tag{B.18}
$$

B.2.3 Oscillator contributions to tree diagrams in D6-brane models

The oscillator contributions in the tree channel read

$$\tilde{\mathcal{K}}^{(0)} = \frac{\vartheta^4\left[\begin{smallmatrix}\frac{1}{2}\\0\end{smallmatrix}\right]}{\eta^{12}}(2l), \tag{B.19}$$

$$\tilde{\mathcal{K}}^{(k)} = \frac{\vartheta^2\left[\begin{smallmatrix}\frac{1}{2}\\0\end{smallmatrix}\right]}{\eta^6}\frac{\vartheta\left[\begin{smallmatrix}\frac{1}{2}\\k/M\end{smallmatrix}\right]\vartheta\left[\begin{smallmatrix}\frac{1}{2}\\-k/M\end{smallmatrix}\right]}{\vartheta\left[\begin{smallmatrix}\frac{1}{2}\\-\frac{1}{2}+k/M\end{smallmatrix}\right]\vartheta\left[\begin{smallmatrix}\frac{1}{2}\\\frac{1}{2}-k/M\end{smallmatrix}\right]}(2l), \tag{B.20}$$

$$\tilde{\mathcal{A}}_{ab}^{(0)} = \frac{\vartheta\left[\begin{smallmatrix}\frac{1}{2}\\0\end{smallmatrix}\right]^3}{\eta^9}\frac{\vartheta\left[\begin{smallmatrix}\frac{1}{2}\\\Delta\varphi\end{smallmatrix}\right]}{\vartheta\left[\begin{smallmatrix}\frac{1}{2}\\\frac{1}{2}+\Delta\varphi\end{smallmatrix}\right]}(2l), \tag{B.21}$$

$$\tilde{\mathcal{A}}_{ab}^{(k)} = \frac{\vartheta\left[\begin{smallmatrix}\frac{1}{2}\\0\end{smallmatrix}\right]}{\eta^3}\frac{\vartheta\left[\begin{smallmatrix}\frac{1}{2}\\\Delta\varphi\end{smallmatrix}\right]}{\vartheta\left[\begin{smallmatrix}\frac{1}{2}\\\frac{1}{2}+\Delta\varphi\end{smallmatrix}\right]}\frac{\vartheta\left[\begin{smallmatrix}\frac{1}{2}\\k/M\end{smallmatrix}\right]\vartheta\left[\begin{smallmatrix}\frac{1}{2}\\-k/M\end{smallmatrix}\right]}{\vartheta\left[\begin{smallmatrix}\frac{1}{2}\\-\frac{1}{2}+k/M\end{smallmatrix}\right]\vartheta\left[\begin{smallmatrix}\frac{1}{2}\\\frac{1}{2}-k/M\end{smallmatrix}\right]}(2l), \tag{B.22}$$

$$\tilde{\mathcal{M}}_{a}^{(0)} = \frac{\vartheta\left[\begin{smallmatrix}\frac{1}{2}\\0\end{smallmatrix}\right]^3}{\eta^9}\frac{\vartheta\left[\begin{smallmatrix}\frac{1}{2}\\\varphi\end{smallmatrix}\right]}{\vartheta\left[\begin{smallmatrix}\frac{1}{2}\\\frac{1}{2}+\varphi\end{smallmatrix}\right]}(2l-\frac{i}{2}), \tag{B.23}$$

$$\tilde{\mathcal{M}}_{a}^{(k)} = \frac{\vartheta\left[\begin{smallmatrix}\frac{1}{2}\\0\end{smallmatrix}\right]}{\eta^3}\frac{\vartheta\left[\begin{smallmatrix}\frac{1}{2}\\\varphi\end{smallmatrix}\right]}{\vartheta\left[\begin{smallmatrix}\frac{1}{2}\\\frac{1}{2}+\varphi\end{smallmatrix}\right]}\frac{\vartheta\left[\begin{smallmatrix}\frac{1}{2}\\k/M\end{smallmatrix}\right]\vartheta\left[\begin{smallmatrix}\frac{1}{2}\\-k/M\end{smallmatrix}\right]}{\vartheta\left[\begin{smallmatrix}\frac{1}{2}\\-\frac{1}{2}+k/M\end{smallmatrix}\right]\vartheta\left[\begin{smallmatrix}\frac{1}{2}\\\frac{1}{2}-k/M\end{smallmatrix}\right]}(2l-\frac{i}{2}). \tag{B.24}$$

Appendix C

Boundary state approach for O6-plane/D6-brane interactions

C.1 Construction of crosscap states

A comprehensive introduction into the boundary state approach to D-branes is given in [50] and references therein. Appendix A of [5] contains the construction of crosscap states in related models.

C.1.1 Oscillator part

Crosscap states have to fulfill

$$\left[X^i_{L,R}(\sigma,0) - \Theta^k \mathcal{R}_3 X^i_{R,L}(\sigma+\pi,0)\right] |\Omega\mathcal{R}_3\Theta^k\rangle = 0. \tag{C.1}$$

Inserting the mode expansion (A.2), (A.3) gives the constraints in terms of bosonic oscillators

$$\begin{aligned}
(\alpha^\mu_n + (-1)^n \tilde{\alpha}^\mu_{-n})|\Omega\mathcal{R}_3\Theta^k,\eta\rangle &= 0,\\
(\alpha^i_r + (-1)^r e^{2\pi i k v_i} \tilde{\alpha}^{\bar{i}}_{-r})|\Omega\mathcal{R}_3\Theta^k,\eta\rangle &= 0,\\
(\alpha^{\bar{i}}_r + (-1)^r e^{-2\pi i k v_i} \tilde{\alpha}^{i}_{-r})|\Omega\mathcal{R}_3\Theta^k,\ \eta\rangle &= 0.
\end{aligned} \tag{C.2}$$

The constraints for the fermionic oscillators are ($\eta = \pm 1$)

$$\begin{aligned}
(\psi^\mu_r + i\eta e^{-i\pi r} \tilde{\psi}^\mu_{-r})|\Omega\mathcal{R}_3\Theta^k,\eta\rangle &= 0,\\
(\psi^i_r + i\eta e^{-i\pi r} e^{2\pi i k v_i} \tilde{\psi}^{\bar{i}}_{-r})|\Omega\mathcal{R}_3\Theta^k,\eta\rangle &= 0,\\
(\psi^{\bar{i}}_r + i\eta e^{-i\pi r} e^{-2\pi i k v_i} \tilde{\psi}^{i}_{-r})|\Omega\mathcal{R}_3\Theta^k,\eta\rangle &= 0.
\end{aligned} \tag{C.3}$$

A solution is provided by

$$
\begin{aligned}
|\Omega\mathcal{R}_3\Theta^k,\eta\rangle = \mathcal{N}_C \exp\ \Big\{ & -\sum_n \frac{(-1)^n}{n}\alpha^\mu_{-n}\tilde{\alpha}^\mu_{-n} - \sum_{i\in\{1,2,3\}}\sum_n \frac{(-1)^n}{n} e^{-2\pi i k v_i}\alpha^i_{-n}\tilde{\alpha}^i_{-n} \\
& - \sum_{\bar{i}\in\{\bar{1},\bar{2},\bar{3}\}}\sum_n \frac{(-1)^n}{n} e^{2\pi i k v_i}\alpha^{\bar{i}}_{-n}\tilde{\alpha}^{\bar{i}}_{-n} \\
& - i\eta\sum_r e^{-i\pi r}\psi^\mu_{-r}\tilde{\psi}^\mu_{-r} - i\eta\sum_{i\in\{1,2,3\}}\sum_r e^{-i\pi r}e^{-2\pi i k v_i}\psi^i_{-r}\tilde{\psi}^i_{-r} \\
& - i\eta\sum_{\bar{i}\in\{\bar{1},\bar{2},\bar{3}\}}\sum_r e^{-i\pi r}e^{2\pi i k v_i}\psi^{\bar{i}}_{-r}\tilde{\psi}^{\bar{i}}_{-r}\Big\}|0,\eta\rangle,
\end{aligned}
\tag{C.4}
$$

where $r\in\mathbb{Z}(\mathbb{Z}+\frac{1}{2})$ in the RR (NSNS) sector, $n\in\mathbb{Z}$ and $|0,\eta\rangle$ is the groundstate which depends on the spin structure η in the RR sector. The sums are meant to contain creation operators only. The vacuum state contains the momentum and winding modes discussed in section C.1.3.

C.1.2 Zero modes and GSO invariant states

We present the following discussion for the crosscap states. The GSO projections on boundary states are completely analogous.

NSNS sector

In the NSNS sectors, the GSO projection on the groundstate is determined by requiring tachyonic groundstates to be unphysical. Therefore, the GSO invariant combination is

$$
|\Omega\mathcal{R}_3\Theta^k\rangle_{NSNS} = |\Omega\mathcal{R}_3\Theta^k,+\rangle_{NSNS} - |\Omega\mathcal{R}_3\Theta^k,-\rangle_{NSNS}. \tag{C.5}
$$

Untwisted RR sector

Defining ($i=1,2,3$ and $\eta=\pm1$)

$$
\begin{aligned}
\psi^\mu_\eta &= \frac{1}{\sqrt{2}}\left(\psi^\mu_0 + i\eta\tilde{\psi}^\mu_0\right), \\
\psi^i_\eta &= \frac{1}{\sqrt{2}}\left(\psi^i_0 + i\eta\tilde{\psi}^{\bar{i}}_0\right), \qquad \psi^{\bar{i}}_\eta = \frac{1}{\sqrt{2}}\left(\psi^{\bar{i}}_0 + i\eta\tilde{\psi}^i_0\right),
\end{aligned}
$$

the non-trivial commutation relations are

$$
\begin{aligned}
\{\psi^\mu_+,\psi^\mu_-\} &= 1, \\
\left\{\psi^i_+,\psi^{\bar{i}}_-\right\} &= \left\{\psi^i_-,\psi^{\bar{i}}_+\right\} = 1.
\end{aligned}
$$

The crosscap conditions from the zero modes in the RR sector on the groundstate then read

$$\left.\begin{array}{c}\psi_\eta^\mu\\ \psi_\eta^i\\ \psi_\eta^{\bar{i}}\end{array}\right\}|\Omega\mathcal{R}_3\Theta^k,\eta\rangle^0_{RR}=0, \tag{C.6}$$

and the zero mode parts of the GSO projections are given by

$$\begin{aligned}(-1)^F &= \prod_{m=2}^{9}\sqrt{2}\psi_0^m \qquad\qquad (C.7)\\ &= \prod_{\mu=2,3}(\psi_+^\mu+\psi_-^\mu)\cdot\prod_{i=1,2,3}\frac{1}{2i}\left(\psi_+^i+\psi_-^i+\psi_+^{\bar{i}}+\psi_-^{\bar{i}}\right)\left(\psi_+^i+\psi_-^i-\psi_+^{\bar{i}}-\psi_-^{\bar{i}}\right),\\ (-1)^{\tilde{F}} &= \prod_{m=2}^{9}\sqrt{2}\tilde{\psi}_0^m \qquad\qquad (C.8)\\ &= \prod_{\mu=2,3}\frac{1}{i}(\psi_+^\mu-\psi_-^\mu)\cdot\prod_{i=1,2,3}\frac{1}{2i}\left(\psi_+^i-\psi_-^i+\psi_+^{\bar{i}}-\psi_-^{\bar{i}}\right)\left(\psi_+^i-\psi_-^i-\psi_+^{\bar{i}}+\psi_-^{\bar{i}}\right).\end{aligned}$$

Defining

$$|\Omega\mathcal{R}_3\Theta^k,-\rangle^0_{RR}\equiv\left[\left(\prod_{\mu=2,3}\psi_-^\mu\right)\left(\prod_{i=1,2,3}\psi_-^i\psi_-^{\bar{i}}\right)\right]|\Omega\mathcal{R}_3\Theta^k,+\rangle^0_{RR}, \tag{C.9}$$

the action of the complete GSO projector can be rephrased as

$$(-1)^F|\Omega\mathcal{R}_3\Theta^k,+\rangle_{RR}=-(-1)^{\tilde{F}}|\Omega\mathcal{R}_3\Theta^k,+\rangle_{RR}=-i|\Omega\mathcal{R}_3\Theta^k,-\rangle_{RR}, \tag{C.10}$$
$$(-1)^F|\Omega\mathcal{R}_3\Theta^k,-\rangle_{RR}=-(-1)^{\tilde{F}}|\Omega\mathcal{R}_3\Theta^k,-\rangle_{RR}=i|\Omega\mathcal{R}_3\Theta^k,+\rangle_{RR}. \tag{C.11}$$

GSO invariant states are given by

$$\begin{aligned}|\Omega\mathcal{R}_3\Theta^k\rangle &= |\Omega\mathcal{R}_3\Theta^k\rangle_{NSNS}+|\Omega\mathcal{R}_3\Theta^k\rangle_{RR},\\ |\Omega\mathcal{R}_3\Theta^k\rangle_{NSNS} &= |\Omega\mathcal{R}_3\Theta^k,+\rangle_{NSNS}-|\Omega\mathcal{R}_3\Theta^k,-\rangle_{NSNS},\\ |\Omega\mathcal{R}_3\Theta^k\rangle_{RR} &= |\Omega\mathcal{R}_3\Theta^k,+\rangle_{RR}-i|\Omega\mathcal{R}_3\Theta^k,-\rangle_{RR}.\end{aligned} \tag{C.12}$$

The total crosscap state has to be invariant under the orbifold group (i.e. it contains the 'complete projector'):

$$|C\rangle=\sum_{k=0}^{M-1}|\Omega\mathcal{R}_3\Theta^k\rangle. \tag{C.13}$$

C.1.3 Lattice part

From (C.1) we also obtain

$$\left(x^i - e^{2\pi i k v_i}[x^{\bar{i}} + \frac{1}{2}(p_L^{\bar{i}} - p_R^{\bar{i}})]\right)|\Omega\mathcal{R}_3\Theta^k\rangle = 0 \tag{C.14}$$

by inserting the mode expansion (A.2), (A.3). From this we can read off that the crosscap state $|\Omega\mathcal{R}_3\Theta^k\rangle$ is confined to a line on T_i which is tilted by the angle $-\pi k v_i$ relative to the real axis. Finally, conditions on the momenta arise:

$$\begin{aligned} p^\mu|\Omega\mathcal{R}_3\Theta^k\rangle &= 0, \\ (p_L^i + e^{2\pi i k v_i} p_R^{\bar{i}})|\Omega\mathcal{R}_3\Theta^k\rangle &= 0, \\ (p_R^i + e^{2\pi i k v_i} p_L^{\bar{i}})|\Omega\mathcal{R}_3\Theta^k\rangle &= 0. \end{aligned} \tag{C.15}$$

Inserting $p_{L,R} = P \pm \alpha' W$ for the compact momenta, (C.15) indicates that on each T_i, there are Kaluza-Klein momenta perpendicular and windings parallel to the position of the crosscap state.

C.2 Boundary states

Similarly to a crosscap state, the boundary state for a D6-brane at angle $\pi\varphi$ on T_1 relative to the X^4 axis is given by

$$\begin{aligned} |\varphi, \Theta^k; \eta\rangle = \mathcal{N}_B \exp \Big\{ & -\sum_n \frac{1}{n}\alpha^\mu_{-n}\tilde{\alpha}^\mu_{-n} - \sum_n \frac{1}{n} e^{2\pi i\varphi}\alpha^1_{-n}\tilde{\alpha}^1_{-n} \\ & - \sum_{i\in\{2,3\}}\sum_n \frac{1}{n} e^{-2\pi i k v_i}\alpha^i_{-n}\tilde{\alpha}^i_{-n} - \sum_n \frac{1}{n} e^{-2\pi i\varphi}\alpha^{\bar{1}}_{-n}\tilde{\alpha}^{\bar{1}}_{-n} \\ & - \sum_{\bar{i}\in\{\bar{2},\bar{3}\}}\sum_n \frac{1}{n} e^{2\pi i k v_i}\alpha^{\bar{i}}_{-n}\tilde{\alpha}^{\bar{i}}_{-n} \\ & - i\eta\sum_r \psi^\mu_{-r}\tilde{\psi}^\mu_{-r} - i\eta\sum_r e^{2\pi i\varphi}\psi^1_{-r}\tilde{\psi}^1_{-r} \\ & - i\eta\sum_{i\in\{2,3\}}\sum_r e^{-2\pi i k v_i}\psi^i_{-r}\tilde{\psi}^i_{-r} - i\eta\sum_r e^{-2\pi i\varphi}\psi^{\bar{1}}_{-r}\tilde{\psi}^{\bar{1}}_{-r} \\ & - i\eta\sum_{\bar{i}\in\{\bar{2},\bar{3}\}}\sum_r e^{2\pi i k v_i}\psi^{\bar{i}}_{-r}\tilde{\psi}^{\bar{i}}_{-r}\Big\}|0,\eta\rangle. \end{aligned} \tag{C.16}$$

The oscillator moding is the same as for the crosscap. The NSNS vacuum is again independent of the spin structure η, and the vacuum states contain the lattice contributions.

Using the analogous equations to (C.12), the GSO invariant boundary state is given by

$$|B_\varphi\rangle = \sum_{k=0}^{M-1} |\varphi, \Theta^k\rangle. \tag{C.17}$$

Discrete momenta exist in the compact directions perpendicular to the position of the boundary state while windings are parallel.

C.3 Tree channel amplitudes

Using equation (C.13) and (C.17), the tree channel amplitudes read

$$\begin{aligned}
\tilde{\mathcal{K}}_{total} &= \tilde{\mathcal{K}}_{RR} + \tilde{\mathcal{K}}_{NSNS} = \int_0^\infty \mathrm{d}l \langle C|e^{-2\pi l H}|C\rangle, \\
\tilde{\mathcal{A}}_{total} &= \tilde{\mathcal{A}}_{RR} + \tilde{\mathcal{A}}_{NSNS} = \int_0^\infty \mathrm{d}l \sum_{\varphi,\varphi'} \langle B_\varphi|e^{-2\pi l H}|B_{\varphi'}\rangle, \\
\tilde{\mathcal{M}}_{total} &= \tilde{\mathcal{M}}_{RR} + \tilde{\mathcal{M}}_{NSNS} = \int_0^\infty \mathrm{d}l \sum_{\varphi} \left(\langle C|e^{-2\pi l H}|B_\varphi\rangle + h.c.\right).
\end{aligned} \tag{C.18}$$

As we mainly focus on computing the RR exchange in this thesis, we will use the abbreviation $\tilde{\mathcal{K}} \equiv \tilde{\mathcal{K}}_{RR}$ etc. The normalizations $\mathcal{N}_C, \mathcal{N}_B$ are determined from the Klein bottle and annulus amplitude via worldsheet duality. The following equation holds

$$\langle \Omega\mathcal{R}_3\Theta^k|e^{-2\pi l H}|\Omega\mathcal{R}_3\Theta^{k'}\rangle = \begin{cases} \mathcal{N}_C^2 \tilde{\mathcal{K}}^{(0)} \tilde{\mathcal{L}}_1 \tilde{\mathcal{L}}_2 \tilde{\mathcal{L}}_3 & \text{for } k = k', \\ 4\sin^2(\pi(k-k')/M)\mathcal{N}_C^2 \tilde{\mathcal{K}}^{(k-k')} \tilde{\mathcal{L}}_1 & \text{for } k \neq k', \end{cases} \tag{C.19}$$

where $\tilde{\mathcal{K}}^{(k-k')} \equiv \tilde{\mathcal{K}}^{(k-k')}(2l)$ contains the oscillator contribution (for notation see (B.19), (B.20)) and $\tilde{\mathcal{L}}_i \equiv \tilde{\mathcal{L}}_i(l)$ denotes the lattice contribution for the two torus T_i listed in table B.1. For $\mathbb{Z}_{2,3}$, all $|\Omega\mathcal{R}_3\Theta^k\rangle$ are extended along the axes of $T_{2,3}$ in the case of the **A** lattice and diagonal to the axes for the **B** lattice.

Since the D6-branes lie on top of the O6-planes on $T_{2,3}$ in our models, the positions of the O6-planes can be read off from figures 2.4 and 2.5. All $|\Omega\mathcal{R}_3\Theta^k\rangle$ have the same relative orientation with respect to the tori $T_{2,3}$, hence they all provide the same lattice contribution. All choices **AA**, **AB**, **BB** lead to consistent models. The situation is different for $\mathbb{Z}_{4,6}$. In these models, all $|\Omega\mathcal{R}_3\Theta^{2k}\rangle$ have the same orientation relative to the lattice while all $|\Omega\mathcal{R}_3\Theta^{2k+1}\rangle$ have the other possible one. $|\Omega\mathcal{R}_3\Theta^{2k}\rangle$ on the lattice **A** gives the same contribution as $|\Omega\mathcal{R}_3\Theta^{2k+1}\rangle$ on **B** and vice versa,

$$\left.\begin{array}{l} \langle \Omega\mathcal{R}_3\Theta^{2k}|e^{-2\pi l H}|\Omega\mathcal{R}_3\Theta^{2k}\rangle \\ +\langle \Omega\mathcal{R}_3\Theta^{2k+1}|e^{-2\pi l H}|\Omega\mathcal{R}_3\Theta^{2k+1}\rangle \end{array}\right\} \longrightarrow \begin{cases} 2\tilde{\mathcal{L}}_{\mathbf{A}}\tilde{\mathcal{L}}_{\mathbf{B}} & \text{for } \mathbf{AB}, \\ \tilde{\mathcal{L}}_{\mathbf{A}}^2 + \tilde{\mathcal{L}}_{\mathbf{B}}^2 & \text{for } \mathbf{AA}/\mathbf{BB}. \end{cases} \tag{C.20}$$

By modular transformation from the loop channel, one recovers the correct result for **AB**. But for **AA** or **BB**, the loop channel amplitude gives $(4\tilde{\mathcal{L}}_{\mathbf{A}}^2 + \tilde{\mathcal{L}}_{\mathbf{B}}^2)$ for $\mathbb{Z}_4$ and $(\tilde{\mathcal{L}}_{\mathbf{A}}^2 + 9\tilde{\mathcal{L}}_{\mathbf{B}}^2)$ for $\mathbb{Z}_6$ as can be read off from table B.1. This means that only the **AB**-lattice is consistent with worldsheet duality.

Appendix D

Chiral D6-brane spectra

In this appendix we list the fermionic groundstates of section 2.2.1 and 3.1.2 and the chiral spectrum for the D6-brane model in section 2.3.2.

Fermionic states on $T^2 \times T^4/\mathbb{Z}_M$						
on T^2	on $T^4/\mathbb{Z}_M$	state	$\frac{\alpha'}{4}\text{mass}^2$	chirality	$\mathbb{Z}_2$	$(\mathbb{Z}_3)$
$\Delta\varphi = 0$	$\frac{k}{M} = 0$	$\|0\rangle_R$	0	L	$+$	1
		$\psi_0^0\psi_0^1\|0\rangle_R$	0	R	$+$	1
		$\psi_0^0\psi_0^2\|0\rangle_R$	0	R	$-$	α
		$\psi_0^0\psi_0^3\|0\rangle_R$	0	R	$-$	α^2
		$\psi_0^1\psi_0^2\|0\rangle_R$	0	L	$-$	α
		$\psi_0^1\psi_0^3\|0\rangle_R$	0	L	$-$	α^2
		$\psi_0^2\psi_0^3\|0\rangle_R$	0	L	$+$	1
		$\psi_0^0\psi_0^1\psi_0^2\psi_0^3\|0\rangle_R$	0	R	$+$	1
$\Delta\varphi = 0$	$0 < \frac{k}{M} \leqslant \frac{1}{2}$	$\|0\rangle_R$	0	L	$+$	
		$\psi_0^0\psi_0^1\|0\rangle_R$	0	R	$+$	
$\Delta\varphi \neq 0$	$\frac{k}{M} = 0$	$\|0\rangle_R$	0	L	$+$	1
		$\psi_0^0\psi_0^2\|0\rangle_R$	0	R	$-$	α
		$\psi_0^0\psi_0^3\|0\rangle_R$	0	R	$-$	α^2
		$\psi_0^2\psi_0^3\|0\rangle_R$	0	L	$+$	1
$\Delta\varphi \neq 0$	$0 < \frac{k}{M} \leqslant \frac{1}{2}$	$\|0\rangle_R$	0	L	$+$	
		$\psi_0^0\psi_{-\Delta\varphi}^1\|0\rangle_R$	$\Delta\varphi$	(R)	$(+)$	

Table D.1: Fermionic groundstates for the open string sector of D6-brane models. The last but one column denotes the $\mathbb{Z}_2$ eigenvalue of the corresponding massless state. The last column denotes the $\mathbb{Z}_3$ eigenvalue for D8-brane models where $\alpha \equiv e^{2\pi i/3}$.

Chiral spectrum for intersecting D6-branes, Ex. 2, Part 1																		
	rep.	mult	Q_1	Q_2	Q_3	Q_4	Q_5	Q_6	Q_7	Q_8	Q_9	Q_{10}	$\tilde{Q}_1$	$\tilde{Q}_2$	$\tilde{Q}_3$	$\tilde{Q}_4$	$\tilde{Q}_5$	$\tilde{Q}_6$
$11'U$	$(\mathbf{3},\mathbf{3},1,1;1,1)$	4	1	1	0	0	0	0	0	0	0	0	2	0	0	0	0	0
	$(1,1,\mathbf{3},\mathbf{3};1,1)$	4	0	0	1	1	0	0	0	0	0	0	0	2	0	0	0	0
	$(\mathbf{3},1,1,1;1,1)$	4	-2	0	0	0	0	0	0	0	0	0	-2	0	-2	0	0	0
	$(1,\mathbf{3},1,1;1,1)$	4	0	-2	0	0	0	0	0	0	0	0	-2	0	2	0	0	0
	$(1,1,\mathbf{3},1;1,1)$	4	0	0	-2	0	0	0	0	0	0	0	0	-2	0	-2	0	0
	$(1,1,1,\mathbf{3};1,1)$	4	0	0	0	-2	0	0	0	0	0	0	0	-2	0	2	0	0
$11'T$	$(\bar{\mathbf{3}},1,1,\bar{\mathbf{3}};1,1)$	2	-1	0	0	-1	0	0	0	0	0	0	-1	-1	-1	1	0	0
	$(1,\bar{\mathbf{3}},\bar{\mathbf{3}},1;1,1)$	2	0	-1	-1	0	0	0	0	0	0	0	-1	-1	1	-1	0	0
$12U$	$(\mathbf{3},1,1,1;\bar{\mathbf{2}},1)$	2	1	0	0	0	-1	0	0	0	0	0	1	0	4	0	4	0
	$(\bar{\mathbf{3}},1,1,1;\bar{\mathbf{2}},1)$	2	-1	0	0	0	-1	0	0	0	0	0	-1	0	2	0	4	0
	$(1,\mathbf{3},1,1;\mathbf{2},1)$	2	0	1	0	0	1	0	0	0	0	0	1	0	-4	0	-4	0
	$(1,\bar{\mathbf{3}},1,1;\mathbf{2},1)$	2	0	-1	0	0	1	0	0	0	0	0	-1	0	-2	0	-4	0
	$(1,1,\mathbf{3},1;1,\bar{\mathbf{2}})$	2	0	0	1	0	0	-1	0	0	0	0	0	1	0	4	0	4
	$(1,1,\bar{\mathbf{3}},1;1,\bar{\mathbf{2}})$	2	0	0	-1	0	0	-1	0	0	0	0	0	-1	0	2	0	4
	$(1,1,1,\mathbf{3};1,\mathbf{2})$	2	0	0	0	1	0	1	0	0	0	0	0	1	0	-4	0	-4
	$(1,1,1,\bar{\mathbf{3}};1,\mathbf{2})$	2	0	0	0	-1	0	1	0	0	0	0	0	-1	0	-2	0	-4
$12T$	$(\bar{\mathbf{3}},1,1,1;1,\mathbf{2})$	1	-1	0	0	0	0	1	0	0	0	0	-1	0	-1	-3	0	-4
	$(1,\bar{\mathbf{3}},1,1;1,\bar{\mathbf{2}})$	1	0	-1	0	0	0	-1	0	0	0	0	-1	0	1	3	0	4
	$(1,1,\bar{\mathbf{3}},1;\mathbf{2},1)$	1	0	0	-1	0	1	0	0	0	0	0	0	-1	-3	-1	-4	0
	$(1,1,1,\bar{\mathbf{3}};\bar{\mathbf{2}},1)$	1	0	0	0	-1	-1	0	0	0	0	0	0	-1	3	1	4	0
$13U$	$(\mathbf{3},1,1,1;1,1)$	6	1	0	0	0	0	0	-1	0	0	0	4	0	1	0	-1	0
	$(\bar{\mathbf{3}},1,1,1;1,1)$	6	-1	0	0	0	0	0	0	1	0	0	-4	0	-1	0	-1	0
	$(1,\mathbf{3},1,1;1,1)$	6	0	1	0	0	0	0	0	-1	0	0	4	0	-1	0	1	0
	$(1,\bar{\mathbf{3}},1,1;1,1)$	6	0	-1	0	0	0	0	1	0	0	0	-4	0	1	0	1	0
	$(1,1,\mathbf{3},1;1,1)$	6	0	0	1	0	0	0	0	0	-1	0	0	4	0	1	0	-1
	$(1,1,\bar{\mathbf{3}},1;1,1)$	6	0	0	-1	0	0	0	0	0	0	1	0	-4	0	-1	0	-1
	$(1,1,1,\mathbf{3};1,1)$	6	0	0	0	1	0	0	0	0	0	-1	0	4	0	-1	0	1
	$(1,1,1,\bar{\mathbf{3}};1,1)$	6	0	0	0	-1	0	0	0	0	1	0	0	-4	0	1	0	1
$13'U$	$(\mathbf{3},1,1,1;1,1)$	10	1	0	0	0	0	0	0	1	0	0	-2	0	1	0	-1	0
	$(\bar{\mathbf{3}},1,1,1;1,1)$	10	-1	0	0	0	0	0	-1	0	0	0	2	0	-1	0	-1	0
	$(1,\mathbf{3},1,1;1,1)$	10	0	1	0	0	0	0	1	0	0	0	-2	0	-1	0	1	0
	$(1,\bar{\mathbf{3}},1,1;1,1)$	10	0	-1	0	0	0	0	0	-1	0	0	2	0	1	0	1	0
	$(1,1,\mathbf{3},1;1,1)$	10	0	0	1	0	0	0	0	0	0	1	0	-2	0	1	0	-1
	$(1,1,\bar{\mathbf{3}},1;1,1)$	10	0	0	-1	0	0	0	0	0	-1	0	0	2	0	-1	0	-1
	$(1,1,1,\mathbf{3};1,1)$	10	0	0	0	1	0	0	0	0	1	0	0	-2	0	-1	0	1
	$(1,1,1,\bar{\mathbf{3}};1,1)$	10	0	0	0	-1	0	0	0	0	0	-1	0	2	0	1	0	1

Chiral spectrum for intersecting D6-branes, Ex. 2, Part 2																						
	rep.	mult	Q_1	Q_2	Q_3	Q_4	Q_5	Q_6	Q_7	Q_8	Q_9	Q_{10}	$\tilde{Q}_1$	$\tilde{Q}_2$	$\tilde{Q}_3$	$\tilde{Q}_4$	$\tilde{Q}_5$	$\tilde{Q}_6$
$13T$	$(\bar{\mathbf{3}},1,1,1;1,1)$	3	-1	0	0	0	0	0	0	0	1	0	-1	-3	-1	0	0	1
	$(1,\bar{\mathbf{3}},1,1;1,1)$	3	0	-1	0	0	0	0	0	0	0	1	-1	-3	1	0	0	-1
	$(1,1,\bar{\mathbf{3}},1;1,1)$	3	0	0	-1	0	0	0	1	0	0	0	-3	-1	0	-1	1	0
	$(1,1,1,\bar{\mathbf{3}};1,1)$	3	0	0	0	-1	0	0	0	1	0	0	-3	-1	0	1	-1	0
$13'T$	$(\bar{\mathbf{3}},1,1,1;1,1)$	5	-1	0	0	0	0	0	0	0	0	-1	-1	3	-1	0	0	1
	$(1,\bar{\mathbf{3}},1,1;1,1)$	5	0	-1	0	0	0	0	0	0	-1	0	-1	3	1	0	0	-1
	$(1,1,\bar{\mathbf{3}},1;1,1)$	5	0	0	-1	0	0	0	0	-1	0	0	3	-1	0	-1	1	0
	$(1,1,1,\bar{\mathbf{3}};1,1)$	5	0	0	0	-1	0	0	-1	0	0	0	3	-1	0	1	-1	0
$23U$	$(1,1,1,1;\mathbf{2},1)$	2	0	0	0	0	1	0	1	0	0	0	-3	0	-3	0	-3	0
	$(1,1,1,1;\mathbf{2},1)$	2	0	0	0	0	1	0	-1	0	0	0	3	0	-3	0	-5	0
	$(1,1,1,1;\bar{\mathbf{2}},1)$	2	0	0	0	0	-1	0	0	1	0	0	-3	0	3	0	3	0
	$(1,1,1,1;\bar{\mathbf{2}},1)$	2	0	0	0	0	-1	0	0	-1	0	0	3	0	3	0	5	0
	$(1,1,1,1;1,\mathbf{2})$	2	0	0	0	0	0	1	0	0	1	0	0	-3	0	-3	0	-3
	$(1,1,1,1;1,\mathbf{2})$	2	0	0	0	0	0	1	0	0	-1	0	0	3	0	-3	0	-5
	$(1,1,1,1;1,\bar{\mathbf{2}})$	2	0	0	0	0	0	-1	0	0	0	1	0	-3	0	3	0	3
	$(1,1,1,1;1,\bar{\mathbf{2}})$	2	0	0	0	0	0	-1	0	0	0	-1	0	3	0	3	0	5
$23T$	$(1,1,1,1;\mathbf{2},1)$	1	0	0	0	0	1	0	0	0	-1	0	0	3	-3	0	-4	-1
	$(1,1,1,1;\bar{\mathbf{2}},1)$	1	0	0	0	0	-1	0	0	0	0	-1	0	3	3	0	4	1
	$(1,1,1,1;1,\mathbf{2})$	1	0	0	0	0	0	1	-1	0	0	0	3	0	0	-3	-1	-4
	$(1,1,1,1;1,\bar{\mathbf{2}})$	1	0	0	0	0	0	-1	0	-1	0	0	3	0	0	3	1	4
$33'U$	$(1,1,1,1;1,1)$	16	0	0	0	0	0	0	1	1	0	0	-6	0	0	0	0	0
	$(1,1,1,1;1,1)$	16	0	0	0	0	0	0	0	0	1	1	0	-6	0	0	0	0
	$(1,1,1,1;1,1)$	6	0	0	0	0	0	0	-2	0	0	0	6	0	0	0	-2	0
	$(1,1,1,1;1,1)$	6	0	0	0	0	0	0	0	-2	0	0	6	0	0	0	2	0
	$(1,1,1,1;1,1)$	6	0	0	0	0	0	0	0	0	-2	0	0	6	0	0	0	-2
	$(1,1,1,1;1,1)$	6	0	0	0	0	0	0	0	0	0	-2	0	6	0	0	0	2
$33'T$	$(1,1,1,1;1,1)$	8	0	0	0	0	0	0	-1	0	0	-1	3	3	0	0	-1	1
	$(1,1,1,1;1,1)$	8	0	0	0	0	0	0	0	-1	-1	0	3	3	0	0	1	-1

Table D.2: Chiral fermionic spectrum for $(T^2 \times T^4/\mathbb{Z}_2)/\Omega\mathcal{R}_3$ with $(n_1, m_1) = (1,1)$, $(n_2, m_2) = (1,0)$, $(n_3, m_3) = (4,1)$ and lattice **aaa** in section 2.3.2. The resulting gauge group is $SU(3)^4 \times SU(2)^2 \times U(1)^6$.

Appendix E

1-loop diagrams for O8-plane/D8-brane interactions

E.1 Lattice contributions on $(T^4/\mathbb{Z}_3)/\Omega\mathcal{R}_1$

The general form of the lattice sums on $T^4/\mathbb{Z}_3$ for one two torus in the loop channel is given by ($\rho \equiv R^2/\alpha'$)

$$\mathcal{L}^R[\alpha](t) \equiv \sum_{m,n\in\mathbb{Z}} e^{-\alpha\pi t(m^2+mn+n^2)/\rho}. \tag{E.1}$$

Using the Poisson resummation formula

$$\sum_{x\in\Gamma} f(x) = \frac{1}{\mathrm{vol}(\Gamma)} \sum_{p\in\Gamma^*} \tilde{f}(p) \tag{E.2}$$

for a d-dimensional lattice Γ and its dual lattice Γ^* with the Fourier transform $\tilde{f}(p) = \int_{\mathbb{R}^d} \mathrm{d}x e^{2\pi i x\cdot p} f(x)$ and defining $t = 1/\kappa l$ gives the lattice sums in the tree channel

$$\mathcal{L}^R[\alpha](t) = l\frac{2\kappa}{\sqrt{3}\alpha}\rho\mathcal{L}^{1/R}\left[\frac{4\kappa}{3\alpha}\right](l). \tag{E.3}$$

For $T^4/\mathbb{Z}_3$, we thus obtain

$$\text{Klein bottle:} \qquad \left(\mathcal{L}^{R_1}\mathcal{L}^{R_2}\right)[1](t) = \frac{64}{3}l^2\omega\left(\mathcal{L}^{1/R_1}\mathcal{L}^{1/R_2}\right)[16/3](l), \tag{E.4}$$

$$\text{Annulus:} \qquad \left(\mathcal{L}^{R_1}\mathcal{L}^{R_2}\right)[2](t) = \frac{4}{3}l^2\omega\left(\mathcal{L}^{1/R_1}\mathcal{L}^{1/R_2}\right)[4/3](l), \tag{E.5}$$

$$\text{Möbius strip:} \qquad \left(\mathcal{L}^{R_1}\mathcal{L}^{R_2}\right)[2](t) = \frac{64}{3}l^2\omega\left(\mathcal{L}^{1/R_1}\mathcal{L}^{1/R_2}\right)[16/3](l), \tag{E.6}$$

where $\omega \equiv \rho_1\rho_2$ is the volume of the orbifold in units of α'.

E.2 Oscillator contributions

Oscillator contributions to the 1-loop amplitudes can be expressed in terms of generalized Jacobi theta functions. The relevant formulas for untwisted sectors without insertions are the same as for models with O6-planes and D6-branes, see (B.15), (B.16), (B.17) for the loop channel and (B.19), (B.21), (B.23) for the tree channel. In addition, an insertion of Θ^k in the trace leads to

$$\text{Klein bottle:} \qquad \mathcal{K}^{(k)} = \frac{\vartheta\begin{bmatrix} 0 \\ \frac{1}{2} \end{bmatrix}^2}{\eta^6} \prod_{i=2,3} \frac{\vartheta\begin{bmatrix} 0 \\ \frac{1}{2}+2kv_i \end{bmatrix}}{\vartheta\begin{bmatrix} \frac{1}{2} \\ \frac{1}{2}+2kv_i \end{bmatrix}}(2t), \tag{E.7}$$

$$\text{Annulus:} \qquad \mathcal{A}_{ab}^{(k)} = i\frac{\vartheta\begin{bmatrix} 0 \\ \frac{1}{2} \end{bmatrix}}{\eta^3} \frac{\vartheta\begin{bmatrix} \Delta\varphi \\ \frac{1}{2} \end{bmatrix}}{\vartheta\begin{bmatrix} \frac{1}{2}+\Delta\varphi \\ \frac{1}{2} \end{bmatrix}} \prod_{i=2,3} \frac{\vartheta\begin{bmatrix} 0 \\ \frac{1}{2}+kv_i \end{bmatrix}}{\vartheta\begin{bmatrix} \frac{1}{2} \\ \frac{1}{2}+kv_i \end{bmatrix}}(t), \tag{E.8}$$

$$\text{Möbius strip:} \qquad \mathcal{M}_{a}^{(k)} = ie^{2\pi i\varphi}\frac{\vartheta\begin{bmatrix} \frac{1}{2} \\ 0 \end{bmatrix}}{\eta^3} \frac{\vartheta\begin{bmatrix} \frac{1}{2}+2\varphi \\ -\varphi \end{bmatrix}}{\vartheta\begin{bmatrix} \frac{1}{2}+2\varphi \\ \frac{1}{2}-\varphi \end{bmatrix}} \prod_{i=2,3} \frac{\vartheta\begin{bmatrix} \frac{1}{2} \\ kv_i \end{bmatrix}}{\vartheta\begin{bmatrix} \frac{1}{2} \\ \frac{1}{2}+kv_i \end{bmatrix}}(t-\frac{i}{2}). \tag{E.9}$$

By modular transformation to the tree channel, one obtains contributions from oscillators in the Θ^k twisted sector,

$$\text{Klein bottle:} \qquad \tilde{\mathcal{K}}^{(k)} = \frac{\vartheta\begin{bmatrix} \frac{1}{2} \\ 0 \end{bmatrix}^2}{\eta^6} \prod_{i=2,3} \frac{\vartheta\begin{bmatrix} \frac{1}{2}-2kv_i \\ 0 \end{bmatrix}}{\vartheta\begin{bmatrix} \frac{1}{2}-2kv_i \\ \frac{1}{2} \end{bmatrix}}(2l), \tag{E.10}$$

$$\text{Annulus:} \qquad \tilde{\mathcal{A}}_{ab}^{(k)} = \frac{\vartheta\begin{bmatrix} \frac{1}{2} \\ 0 \end{bmatrix}}{\eta^3} \frac{\vartheta\begin{bmatrix} \frac{1}{2} \\ \Delta\varphi \end{bmatrix}}{\vartheta\begin{bmatrix} \frac{1}{2} \\ \frac{1}{2}+\Delta\varphi \end{bmatrix}} \prod_{i=2,3} \frac{\vartheta\begin{bmatrix} \frac{1}{2}-kv_i \\ 0 \end{bmatrix}}{\vartheta\begin{bmatrix} \frac{1}{2}-kv_i \\ \frac{1}{2} \end{bmatrix}}(2l), \tag{E.11}$$

$$\text{Möbius strip:} \qquad \tilde{\mathcal{M}}_{a}^{(k)} = \frac{\vartheta\begin{bmatrix} \frac{1}{2} \\ 0 \end{bmatrix}}{\eta^3} \frac{\vartheta\begin{bmatrix} \frac{1}{2} \\ \varphi \end{bmatrix}}{\vartheta\begin{bmatrix} \frac{1}{2} \\ \frac{1}{2}+\varphi \end{bmatrix}}(2l-\frac{i}{2}) \prod_{i=2,3} \frac{\vartheta\begin{bmatrix} -kv_i \\ \frac{1}{2} \end{bmatrix}\vartheta\begin{bmatrix} \frac{1}{2}-kv_i \\ 0 \end{bmatrix}}{\vartheta\begin{bmatrix} \frac{1}{2}-kv_i \\ \frac{1}{2} \end{bmatrix}\vartheta\begin{bmatrix} -kv_i \\ 0 \end{bmatrix}}(4l). \tag{E.12}$$

Appendix F

Tree channel results for $(T^2 \times T^4/\mathbb{Z}_3)/\Omega\mathcal{R}_1$

F.1 Crosscap states

The crosscap conditions for the $\Omega\mathcal{R}_1$-model on $T^4/\mathbb{Z}_3$ where the reflection does not act are given by ($i = 2, 3$)

$$\left[X^i_{L,R}(\sigma,0) - \Theta^k X^i_{R,L}(\sigma+\pi,0)\right] |\Omega\mathcal{R}_1\Theta^k\rangle = 0, \tag{F.1}$$

$$\left[X^{\bar{i}}_{L,R}(\sigma,0) - \Theta^k X^{\bar{i}}_{R,L}(\sigma+\pi,0)\right] |\Omega\mathcal{R}_1\Theta^k\rangle = 0. \tag{F.2}$$

Inserting the mode expansions (A.2), (A.3) gives the following constraints on $T^4/\mathbb{Z}_3$

$$\left.\begin{array}{c} \left[p^i_L + e^{2\pi i k v_i} p^i_R\right] \\ \left[p^{\bar{i}}_L + e^{-2\pi i k v_i} p^{\bar{i}}_R\right] \\ \left[p^i_R + e^{2\pi i k v_i} p^i_L\right] \\ \left[p^{\bar{i}}_R + e^{-2\pi i k v_i} p^{\bar{i}}_L\right] \end{array}\right\} |\Omega\mathcal{R}_1\Theta^k\rangle = 0, \tag{F.3}$$

$$\left.\begin{array}{c} \left[\alpha^i_r + e^{\pi i(2kv_i - r)} \tilde{\alpha}^i_{-r}\right] \\ \left[\alpha^{\bar{i}}_s + e^{\pi i(-2kv_i - s)} \tilde{\alpha}^{\bar{i}}_{-s}\right] \\ \left[\tilde{\alpha}^i_{-r} + e^{\pi i(2kv_i - r)} \alpha^i_r\right] \\ \left[\tilde{\alpha}^{\bar{i}}_{-s} + e^{\pi i(-2kv_i - s)} \alpha^{\bar{i}}_s\right] \end{array}\right\} |\Omega\mathcal{R}_1\Theta^k\rangle = 0. \tag{F.4}$$

The fermionic worldsheet coordinates provide a similar set of constraints.

The set of equations (F.3) states that for $k = 0$ windings along all four directions of the orbifold occur while for $k \neq 0$, only Kaluza-Klein momenta and windings from the first two torus T_1 contribute as discussed in the case of O6-planes in appendix C.1. The equations (F.4) are only mutually consistent if

$r \in \mathbb{Z} + 2kv_i$, $s \in \mathbb{Z} - 2kv_i$. Using the notation $n \in \mathbb{Z}$, $r \in \mathbb{Z}(+1/2)$ for the R (NS) sector, the oscillator constraints can be rewritten as

$$\left.\begin{array}{l}\left[\alpha^i_{n+2kv_i} + (-1)^n \tilde{\alpha}^i_{-n-2kv_i}\right]\\ \left[\alpha^{\bar{i}}_{n-2kv_i} + (-1)^n \tilde{\alpha}^{\bar{i}}_{-n+2kv_i}\right]\end{array}\right\} |\Omega\mathcal{R}_1\Theta^k, \eta\rangle = 0, \tag{F.5}$$

$$\left.\begin{array}{l}\left[\psi^i_{r+2kv_i} + i\eta e^{-i\pi r}\tilde{\psi}^i_{-r-2kv_i}\right]\\ \left[\psi^{\bar{i}}_{r-2kv_i} + i\eta e^{-i\pi r}\tilde{\psi}^{\bar{i}}_{-r+2kv_i}\right]\end{array}\right\} |\Omega\mathcal{R}_1\Theta^k, \eta\rangle = 0. \tag{F.6}$$

A solution to these constraints is provided by

$$\begin{aligned}|\Omega\mathcal{R}_1\Theta^k, \eta\rangle = \mathcal{N}_C^{(k)} \exp \Big\{ & -\sum_n \frac{(-1)^n}{n}\alpha^\mu_{-n}\tilde{\alpha}^\mu_{-n} - \sum_n \frac{(-1)^n}{n}\alpha^1_{-n}\tilde{\alpha}^1_{-n} \\ & - \sum_n \frac{(-1)^n}{n}\alpha^{\bar{1}}_{-n}\tilde{\alpha}^{\bar{1}}_{-n} - \sum_{i\in\{2,3\}}\sum_n \frac{(-1)^n}{n}\alpha^i_{-n+2kv_i}\tilde{\alpha}^{\bar{i}}_{-n+2kv_i} \\ & - \sum_{i\in\{2,3\}}\sum_n \frac{(-1)^n}{n}\alpha^{\bar{i}}_{-n-2kv_i}\tilde{\alpha}^i_{-n-2kv_i} \\ & - i\eta\sum_r e^{-i\pi r}\psi^\mu_{-r}\tilde{\psi}^\mu_{-r} - i\eta\sum_r e^{-i\pi r}\psi^1_{-r}\tilde{\psi}^1_{-r} \\ & -i\ \ \eta\sum_r e^{-i\pi r}\psi^{\bar{1}}_{-r}\tilde{\psi}^{\bar{1}}_{-r} - i\eta\sum_{i\in\{2,3\}}\sum_r e^{-i\pi r}\psi^i_{-r+2kv_i}\tilde{\psi}^{\bar{i}}_{-r+2kv_i} \\ & - i\eta\sum_{i\in\{2,3\}}\sum_r e^{-i\pi r}\psi^{\bar{i}}_{-r-2kv_i}\tilde{\psi}^i_{-r-2kv_i}\Big\}|0, \eta\rangle. \end{aligned} \tag{F.7}$$

The dependence on the lattice is contained in the groundstate $|0, \eta\rangle$ which only depends on η in the RR sector. The sums contain creation operators only.

F.2 Boundary states

In order to reproduce the amplitudes obtained by modular transformation from the loop channel, a boundary state at angle $\pi\varphi$ on T_1 relative to the X^4 axis has to be of the form

$$
\begin{aligned}
|\varphi,\Theta^k;\eta\rangle = \mathcal{N}_B^{(k)} \exp \quad \Big\{ & -\sum_n \frac{1}{n}\alpha^\mu_{-n}\tilde{\alpha}^\mu_{-n} - \sum_n \frac{1}{n} e^{2\pi i\varphi}\alpha^1_{-n}\tilde{\alpha}^1_{-n} \\
- & \sum_n \frac{1}{n} e^{-2\pi i\varphi}\alpha^{\bar{1}}_{-n}\tilde{\alpha}^{\bar{1}}_{-n} - \sum_{i\in\{2,3\}}\sum_n \frac{1}{n}\alpha^i_{-n+2kv_i}\tilde{\alpha}^{\bar{i}}_{-n+2kv_i} \\
- & \sum_{i\in\{2,3\}}\sum_n \frac{1}{n}\alpha^{\bar{i}}_{-n-2kv_i}\tilde{\alpha}^i_{-n-2kv_i} \\
- & i\eta\sum_r \psi^\mu_{-r}\tilde{\psi}^\mu_{-r} - i\eta\sum_r e^{2\pi i\varphi}\psi^1_{-r}\tilde{\psi}^1_{-r} \\
- & i\eta\sum_r e^{-2\pi i\varphi}\psi^{\bar{1}}_{-r}\tilde{\psi}^{\bar{1}}_{-r} - i\eta\sum_{i\in\{2,3\}}\sum_r \psi^i_{-r+2kv_i}\tilde{\psi}^{\bar{i}}_{-r+2kv_i} \\
- & i\eta\sum_{i\in\{2,3\}}\sum_r \psi^{\bar{i}}_{-r-2kv_i}\tilde{\psi}^i_{-r-2kv_i}\Big\}|0,\eta\rangle. \qquad \text{(F.8)}
\end{aligned}
$$

As for the crosscap states, the groundstate $|0,\eta\rangle$ contains Kaluza-Klein momentum and winding eigenvalues from T_1 and windings from $T^4/\mathbb{Z}_3$.

F.3 Zero modes and GSO invariant states for the twisted sectors

The GSO projection for the untwisted sector is very similar to the one for models with D6-branes discussed in appendix C.1.2. For models with D8-branes, it is more appropriate to define the worldsheet spinors ψ^i_η for $i = 2,3$ in the following way,

$$
\psi^i_\eta = \frac{1}{\sqrt{2}}\left(\psi^i_0 + i\eta\tilde{\psi}^i_0\right), \qquad \psi^{\bar{i}}_\eta = \frac{1}{\sqrt{2}}\left(\psi^{\bar{i}}_0 + i\eta\tilde{\psi}^{\bar{i}}_0\right).
$$

Inserting this definition into the subsequent formulas in section C.1.2 gives the correct commutation relations, crosscap conditions and zero mode part of the GSO projection leading to the analogous superposition of states (F.7) and (F.8) with different spin structures as listed at the end of section C.1.2 involving O6-planes and D6-branes.

Twisted RR sectors

For $k \neq 0$, the zero mode conditions read

$$
\left.\begin{matrix} \psi^\mu_\eta \\ \psi^1_\eta \\ \psi^{\bar{1}}_\eta \end{matrix}\right\} |\Omega\mathcal{R}_1\Theta^k,\eta\rangle^0_{RR} = 0. \qquad \text{(F.10)}
$$

The zero mode parts of the GSO projection operators are now given by

$$
\begin{aligned}
(-1)^F &= \prod_{m=2}^{5} \sqrt{2}\psi_0^m && \text{(F.11)}\\
&= \prod_{\mu=2,3} \left(\psi_+^\mu + \psi_-^\mu\right) \cdot \frac{1}{2i} \left(\psi_+^1 + \psi_-^1 + \psi_+^{\bar{1}} + \psi_-^{\bar{1}}\right) \left(\psi_+^1 + \psi_-^1 - \psi_+^{\bar{1}} - \psi_-^{\bar{1}}\right),\\
(-1)^{\tilde{F}} &= \prod_{m=2}^{5} \sqrt{2}\tilde{\psi}_0^m && \text{(F.12)}\\
&= \prod_{\mu=2,3} \frac{1}{i} \left(\psi_+^\mu - \psi_-^\mu\right) \cdot \frac{1}{2i} \left(\psi_+^1 - \psi_-^1 + \psi_+^{\bar{1}} - \psi_-^{\bar{1}}\right) \left(\psi_+^1 - \psi_-^1 - \psi_+^{\bar{1}} + \psi_-^{\bar{1}}\right).
\end{aligned}
$$

Using

$$
|\Omega\mathcal{R}_1\Theta^k, -\rangle^0_{RR} \equiv \left[\left(\prod_{\mu=2,3} \psi_-^\mu\right)\left(\psi_-^1 \psi_-^{\bar{1}}\right)\right] |\Omega\mathcal{R}_1\Theta^k, +\rangle^0_{RR} \qquad \text{(F.13)}
$$

leads to the action of the zero mode part of the GSO projector on the groundstates

$$
\begin{aligned}
(-1)^F |\Omega\mathcal{R}_1\Theta^k, +\rangle^0_{RR} &= -(-1)^{\tilde{F}} |\Omega\mathcal{R}_1\Theta^k, +\rangle^0_{RR} = i|\Omega\mathcal{R}_1\Theta^k, -\rangle^0_{RR}, && \text{(F.14)}\\
(-1)^F |\Omega\mathcal{R}_1\Theta^k, -\rangle^0_{RR} &= -(-1)^{\tilde{F}} |\Omega\mathcal{R}_1\Theta^k, -\rangle^0_{RR} = -i|\Omega\mathcal{R}_1\Theta^k, +\rangle^0_{RR}. && \text{(F.15)}
\end{aligned}
$$

These relations carry over to the excited states. Thus,

$$
|\Omega\mathcal{R}_1\Theta^k, +\rangle_{RR} + i|\Omega\mathcal{R}_1\Theta^k, -\rangle_{RR} \qquad \text{(F.16)}
$$

is invariant under P_{GSO} defined in (1.35). The computation directly carries over to the twisted boundary states.

Appendix G

Low energy spectrum for $(T^2 \times T^4/\mathbb{Z}_3)/\Omega\mathcal{R}_1$

G.1 Bosonic states

The lightest mass eigenstates are distinguished by their Θ eigenvalues. Defining $\alpha \equiv e^{2\pi i/3}$, the lightest bosonic states between D8$_a$ and D8$_b$-branes at angle $\pi\Delta\varphi$ on T_1 are listed in the table G.1. The fermionic states can be extracted from table D.1 by considering only states with $k/M = 0$.

Bosonic open states of $T^2 \times T^4/\mathbb{Z}_3$			
on T^2	state	$\frac{\alpha'}{4}$mass^2	$\mathbb{Z}_3$
$\Delta\varphi = 0$	$\psi^{\mu}_{-1/2}\|0\rangle$	0	1
	$\psi^{1,\bar{1}}_{-1/2}\|0\rangle$	0	1
	$\psi^{2,\bar{3}}_{-1/2}\|0\rangle$	0	α
	$\psi^{\bar{2},3}_{-1/2}\|0\rangle$	0	α^2
$\Delta\varphi \neq 0$	$\psi^{\mu}_{-1/2}\|0\rangle$	$\frac{1}{2}\Delta\varphi$	1
	$\psi^{1}_{\Delta\varphi-1/2}\|0\rangle$	$-\frac{1}{2}\Delta\varphi$	1
	$\psi^{\bar{1}}_{-\Delta\varphi-1/2}\|0\rangle$	$\frac{3}{2}\Delta\varphi$	1
	$\psi^{2,\bar{3}}_{-1/2}\|0\rangle$	$\frac{1}{2}\Delta\varphi$	α
	$\psi^{\bar{2},3}_{-1/2}\|0\rangle$	$\frac{1}{2}\Delta\varphi$	α^2

Table G.1: Bosonic open mass eigenstates of the $(T^2 \times T^4/\mathbb{Z}_3)/\Omega\mathcal{R}_1$ orientifold.

G.2 Chiral spectra of examples 2a and 2b

In this appendix, we list the chiral spectra of the left-right symmetric examples 2a and 2b with intersecting D8-branes in section 3.4.3 and 3.4.4.

Chiral spectrum for intersecting D8-branes, ex. 2a

	mult.	$SU(3)\times SU(2)_L\times SU(2)_R\times SO(8)$	Q_A^1	Q_B^1	Q_B^2	Q_C^1	Q_C^2	Q_{B-L}	Q'	Q''
$AB\alpha^0$	2	$(\overline{\mathbf{3}},\mathbf{2},1,1)$	-1	1	0	0	0	$1/3$	$5/3$	$1/4$
	2	$(\mathbf{3},1,\mathbf{2},1)$	1	0	1	0	0	$-1/3$	$-5/3$	$1/4$
α^1	1	$(1,\mathbf{2},1,\mathbf{8})$	0	-1	0	0	0	0	-1	$-1/4$
	1	$(\mathbf{3},1,\mathbf{2},1)$	1	0	-1	0	0	$-1/3$	$1/3$	$-1/4$
α^2	1	$(1,1,\mathbf{2},\mathbf{8})$	0	0	-1	0	0	0	1	$-1/4$
	1	$(\overline{\mathbf{3}},\mathbf{2},1,1)$	-1	-1	0	0	0	$1/3$	$-1/3$	$-1/4$
$AC\alpha^0$	2	$(\mathbf{3},1,1,1)$	1	0	0	-1	0	$-4/3$	$-2/3$	$-1/2$
	2	$(\overline{\mathbf{3}},1,1,1)$	-1	0	0	0	-1	$4/3$	$2/3$	$-1/2$
α^1	1	$(1,1,1,\mathbf{8})$	0	0	0	1	0	1	0	$1/2$
	1	$(\overline{\mathbf{3}},1,1,1)$	-1	0	0	0	1	$-2/3$	$2/3$	$1/2$
α^2	1	$(1,1,1,\mathbf{8})$	0	0	0	0	1	-1	0	$1/2$
	1	$(\mathbf{3},1,1,1)$	1	0	0	1	0	$2/3$	$-2/3$	$1/2$
$BB'\alpha^0$	2	$(1,\mathbf{2},\mathbf{2},1)$	0	1	1	0	0	0	0	$1/2$
α^1	1	$(1,1,1,1)$	0	-2	0	0	0	0	-2	$-1/2$
α^2	1	$(1,1,1,1)$	0	0	-2	0	0	0	2	$-1/2$
$CC'\alpha^0$	2	$(1,1,1,1)$	0	0	0	-1	-1	0	0	-1
α^1	1	$(1,1,1,1)$	0	0	0	2	0	2	0	1
α^2	1	$(1,1,1,1)$	0	0	0	0	2	-2	0	1
$BC'\alpha^0$	2	$(1,\mathbf{2},1,1)$	0	-1	0	-1	0	-1	-1	$-3/4$
	2	$(1,1,\mathbf{2},1)$	0	0	-1	0	-1	1	1	$-3/4$
α^1	1	$(1,\mathbf{2},1,1)$	0	1	0	0	1	-1	1	$3/4$
α^2	1	$(1,1,\mathbf{2},1)$	0	0	1	1	0	1	-1	$3/4$

Table G.2: Chiral fermionic spectrum for example 2a with intersecting D8-branes. The D8-brane configuration and anomaly-free $U(1)$ charges are recorded in (3.54) and (3.55).

Chiral spectrum for intersecting D8-branes, ex. 2b								
	mult.	$SU(3) \times SU(2)_L \times SU(2)_R \times SO(8)$	Q_A^1	Q_B^1	Q_B^2	Q_C^1	Q_{B-L}	Q'
$AB\alpha^0$	2	$(\overline{\mathbf{3}}, \mathbf{2}, 1, 1)$	-1	1	0	0	$1/3$	1
	2	$(\mathbf{3}, 1, \mathbf{2}, 1)$	1	0	1	0	$-1/3$	-1
α^1	1	$(1, \mathbf{2}, 1, \mathbf{8})$	0	-1	0	0	0	-1
	1	$(\mathbf{3}, 1, \mathbf{2}, 1)$	1	0	-1	0	$-1/3$	1
α^2	1	$(1, 1, \mathbf{2}, \mathbf{8})$	0	0	-1	0	0	1
	1	$(\overline{\mathbf{3}}, \mathbf{2}, 1, 1)$	-1	-1	0	0	$1/3$	-1
$BB'\alpha^0$	2	$(1, \mathbf{2}, \mathbf{2}, 1)$	0	1	1	0	0	0
α^1	1	$(1, 1, 1, 1)$	0	-2	0	0	0	-2
α^2	1	$(1, 1, 1, 1)$	0	0	-2	0	0	2
$BC\alpha^0$	2	$(1, \mathbf{2}, 1, 1)$	0	-1	0	1	-1	1
	2	$(1, 1, \mathbf{2}, 1)$	0	0	-1	-1	1	-1
α^1	1	$(1, 1, \mathbf{2}, 1)$	0	0	1	-1	1	-3
α^2	1	$(1, \mathbf{2}, 1, 1)$	0	1	0	1	-1	3

Table G.3: Chiral fermionic spectrum for example 2b with intersecting D8-branes. The D8-brane configuration is given in (3.56) and the anomaly-free $U(1)$ charges are specified by (3.57).

Bibliography

[1] G. Aldazabal, S. Franco, L. E. Ibáñez, R. Rabadán, and A. M. Uranga, *$D = 4$ chiral string compactifications from intersecting branes*, J. Math. Phys. **42** (2001), 3103–3126, hep-th/0011073.

[2] G. Aldazabal, S. Franco, L. E. Ibáñez, R. Rabadán, and A. M. Uranga, *Intersecting brane worlds*, JHEP **02** (2001), 047, hep-ph/0011132.

[3] C. Angelantonj, *Comments on open-string orbifolds with a non-vanishing B_{ab}*, Nucl. Phys. **B566** (2000), 126–150, hep-th/9908064.

[4] C. Angelantonj, I. Antoniadis, E. Dudas, and A. Sagnotti, *Type-I strings on magnetised orbifolds and brane transmutation*, Phys. Lett. **B489** (2000), 223–232, hep-th/0007090.

[5] C. Angelantonj, R. Blumenhagen, and M. R. Gaberdiel, *Asymmetric orientifolds, brane supersymmetry breaking and non-BPS branes*, Nucl. Phys. **B589** (2000), 545–576, hep-th/0006033.

[6] I. Antoniadis, N. Arkani-Hamed, S. Dimopoulos, and G. R. Dvali, *New dimensions at a millimeter to a Fermi and superstrings at a TeV*, Phys. Lett. **B436** (1998), 257–263, hep-ph/9804398.

[7] N. Arkani-Hamed, S. Dimopoulos, and G. R. Dvali, *The hierarchy problem and new dimensions at a millimeter*, Phys. Lett. **B429** (1998), 263–272, hep-ph/9803315.

[8] C. Bachas, *A way to break supersymmetry*, (1995), hep-th/9503030.

[9] D. Bailin, G. V. Kraniotis, and A. Love, *Standard-like models from intersecting D4-branes*, (2001), hep-th/0108131.

[10] P. Bain and M. Berg, *Effective action of matter fields in four-dimensional string orientifolds*, JHEP **04** (2000), 013, hep-th/0003185.

[11] T. Banks and L. Susskind, *Brane - antibrane forces*, (1995), hep-th/9511194.

[12] M. Berkooz, M. R. Douglas, and R. G. Leigh, *Branes intersecting at angles*, Nucl. Phys. **B480** (1996), 265–278, hep-th/9606139.

[13] M. Bianchi, *A note on toroidal compactifications of the type I superstring and other superstring vacuum configurations with 16 supercharges*, Nucl. Phys. **B528** (1998), 73–94, hep-th/9711201.

[14] M. Bianchi, G. Pradisi, and A. Sagnotti, *Toroidal compactification and symmetry breaking in open string theories*, Nucl. Phys. **B376** (1992), 365–386.

[15] M. Bianchi and A. Sagnotti, *On the systematics of open string theories*, Phys. Lett. **B247** (1990), 517–524.

[16] M. Bianchi and A. Sagnotti, *Twist symmetry and open string Wilson lines*, Nucl. Phys. **B361** (1991), 519–538.

[17] N. D. Birrell and P. C. W. Davies, *Quantum fields in curved space*, Cambridge, Uk: Univ. Pr. (1982) 340p.

[18] R. Blumenhagen, L. Görlich, and B. Körs, *A new class of supersymmetric orientifolds with D-branes at angles*, (1999), hep-th/0002146.

[19] R. Blumenhagen, L. Görlich, and B. Körs, *Supersymmetric 4D orientifolds of type IIA with D6-branes at angles*, JHEP **01** (2000), 040, hep-th/9912204.

[20] R. Blumenhagen, L. Görlich, and B. Körs, *Supersymmetric orientifolds in 6D with D-branes at angles*, Nucl. Phys. **B569** (2000), 209–228, hep-th/9908130.

[21] R. Blumenhagen, L. Görlich, B. Körs, and D. Lüst, *Asymmetric orbifolds, noncommutative geometry and type I string vacua*, Nucl. Phys. **B582** (2000), 44–64, hep-th/0003024.

[22] R. Blumenhagen, L. Görlich, B. Körs, and D. Lüst, *Noncommutative compactifications of type I strings on tori with magnetic background flux*, JHEP **10** (2000), 006, hep-th/0007024.

[23] R. Blumenhagen, L. Görlich, B. Körs, and D. Lüst, *Magnetic flux in toroidal type I compactification*, Fortsch. Phys. **49** (2001), 591–598, hep-th/0010198.

[24] R. Blumenhagen, B. Körs, and D. Lüst, *Type I strings with F- and B-flux*, JHEP **02** (2001), 030, hep-th/0012156.

[25] R. Blumenhagen, B. Körs, and D. Lüst, *Moduli stabilization for intersecting brane worlds in type 0' string theory*, (2002), `hep-th/0202024`.

[26] R. Blumenhagen, B. Körs, D. Lüst, and T. Ott, *Intersecting brane worlds on tori and orbifolds*, (2001), `hep-th/0112015`.

[27] R. Blumenhagen, B. Körs, D. Lüst, and T. Ott, *The standard model from stable intersecting brane world orbifolds*, Nucl. Phys. **B616** (2001), 3–33, `hep-th/0107138`.

[28] P. Candelas, G. T. Horowitz, A. Strominger, and E. Witten, *Vacuum configurations for superstrings*, Nucl. Phys. **B258** (1985), 46–74.

[29] D. Cremades, L. E. Ibáñez, and F. Marchesano, *Intersecting brane models of particle physics and the Higgs mechanism*, (2002), `hep-th/0203160`.

[30] D. Cremades, L. E. Ibáñez, and F. Marchesano, *SUSY quivers, intersecting branes and the modest hierarchy problem*, (2002), `hep-th/0201205`.

[31] M. Cvetič, L. L. Everett, P. Langacker, and J. Wang, *Blowing-up the four-dimensional Z_3 orientifold*, JHEP **04** (1999), 020, `hep-th/9903051`.

[32] M. Cvetič and P. Langacker, *$D = 4$ $N = 1$ type IIB orientifolds with continuous Wilson lines, moving branes, and their field theory realization*, Nucl. Phys. **B586** (2000), 287–302, `hep-th/0006049`.

[33] M. Cvetič, G. Shiu, and A. M. Uranga, *Chiral four-dimensional $N = 1$ supersymmetric type IIA orientifolds from intersecting D6-branes*, Nucl. Phys. **B615** (2001), 3–32, `hep-th/0107166`.

[34] M. Cvetič, G. Shiu, and A. M. Uranga, *Chiral type II orientifold constructions as M theory on G_2 holonomy spaces*, (2001), `hep-th/0111179`.

[35] M. Cvetič, G. Shiu, and A. M. Uranga, *Three-family supersymmetric standard like models from intersecting brane worlds*, Phys. Rev. Lett. **87** (2001), 201801, `hep-th/0107143`.

[36] M. Cvetič, A. M. Uranga, and J. Wang, *Discrete Wilson lines in $N = 1$ $D = 4$ type IIB orientifolds: A systematic exploration for Z_6 orientifold*, Nucl. Phys. **B595** (2001), 63–92, `hep-th/0010091`.

[37] A. Dabholkar, *Lectures on orientifolds and duality*, (1997), `hep-th/9804208`.

[38] J. Dai, R. G. Leigh, and J. Polchinski, *New connections between string theories*, Mod. Phys. Lett. **A4** (1989), 2073–2083.

[39] S. P. de Alwis, *A note on brane tension and M-theory*, Phys. Lett. **B388** (1996), 291–295, hep-th/9607011.

[40] L. J. Dixon, J. A. Harvey, C. Vafa, and E. Witten, *Strings on orbifolds*, Nucl. Phys. **B261** (1985), 678–686.

[41] L. J. Dixon, J. A. Harvey, C. Vafa, and E. Witten, *Strings on orbifolds. 2*, Nucl. Phys. **B274** (1986), 285–314.

[42] M. R. Douglas, *Branes within branes*, (1995), hep-th/9512077.

[43] M. R. Douglas and G. W. Moore, *D-branes, quivers, and ALE instantons*, (1996), hep-th/9603167.

[44] W. Fischler and L. Susskind, *Dilaton tadpoles, string condensates and scale invariance*, Phys. Lett. **B171** (1986), 383.

[45] W. Fischler and L. Susskind, *Dilaton tadpoles, string condensates and scale invariance. 2*, Phys. Lett. **B173** (1986), 262.

[46] A. Font, L. E. Ibáñez, H. P. Nilles, and F. Quevedo, *Yukawa couplings in degenerate orbifolds: Towards a realistic $SU(3)\times SU(2)\times U(1)$ superstring*, Phys. Lett. **210B** (1988), 101.

[47] S. Förste, *Strings, branes and extra dimensions*, Fortsch. Phys. **50** (2002), 221–403, hep-th/0110055.

[48] S. Förste, G. Honecker, and R. Schreyer, *Orientifolds with branes at angles*, JHEP **06** (2001), 004, hep-th/0105208.

[49] S. Förste, G. Honecker, and R. Schreyer, *Supersymmetric $Z_N \times Z_M$ orientifolds in 4D with D-branes at angles*, Nucl. Phys. **B593** (2001), 127–154, hep-th/0008250.

[50] M. R. Gaberdiel, *Lectures on non-BPS Dirichlet branes*, Class. Quant. Grav. **17** (2000), 3483–3520, hep-th/0005029.

[51] J. Garcia-Bellido, R. Rabadán, and F. Zamora, *Inflationary scenarios from branes at angles*, JHEP **01** (2002), 036, hep-th/0112147.

[52] D. M. Ghilencea, H. P. Nilles, and S. Stieberger, *Divergences in Kaluza-Klein models and their string regularization*, (2001), hep-th/0108183.

[53] E. G. Gimon and C. V. Johnson, *K3 orientifolds*, Nucl. Phys. **B477** (1996), 715–745, hep-th/9604129.

[54] E. G. Gimon and J. Polchinski, *Consistency conditions for orientifolds and D-manifolds*, Phys. Rev. **D54** (1996), 1667–1676, hep-th/9601038.

[55] A. Giveon, M. Porrati, and E. Rabinovici, *Target space duality in string theory*, Phys. Rept. **244** (1994), 77–202, `hep-th/9401139`.

[56] F. Gliozzi, J. Scherk, and D. I. Olive, *Supersymmetry, supergravity theories and the dual spinor model*, Nucl. Phys. **B122** (1977), 253–290.

[57] J. Govaerts, *Quantum consistency of open string theories*, Phys. Lett. **B220** (1989), 77.

[58] M. B. Green, J. H. Schwarz, and E. Witten, *Superstring theory. Vol. 1: Introduction*, Cambridge, Uk: Univ. Pr. (1987) 469 P. (Cambridge Monographs On Mathematical Physics).

[59] M. B. Green, J. H. Schwarz, and E. Witten, *Superstring theory. Vol. 2: Loop amplitudes, anomalies and phenomenology*, Cambridge, Uk: Univ. Pr. (1987) 596 P. (Cambridge Monographs On Mathematical Physics).

[60] D. J. Gross, J. A. Harvey, E. J. Martinec, and R. Rohm, *Heterotic string theory 1. The free heterotic string*, Nucl. Phys. **B256** (1985), 253.

[61] D. J. Gross, J. A. Harvey, E. J. Martinec, and R. Rohm, *The heterotic string*, Phys. Rev. Lett. **54** (1985), 502–505.

[62] D. J. Gross, J. A. Harvey, E. J. Martinec, and R. Rohm, *Heterotic string theory. 2. the interacting heterotic string*, Nucl. Phys. **B267** (1986), 75.

[63] A. Hashimoto and IV Taylor, W., *Fluctuation spectra of tilted and intersecting D-branes from the Born-Infeld action*, Nucl. Phys. **B503** (1997), 193–219, `hep-th/9703217`.

[64] G. Honecker, *Non-supersymmetric orientifolds with D-branes at angles*, (2001), `hep-th/0112174`.

[65] G. Honecker, *Intersecting brane world models from D8-branes on* $(T^2 \times T^4/Z_3)/\Omega\mathcal{R}_1$ *type IIA orientifolds*, JHEP **01** (2002), 025, `hep-th/0201037`.

[66] P. Hořava, *Strings on world sheet orbifolds*, Nucl. Phys. **B327** (1989), 461.

[67] P. Hořava and E. Witten, *Eleven-dimensional supergravity on a manifold with boundary*, Nucl. Phys. **B475** (1996), 94–114, `hep-th/9603142`.

[68] P. Hořava and E. Witten, *Heterotic and type i string dynamics from eleven dimensions*, Nucl. Phys. **B460** (1996), 506–524, `hep-th/9510209`.

[69] L. E. Ibáñez, *Standard model engineering with intersecting branes*, (2001), `hep-ph/0109082`.

[70] L. E. Ibáñez, J. E. Kim, H. P. Nilles, and F. Quevedo, *Orbifold compactifications with three families of $SU(3) \times SU(2) \times U(1)^n$*, Phys. Lett. **B191** (1987), 282–286.

[71] L. E. Ibáñez, F. Marchesano, and R. Rabadán, *Getting just the standard model at intersecting branes*, JHEP **11** (2001), 002, `hep-th/0105155`.

[72] L. E. Ibáñez, C. Muñoz, and S. Rigolin, *Aspects of type I string phenomenology*, Nucl. Phys. **B553** (1999), 43–80, `hep-ph/9812397`.

[73] L. E. Ibáñez, H. P. Nilles, and F. Quevedo, *Orbifolds and Wilson lines*, Phys. Lett. **B187** (1987), 25–32.

[74] N. Ishibashi and T. Onogi, *Open string model building*, Nucl. Phys. **B318** (1989), 239.

[75] Z. Kakushadze, *Geometry of orientifolds with NS-NS B-flux*, Int. J. Mod. Phys. **A15** (2000), 3113–3196, `hep-th/0001212`.

[76] T. Kaluza, *On the problem of unity in physics*, Sitzungsber. Preuss. Akad. Wiss. Berlin (Math. Phys.) **K1** (1921), 966–972.

[77] H. Kataoka and M. Shimojo, *$SU(3) \times SU(2) \times U(1)$ chiral models from intersecting D4/D5 branes*, (2001), `hep-th/0112247`.

[78] O. Klein, *Quantum theory and five-dimensional theory of relativity. (in german and english)*, Z. Phys. **37** (1926), 895–906.

[79] C. Kokorelis, *GUT model hierarchies from intersecting branes*, (2002), `hep-th/0203187`.

[80] B. Körs, *Open strings in magnetic background fields*, Fortsch. Phys. **49** (2001), 759–867.

[81] Z. Lalak, S. Lavignac, and H. P. Nilles, *String dualities in the presence of anomalous U(1) symmetries*, Nucl. Phys. **B559** (1999), 48–70, `hep-th/9903160`.

[82] J. Lauer, J. Mas, and H. P. Nilles, *Duality and the role of nonperturbative effects on the world sheet*, Phys. Lett. **B226** (1989), 251.

[83] J. Lauer, J. Mas, and H. P. Nilles, *Twisted sector representations of discrete background symmetries for two-dimensional orbifolds*, Nucl. Phys. **B351** (1991), 353–424.

[84] A. Lerda and R. Russo, *Stable non-BPS states in string theory: A pedagogical review*, Int. J. Mod. Phys. **A15** (2000), 771–820, `hep-th/9905006`.

[85] M. Li, *Boundary states of D-branes and Dy-strings*, Nucl. Phys. **B460** (1996), 351–361, `hep-th/9510161`.

[86] D. Lüst and S. Theisen, *Lectures on string theory*, Lect. Notes Phys. **346** (1989), 1–346.

[87] J. D. Lykken, *Weak scale superstrings*, Phys. Rev. **D54** (1996), 3693–3697, `hep-th/9603133`.

[88] N. S. Manton, *The Schwinger model and its axial anomaly*, Annals Phys. **159** (1985), 220–251.

[89] H. P. Nilles, *Supersymmetry, supergravity and particle physics*, Phys. Rept. **110** (1984), 1.

[90] H. P. Nilles, M. Olechowski, and M. Yamaguchi, *Supersymmetry breaking and soft terms in M-theory*, Phys. Lett. **B415** (1997), 24–30, `hep-th/9707143`.

[91] H. P. Nilles, M. Olechowski, and M. Yamaguchi, *Supersymmetry breakdown at a hidden wall*, Nucl. Phys. **B530** (1998), 43–72, `hep-th/9801030`.

[92] J. Park, R. Rabadán, and A. M. Uranga, *Orientifolding the conifold*, Nucl. Phys. **B570** (2000), 38–80, `hep-th/9907086`.

[93] J. Polchinski, *String theory. Vol. 1: An introduction to the bosonic string*, Cambridge, UK: Univ. Pr. (1998) 402 p.

[94] J. Polchinski, *String theory. Vol. 2: Superstring theory and beyond*, Cambridge, UK: Univ. Pr. (1998) 531 p.

[95] J. Polchinski, *Dirichlet-branes and Ramond-Ramond charges*, Phys. Rev. Lett. **75** (1995), 4724–4727, `hep-th/9510017`.

[96] J. Polchinski, *TASI lectures on D-branes*, (1996), `hep-th/9611050`.

[97] J. Polchinski and Y. Cai, *Consistency of open superstring theories*, Nucl. Phys. **B296** (1988), 91.

[98] J. Polchinski and E. Witten, *Evidence for heterotic - type I string duality*, Nucl. Phys. **B460** (1996), 525–540, `hep-th/9510169`.

[99] G. Pradisi and A. Sagnotti, *Open string orbifolds*, Phys. Lett. **B216** (1989), 59.

[100] R. Rabadán, *Branes at angles, torons, stability and supersymmetry*, Nucl. Phys. **B620** (2002), 152–180, `hep-th/0107036`.

[101] R. Rabadán and A. M. Uranga, *Type IIB orientifolds without untwisted tadpoles, and non- BPS D-branes*, JHEP **01** (2001), 029, hep-th/0009135.

[102] C. Rovelli, *Strings, loops and others: A critical survey of the present approaches to quantum gravity*, (1997), gr-qc/9803024.

[103] A. Sagnotti, *Open strings and their symmetry groups*, Talk presented at the Cargese Summer Institute on Non- Perturbative Methods in Field Theory, Cargese, France, Jul 16-30, 1987.

[104] R. Schreyer, *Supersymmetric orientifolds with D-branes at angles*, (2001), Ph.D. thesis.

[105] J. H. Schwarz, *The power of M theory*, Phys. Lett. **B367** (1996), 97–103, hep-th/9510086.

[106] N. Seiberg and E. Witten, *Spin structures in string theory*, Nucl. Phys. **B276** (1986), 272.

[107] A. Sen, *Non-BPS D-branes in string theory*, Class. Quant. Grav. **17** (2000), 1251–1256.

[108] G. Shiu and S. H. H. Tye, *TeV scale superstring and extra dimensions*, Phys. Rev. **D58** (1998), 106007, hep-th/9805157.

[109] A. Strominger and E. Witten, *New manifolds for superstring compactification*, Commun. Math. Phys. **101** (1985), 341.

[110] P. K. Townsend, *The eleven-dimensional supermembrane revisited*, Phys. Lett. **B350** (1995), 184–187, hep-th/9501068.

[111] E. Witten, *String theory dynamics in various dimensions*, Nucl. Phys. **B443** (1995), 85–126, hep-th/9503124.

[112] E. Witten, *Strong coupling expansion of Calabi-Yau compactification*, Nucl. Phys. **B471** (1996), 135–158, hep-th/9602070.

[113] E. Witten, *Toroidal compactification without vector structure*, JHEP **02** (1998), 006, hep-th/9712028.